

**METAL NANO PARTICLE-CORED DENDRIMERS: SYNTHESIS,
CHARACTERIZATION AND THEIR USE AS CATALYST IN
SELECTED ORGANIC TRANSFORMATIONS**

THESIS SUBMITTED TO
THE UNIVERSITY OF KERALA
FOR THE DEGREE OF
DOCTOR OF PHILOSOPHY
IN CHEMISTRY
UNDER THE FACULTY OF SCIENCE

By
RATHEESH KUMAR V. K.

PHOTOSCIENCES AND PHOTONICS
CHEMICAL SCIENCES AND TECHNOLOGY DIVISION
NATIONAL INSTITUTE FOR INTERDISCIPLINARY SCIENCE AND TECHNOLOGY
COUNCIL OF SCIENTIFIC AND INDUSTRIAL RESEARCH
TRIVANDRUM – 695 019
KERALA, INDIA

DECEMBER 2010

DECLARATION

I hereby declare that the Ph.D. thesis entitled "**Metal Nano Particle-Cored Dendrimers: Synthesis, Characterization and their Use as Catalyst in Selected Organic Transformations**" is an independent work carried out by me at the Photosciences and Photonics Section, Chemical Sciences and Technology Division, National Institute for Interdisciplinary Science and Technology (NIIST), CSIR, Trivandrum, under the supervision of Dr. K. R. Gopidas and the same has not been submitted elsewhere for any other degree, diploma or title.

In keeping with the general practice of reporting the scientific observations, due acknowledgement has been made wherever the work described is based on the findings of other investigators.

Ratheesh Kumar V. K.

**NATIONAL INSTITUTE FOR INTERDISCIPLINARY SCIENCE
AND TECHNOLOGY (NIIST)**



(Formerly Regional Research Laboratory)
Council of Scientific & Industrial Research (CSIR)
Industrial Estate P O Trivandrum – 695 019, Kerala, INDIA.



Dr. K. R. Gopidas

Scientist and Head
Photosciences and Photonics
Chemical Sciences and Technology Division

Tel: 91 471 2515 390
Fax: +91 471 2491 712
E-mail: gopidaskr@gmail.com

December 01, 2010

CERTIFICATE

This is to certify that the work embodied in the thesis entitled "**Metal Nano Particle-Cored Dendrimers: Synthesis, Characterization and their Use as Catalyst in Selected Organic Transformations**" has been carried out by Mr. Ratheesh Kumar V. K. under my supervision and guidance at the Photosciences and Photonics Section, Chemical Sciences and Technology Division, National Institute for Interdisciplinary Science and Technology (NIIST), CSIR, Trivandrum and the same has not been submitted elsewhere for a degree.

K. R. Gopidas
(Thesis Supervisor)

ACKNOWLEDGEMENTS

It is with great pleasure I express my deep sense of gratitude to Dr. K. R. Gopidas, my thesis supervisor, for suggesting the research problem and for his encouraging and inspiring guidance which moulded the successful completion of this work.

I gratefully acknowledge the encouraging interactions that I had with Professor M. V. George during my stay at NIIST.

I thank Dr. Suresh Das, present director, Professor T. K. Chandrasekhar and Dr. B. C. Pai, former directors of NIIST, Trivandrum, for providing me the necessary facilities and infrastructure of the institute for carrying out this work.

My sincere thanks are due to Dr. A. Ajayaghosh, Dr. D. Ramaiah, Dr. K. George Thomas and Dr. A. Srinivasan, present and former scientists of the Photosciences and Photonics Section for their support and valuable discussions at different stages of this work.

I am thankful to

- ❖ *Dr. B. Bijitha, Dr. G. Ajayakumar, Dr. K. Sreenath and Dr. C. V. Suneesh, former members of the Photosciences and Photonics Section for their support and encouragement.*
- ❖ *Ms. Deepthi L. Sivadas, Mr. Jomon Mathew, Mr. K. Retheesh, Mr. M. V. Vinayak, Ms. A. M. Rakhi, Mr. Tony George Thomas, Ms. K. Sreedevi, Mr. T. M. Lakshmikanth, Ms. Divya R. Nair and all other members of Photosciences and Photonics Group for their help and cooperation.*
- ❖ *Ms. Saumini Mathew, Mr. Adarsh, Mr. Preethanuj for NMR, Ms. S. Viji for HRMS, Mr. P. Guruswamy for XRD, Mr. Kiran for TEM, Mr. S. Veluswamy for TGA, Mrs. Sarada Nair and Mr. Robert Philip for general help.*
- ❖ *All my friends at NIIST for their support.*
- ❖ *All my teachers for their encouragement at different stages of my academic career.*

I am deeply grateful to my family for their support, love and wishes.

Finally, I thank UGC, CSIR and DST for the financial support.

Ratheesh Kumar V. K.

CONTENTS

	Page
Declaration	i
Certificate	ii
Acknowledgements	iii
List of Tables	vii
List of Figures	vii
List of Abbreviations	ix
Preface	xii

CHAPTER 1: Dendrimer Stabilized Metal Nanoparticles: An Overview

1.1	Introduction	1
1.2	Synthesis of Metal Nanoparticles	3
1.2.1	Electrostatic Stabilization	4
1.2.2	Steric Stabilization	5
1.2.3	Electrosteric Stabilization	6
1.3	Dendrimers	7
1.3.1	Synthesis of Dendrimers	8
1.3.2	Dendrimers as Nanoparticle Protecting Agents	10
1.4	Origin of Present Work	38
1.5	Electrochemical Grafting of Aryl Groups on Electrode Surfaces	40
1.6	Outline of the Thesis	45

CHAPTER 2: Synthesis and Characterization of Gold Nanoparticle-Cored Dendrimers Stabilized by Direct Carbon-Metal Bonds

2.1	Abstract	48
-----	----------	----

2.2	Introduction	49
2.3	Results and Discussions	52
2.3.1	Syntheses	52
2.3.2	Characterization of Diazodendrons and AuG_n	61
2.3.3	Control Experiments	72
2.3.4	Stability of AuG_n	75
2.3.5	Structure of AuG_n	75
2.4	Conclusion	79
2.5	Experimental	80
2.5.1	Materials and Methods	80
2.5.2	Synthesis of AuG₁	81
2.5.3	Synthesis of AuG₂	83
2.5.4	Synthesis of AuG₃	86
2.5.5	Synthesis of AuG₄	89
2.5.6	Control Experiments	91

CHAPTER 3: **Synthesis and Characterization of Palladium**

Nanoparticle-Cored Dendrimers Stabilized by Direct Carbon-Metal Bonds

3.1	Abstract	95
3.2	Introduction	96
3.3	Results and Discussions	100
3.3.1	Syntheses	100
3.3.2	Characterization of PdG_n	102
3.3.3	Control Experiments	109
3.4	Conclusion	109
3.5	Experimental	110
3.5.1	Materials and Methods	110

3.5.2	Synthesis of PdG₁	111
3.5.3	Synthesis of PdG₂	112
3.5.4	Synthesis of PdG₃	113
3.5.5	Synthesis of PdG₄	114

CHAPTER 4: Catalytic Applications of Palladium Nanoparticle-Cored G₁ Dendrimer

4.1	Abstract	116
4.2	Introduction	117
4.3	Results and Discussions	124
4.3.1	Catalytic Features of PdG₁	124
4.3.2	Hydrogenation Reactions Using PdG₁	126
4.3.3	PdG₁ Catalyzed C-C Bond Forming Reactions	135
4.3.4	Suzuki Reactions	136
4.3.5	Stille Reactions	146
4.3.6	Hiyama Reactions	148
4.3.7	Heck Reactions	150
4.4	Conclusion	152
4.5	Experimental	154
4.5.1	Materials and Methods	154
4.5.2	Reaction Conditions and Product Characterization Data for PdG₁ Catalyzed Reactions	154
	List of Publications	166
	References	168

List of Tables

	Page
1. Table 2.1	77
2. Table 4.1	120
3. Table 4.2	129
4. Table 4.3	130
5. Table 4.4	132
6. Table 4.5	133
7. Table 4.6	135
8. Table 4.7	137
9. Table 4.8	139
10. Table 4.9	140
11. Table 4.10	141
12. Table 4.11	142
13. Table 4.12	143
14. Table 4.13	144
15. Table 4.14	148
16. Table 4.15	150
17. Table 4.16	152

List of Figures

1. Figure 1.1	5
2. Figure 1.2	6
3. Figure 1.3	6

4.	Figure 1.4	8
5.	Figure 1.5	8
6.	Figure 1.6	12
7.	Figure 1.7	13
8.	Figure 1.8	14
9.	Figure 1.9	15
10.	Figure 1.10	21
11.	Figure 1.11	22
12.	Figure 1.12	23
13.	Figure 1.13	26
14.	Figure 1.14	27
15.	Figure 1.15	27
16.	Figure 1.16	35
17.	Figure 2.1	51
18.	Figure 2.2	52
19.	Figure 2.3	54
20.	Figure 2.4	55
21.	Figure 2.5	57
22.	Figure 2.6	58
23.	Figure 2.7	61
24.	Figure 2.8	63
25.	Figure 2.9	64
26.	Figure 2.10	67

27.	Figure 2.11	68
28.	Figure 2.12	70
29.	Figure 2.13	72
30.	Figure 2.14	73
31.	Figure 2.15	74
32.	Figure 2.16	77
33.	Figure 3.1	102
34.	Figure 3.2	103
35.	Figure 3.3	105
36.	Figure 3.4	106
37.	Figure 3.5	107
38.	Figure 3.6	108
39.	Figure 4.1	125
40.	Figure 4.2	134
41.	Figure 4.3	143

List of Abbreviations

acac	Acetylacetone
AFM	Atomic Force Microscopy
Aq.	Aqueous
BE	Binding Energy
BINAP	2,2'-bis(diphenylphosphino)-1,1'-binaphthyl
CCD	Charge-Coupled Device

Conc.	Concentrated
CVD	Chemical Vapour Deposition
DCC	Dicyclohexylcarbodiimide
DCM	Dichloromethane
DEN	Dendrimer-Encapsulated Nanoparticle
Dil.	Dilute
DMAP	4-Dimethylaminopyridine
DMF	Dimethylformamide
DTA	Differential Thermal Analysis
EDX	Energy Dispersive X-Ray
EI	Electron Ionization
en	ethylenediamine
ESR	Electron Spin Resonance
FAB	Fast Atom Bombardment
GC-MS	Gas Chromatograph-Mass Spectrometer
HOPG	Highly Oriented Pyrolytic Graphite
HRMS	High Resolution Mass Spectrum
IR	Infrared
LMCT	Ligand to Metal Charge Transfer
M	Molar
MPC	Monolayer Protected Cluster
NCD	Nanoparticle-Cored Dendrimer
NMR	Nuclear Magnetic Resonance

PAMAM	Poly(amidoamine)
PPD	Poly(oxymethylphenylene)
PPI	Poly(propyleneimine)
SAM	Self Assembled Monolayer
SIS	Sterically Induced Stoichiometry
SPR	Surface Plasmon Resonance
STM	Scanning Tunneling Microscopy
TBAF	Tetrabutylammonium fluoride
TEM	Transmission Electron Microscopy
TGA	Thermogravimetric Analysis
THF	Tetrahydrofuran
TLC	Thin Layer Chromatogram
TOAB	Tetra- <i>n</i> -octylammonium bromide
TOF	Turn-over Frequency
TON	Turn-over Number
UV	Ultraviolet

PREFACE

Nanoparticle-Cored Dendrimers (NCDs) are inorganic-organic hybrid materials possessing nanometer size metal clusters at the core surrounded by a shell of dendrons of different generations that are radially attached to the core. The sterically induced assembly of cone shaped dendron shells around the metal core makes these core-shell materials to enclose large voids close to the nanoparticle surface. This sterically restricted assembly envisaged by NCDs enables them to function as 'nanoreactors' for metal catalyzed organic transformations. Significant progress has been achieved during the last decades in the design and synthesis of NCDs containing different metals and dendrons of different structures. Most of the synthetic approaches for the preparation of NCDs involve anchoring of the dendrons on to the metal surface through soft atoms like S, N, P or O which makes their stability always challenging. This makes the synthesis of NCDs with strong metal-ligand interaction an active area of research and our work is an attempt in this direction. Work described in this thesis involves the synthesis and characterization of gold and palladium NCDs stabilized by direct metal-carbon linkages. The synthesis of these core-shell materials are achieved by the simultaneous reduction of the metal ion precursor and a diazodendron using a suitable reducing agent. The NCDs thus prepared were purified and characterized. The ability of these NCDs to catalyze various reactions was also studied.

A detailed literature review regarding the different approaches for the synthesis and characterization of dendrimer stabilized nanoparticles is presented in the first chapter of this thesis. The advantages and disadvantages of different synthetic strategies adopted for the preparation of NCDs are also presented in this chapter along with the potential applications of dendrimer stabilized nanoparticles.

Second chapter of the thesis describes the synthesis and characterization of gold nanoparticle-cored dendrimers of generation 1-4 (AuG_n), stabilized by direct metal-carbon linkage. The synthesis was carried out by the simultaneous reduction of different generation diazo functionalized dendrons (G_1 - G_4) and Au(III) using sodium borohydride as the reducing agent. The diazodendrons and NCDs were characterized

using FT-IR, NMR, UV-visible spectroscopies as well as TEM and TG analysis. TEM studies confirmed the formation of nearly monodisperse, spherical gold nanoparticles with size around 5 nm. In order to confirm the direct bonding interaction of the dendrons with the metal nanoparticle, different control experiments were also carried out. These studies ruled out the possible encapsulation of nanoparticles inside the macromolecules. Studies were also carried out to check the stability of the NCDs and these details are also discussed in this chapter.

Synthesis and characterization details for the preparation of palladium nanoparticle-cored dendrimers of generation 1-4 (**PdG_n**), are reported in the third chapter. The synthesis was carried out by the reduction of Pd(II) in presence of diazo functionalized Fréchet type poly(arylether) dendrons of different generations (G₁-G₄). The isolated products were well characterized by different spectroscopic techniques like FT-IR, NMR, UV-visible as well as TEM analysis. The formation of almost monodisperse spherical particles having 2-4 nm size was confirmed by TEM analysis.

We have studied the use of **PdG₁** as catalyst for different organic transformations and the results are discussed in the fourth chapter. **PdG₁** was used for the catalytic hydrogenation of different multifunctional organic molecules and the results show that the present catalytic system is effective for the efficient and selective hydrogenation of olefins and acetylenes in multifunctional organic molecules possessing functional moieties like -NO₂, -CHO and halides which are very sensitive to hydrogenation reaction conditions. These chemoselective hydrogenation reactions were conducted at room temperature using a hydrogen balloon and all these reactions proceeded smoothly to almost completion with good yields at short reaction times and the catalyst showed good recyclability. The ability of **PdG₁** to catalyze different C-C bond forming reactions such as Suzuki, Stille, Heck and Hiyama couplings was also investigated. Our studies showed that **PdG₁** can act as an efficient catalyst for Suzuki and Stille couplings with almost quantitative yields. These reactions required only mild conditions and short reaction times and the catalyst showed good recyclability. Our results showed that **PdG₁** is a promising catalyst for different C-C bond forming reactions.

Chapter 1

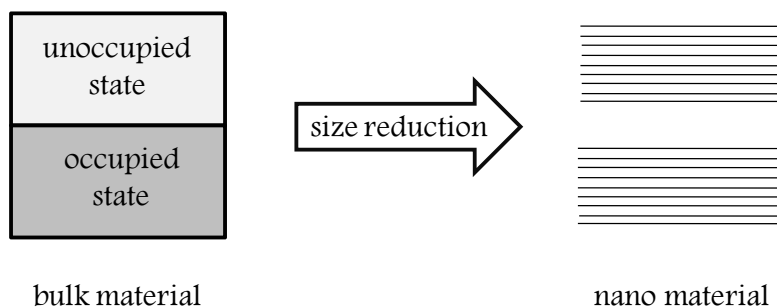
Dendrimer Stabilized Metal Nanoparticles: An Overview

1.1 Introduction

Nanoparticles or nano-sized particles are of great scientific interest because they serve as a bridge between bulk materials and the molecular world. Bulk materials exhibit size-independent physical properties whereas the properties of nanoparticles are often size dependent. For bulk materials larger than one micrometer the percentage of atoms on the surface is insignificantly small compared to atoms present in the bulk. In the case of nanoparticles, the number of atoms present on the surface is significant compared to atoms in the bulk. The interesting and sometimes unexpected properties of nanoparticles are therefore mainly due to the large surface area of the material, which dominates the contributions made by the small bulk of the material [El-Sayed 2001; 2004; Shenhar 2003].

The electronic and optical properties of nanoparticles depend on the size and shape of these materials. Size dependent electronic and optical properties arise due to confinement of electrons within the dimensions of the small particles and this can be best explained using the 3D model of particle in a box problem. In the case of bulk metals, for

example, the electrons are free to move leading to a merging of the valence and conduction band levels (Scheme 1.1). As the size of the metal particles decrease the electron movement becomes confined within well defined atomic/molecular orbitals with definite energy boundaries. The smaller the allowed space for electron motion, the stronger will be the confinement leading to larger differences between the allowed energy levels. Thus when a metal particle is progressively reduced in size electron confinement leads to progressive separation of valence and conduction bands [Jain 2008; Cao 2008]. This would lead to a metallic \rightarrow insulator transformation as shown in Scheme 1.1.



Scheme 1.1 Difference in the arrangement of energy levels in bulk and nano metal.

During the last several years the science dealing with the synthesis and study of nanomaterials has seen tremendous advancement. At the core of these studies lies the desire to gain a deeper insight into the peculiar chemical properties and reactivities of particles comprising of only a small number of atoms. Application of nanochemistry to the synthesis, modification and stabilization of individual nanoparticles also gained considerable importance during this period. Other areas worth mentioning include the studies dealing with altering the properties of

synthesized nanoparticles by regulating sizes and shapes and directed self-assembly of nanoparticles to give more complex structures. In the following sections some of these important aspects are reviewed.

1.2 Synthesis of Metal Nanoparticles

Nanoparticle synthesis in general is achieved either by a top-down approach or by a bottom-up strategy [Pachón 2008]. Chiseling of macro objects to nanosize is the core concept of top-down strategy and attrition or milling is a typical top-down method to make nanoparticles [Cao 2008]. Other methods for the synthesis of nanoparticles include redox surface techniques, thermal and photochemical decomposition of metal complex precursors, sonochemical methods and laser ablation [Micheaud 1998; Angel 2000; Navaladian 2007; Allmond 2007; Song 2007].

Among others, the biggest problem with top-down approach is the imperfection of the surface structure. It is well known that the conventional top-down techniques such as lithography can cause significant crystallographic damage to the processed patterns [Temperley 1952] and additional defects may be introduced even during the etching steps [Burton 1949]. Such imperfections would have a significant impact on physical properties and surface chemistry of nanostructures and nanomaterials, since the surface to volume ratio in nanostructures and nanomaterials is very large.

The bottom-up approach involves building the nanoparticles through an atom by atom approach. Chemical reduction of metal ions to give metal nanoparticles is one of the most frequently used techniques in

this category. The commonly used wet chemical reduction method for the synthesis of nanoparticles was discovered by Michael Faraday about 150 years ago [Faraday 1857]. Later, Turkevich *et al.* [Turkevich 1951; Turkevich 1970] reported the first reproducible synthesis of gold nanoparticles by the citrate reduction of Au(III) ions and proposed a 3 step mechanism consisting of nucleation, growth and agglomeration for nanoparticle formation [Gröschel 2004]. In the chemical reduction method, the precursor metal ion is reduced to form the zero-valent metal atoms. These atoms, owing to their high surface energy, will undergo aggregation leading to the formation of nano clusters. But, if the growth of the particles is not arrested at this stage the growth process will continue which would eventually lead to the precipitation of the metal. In order to arrest the growth of nanoparticles, stabilizers are added during the synthesis. Stabilizers used for this purpose can provide protection for nanoparticles against aggregation in three ways.

1.2.1 Electrostatic Stabilization

When a nanoparticle is formed in a polar solvent or in an electrolyte solution, a surface charge will be developed due to reasons such as (1) preferential adsorption of ions, (2) dissociation of surface charged species, (3) isomorphic substitution of ions, (4) accumulation or depletion of electrons at the surface and (5) physical adsorption of charged species on to the surface. Since all the particles are having the same type of charges the electrostatic repulsion between the charges on different nano clusters will protect them against aggregation as shown in Figure 1.1. This type of

stabilization is weak and mostly present in liquid phase only. The advent of ionic liquids for stabilizing nanoparticles increased the scope of this approach [Dupont 2002].

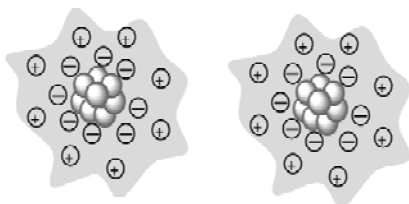


Figure 1.1 Electrostatic stabilization of nanoparticles.

1.2.2 Steric Stabilization

Steric stabilization involves the protection of nanoparticles against aggregation by way of protecting their surfaces using polymers or sterically crowded molecules like dendrimers [Astruc 2005]. The steric hindrance provided by the surface covered polymer prevents the aggregation of nanoparticles into bigger particles as shown in Figure 1.2, which illustrate the stabilization of Pd nanoparticles by a block copolymer [Fink 1998]. As the stabilizing ligand covers the nanoparticle surface almost completely, effective use of surface properties of the nanoparticle will become difficult in these types of assemblies. For example, if the nanoparticle is intended for use as catalyst, then the nanoparticle surface should be accessible to the reactants. Protection of the surface with polymers would restrict the approach of reactants to the surface.

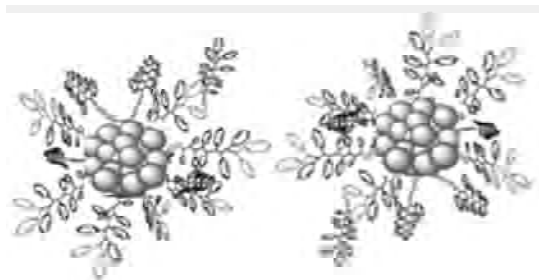


Figure 1.2 Stabilization of nanoparticles using sterically crowded ligands.

1.2.3 Electrosteric Stabilization

This mode of stabilization involves wrapping the surface of nanoparticles with polymer stabilizers bearing charged groups. The polymer support will provide a steric hindrance whereas the charged functional groups like sulphonate present on the polymer chain will form an electrical barrier against aggregation. Different polyelectrolyte block copolymers like poly(alkylmethacrylate-*b*-sulfonated glycidylmethacrylate), poly(ethylene-*b*-styrenesulfonate) are examples of ligands which provide stabilization for the nanoparticles through electrosteric passivation [Leemans 1991]. A schematic representation of electrosteric stabilization is shown in Figure 1.3.

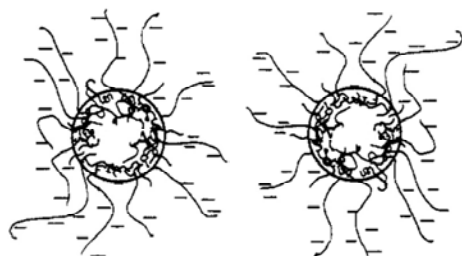


Figure 1.3 Nanoparticles stabilized through electrosteric stabilization.

Even though the use of stabilizers cannot be avoided in nanoparticle synthesis, their presence on the metal surface can hinder the

effective use of surface properties of nanoparticles. For example, large number of metal nanoparticles is prepared for catalytic applications. The catalytic activity of nanoparticles would depend on the free area available on the surface which is inversely related to the number of stabilizing ligands attached on to the surface. Thus it is essential to find a balance between the number of ligands attached on to the particle surface and the free surface area available for catalytic activity. There has been extensive research in this area to identify the best suited ligand which provides maximum protection against particle aggregation with minimum occupancy on the nanoparticle surface. Dendrimers are a class of molecules that has been extensively investigated in this context. The three dimensional topologies attained by dendrimer stabilizers are expected to prevent the nanoparticles from possible aggregation and also provide ample free metal surface enabling their use as catalyst for several applications. A brief description of dendrimers and their use as protecting ligands is provided in the following section.

1.3 Dendrimers

The word dendrimer, first used by Tomalia *et al.* in 1980s, came from the Greek words *dendri* (tree-branch-like) and *meros* (part-of). Dendrimers are large, complex, nearly perfect monodisperse macromolecules with a regular and highly branching three dimensional architecture [Tomalia 1990; Fréchet 2001; Grayson 2001]. A schematic representation of the structure of a dendrimer is given in Figure 1.4.

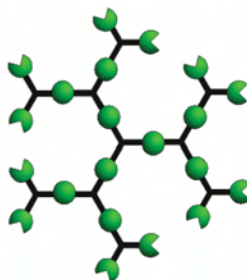


Figure 1.4 Schematic representation of a dendrimer.

The structure of a typical dendrimer is featured by three distinct parts namely, (i) the core unit or focal point, which controls the directionality of the dendrimer, (ii) the branching units, which determines the generation number and size of the molecule, and (iii) the peripheral groups upon which the solubility of the unit as a whole depends. The peripheral crowding also controls the access of guest molecules towards the interior of the dendrimer [Tomalia 2005]. Pictorial representation of a dendrimer showing the different parts is given in Figure 1.5.

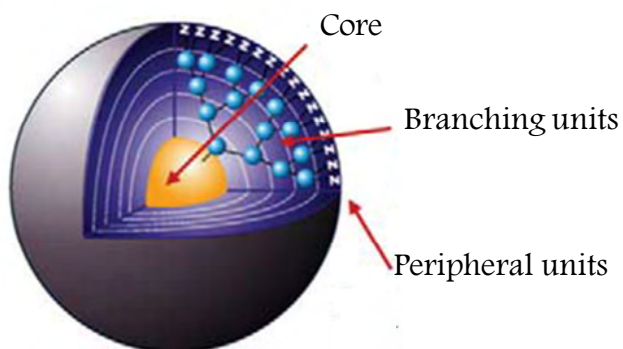


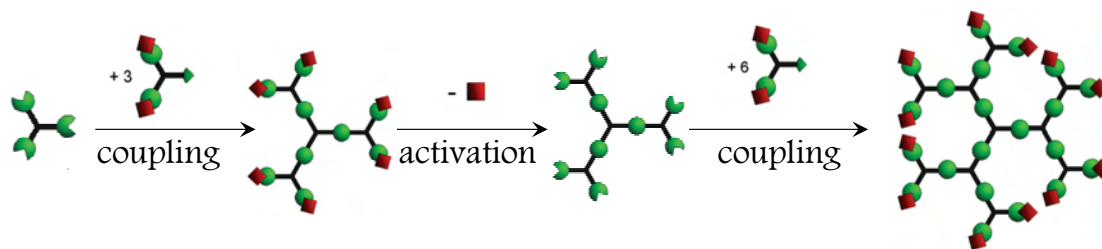
Figure 1.5 Different parts of a dendritic structure.

1.3.1 Synthesis of Dendrimers

The synthesis of dendrimers can be done either starting from the core towards the periphery or vice versa. Depending upon the direction of building up of these macromolecules, two synthetic approaches are generally observed.

1.3.1.1 Divergent synthesis

The divergent approach of dendrimer synthesis was reported by the groups of Tomalia [Tomalia 1985; Fréchet 2001] and Newkome [1985]. In this approach, growth will start from the structural unit which will become the core of the dendrimer, and the growth will repeat outwards to the periphery. Reaction of a multifunctional core with monomer units leads to the formation of the next higher generation dendrimer with increased number of peripheral functionalities. These new surface groups upon activation (usually by the conversion to a reactive functionality) followed by coupling with monomers result in the progression of the dendrimer generation as shown in Scheme 1.2.

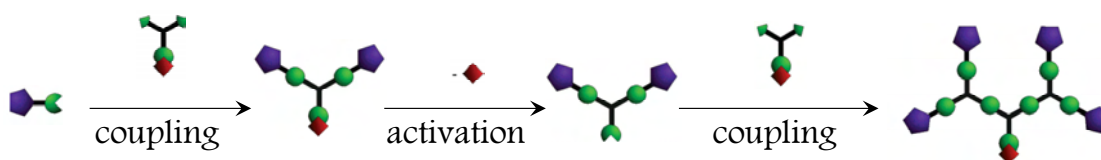


Scheme 1.2 Divergent synthesis of dendrimers.

Examples of dendrimers synthesized by the divergent route include poly(amidoamine) and poly(propyleneimine) dendrimers [Fréchet 2001]. As we go from one generation to the next higher generation, the number of terminal groups doubles. When the number of terminal groups is very large, chances of complete coupling of monomers with the terminal reactive groups become less, leading to the formation of defective dendrimers.

1.3.1.2 Convergent synthesis

This method was introduced by Hawker and Fréchet in 1990 [Hawker 1990 (a)] and in this methodology, the synthesis will start from the periphery and move towards the core. The molecule which will become the terminal group of the dendrimer will react with a multifunctional spacer molecule. This will then undergo activation followed by coupling sequentially to result in the formation of the dendrimer structure [Hawker 1990]. A schematic representation of the convergent synthetic sequence is given in Scheme 1.3.



Scheme 1.3 Convergent approach for dendrimer synthesis.

As the number of reaction at each coupling stage is limited, the dendrimers synthesized through this approach will be free from defects arising due to incomplete reactions as with the case of divergent approach. But, the presence of the reactive functionality at the focal point of the growing dendron makes it difficult for preparing higher generation dendrons due to steric reasons. Most important examples of dendrimers synthesized through this approach are the poly(arylether) dendrimers.

1.3.2 Dendrimers as Nanoparticle-Protecting Agents

Dendrimer-protected nanoparticles are of two types, (1) Dendrimer encapsulated nanoparticles (DEN) and (2) Nanoparticle-cored dendrimers

(NCD). Detailed description of these systems is given in the following sections.

1.3.2.1 Dendrimer Encapsulated Nanoparticles (DEN)

Dendrimer encapsulated nanoparticles are nanocomposites of dendrimer and metal nanoparticles where the passivation of metal particles against aggregation is achieved through encapsulation of the nanoparticles by a higher generation dendrimer. This encapsulation need not involve a direct bonding interaction between the nanoparticle and dendrimer. After the pioneering efforts by the groups of Crooks [Zhao 1998], Tomalia [Balogh 1998], and Esumi [Esumi 1998], the field of dendrimer encapsulated nanoparticles has been well established especially in the field of catalysis.

Synthesis of DENs makes use of the ability of metal ions to form localized domains inside a dendrimer which can be subsequently reduced to zero valent metal nanostructures. Typical synthesis of DEN involves 2 steps, via, sorption of the metal ions into the interior of the dendrimer followed by the reduction of the encapsulated metal ions into metal nanoparticles. The PAMAM or PPI dendrimers (Figure 1.6) are most suited for these applications mainly because of the presence of amino groups which can assist the initial sorption of metal ions and also because of their commercial availability.

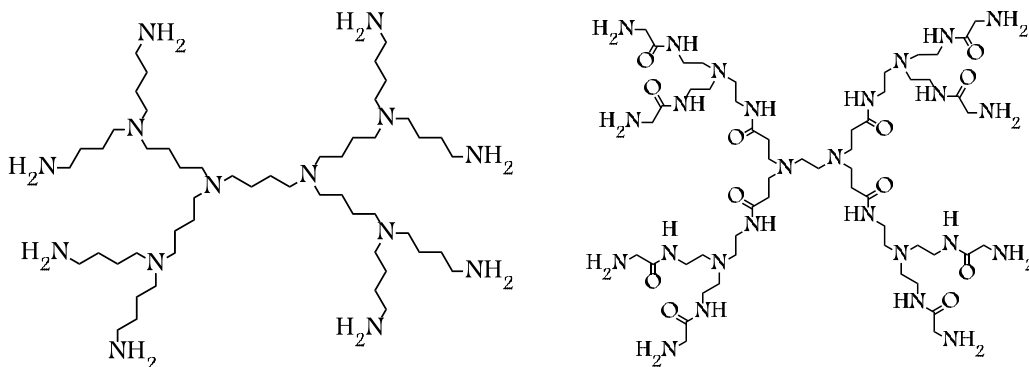
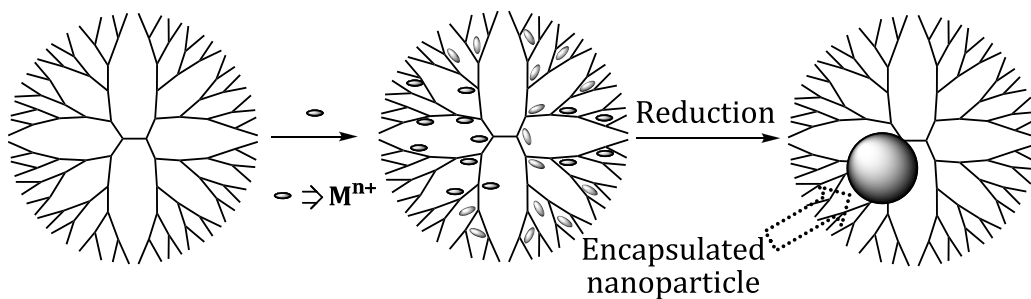


Figure 1.6 First generation poly(propyleneimine) (PPI) and poly(amidoamine) (PAMAM) dendrimers.

Initial uptake of the metal ions into the dendrimer is mainly achieved through the electrostatic gradient presented by electroactive groups such as amino or amide, present in the dendrimer back bone. For instance, in the case of PAMAM dendrimers, two types of amino groups are present, the more basic surface primary amines and the less basic interior tertiary amines. Hence, tuning the pH of the solution will selectively protonate the labile surface amines thereby making the metal ions to flow towards the interior tertiary amines which will remain unprotonated under the used set of conditions. A general scheme for the formation of DEN is shown in Scheme 1.4 [Crooks 2001; Niu 2003; Scott 2005]



Scheme 1.4 Scheme for the synthesis of dendrimer encapsulated metal nanoparticles.

Copper (II) was the first metal ion used for the synthesis of DEN, because of the easiness of following the reaction through UV-visible and ESR spectroscopy. Figure 1.7 shows the absorption spectrum of Cu(II) in the absence of PAMAM dendrimer which is featured by the presence of a weak broad absorption around 800 nm, corresponding to the $d-d$ transition (spectrum 1 in Figure 1.7). Upon addition of the dendrimer, absorption maximum of the $d-d$ transition shifts towards 605 nm (spectrum 2 in Figure 1.7) and a new peak emerges at 300 nm, corresponding to the ligand-to-metal charge-transfer transition (LMCT).

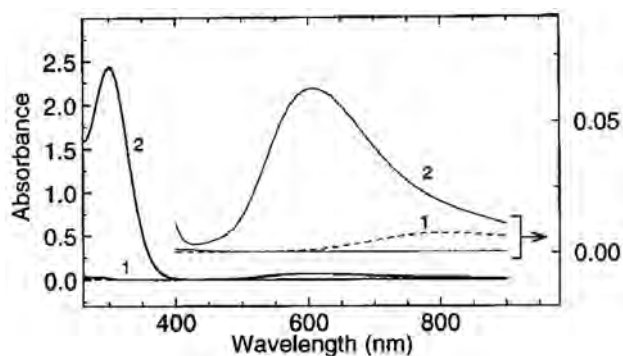


Figure 1.7 UV-Visible absorption spectra of aqueous solution of Cu(II) before (1) and after (2) the addition of G₄ PAMAM dendrimer.

Reduction of Cu(II)-dendrimer complex using NaBH₄ resulted in the formation of copper nano clusters, evidenced by the disappearance of the absorption bands at 605 and 300 nm with the simultaneous formation of a monotonically increasing absorption profile with an exponential shape towards shorter wavelength (Figure 1.8). This was associated with a visible change in the colour of the solution from blue to golden brown. The metal cluster so formed was found to be stable for one week under oxygen

free conditions, but in presence of oxygen, Cu(0) was immediately oxidized to Cu(II).

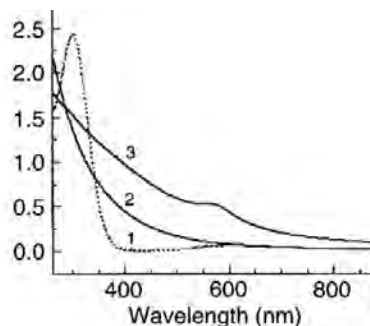
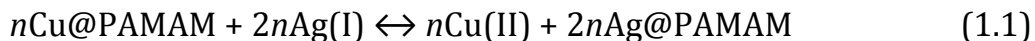


Figure 1.8 Absorption changes during the reduction of PAMAM-entrapped Cu(II) at different time intervals (1-3).

The most important condition for the formation of dendrimer encapsulated nanoparticles by direct reduction method is the initial extraction of metal ions into the dendrimer interior and hence this method is limited to metal ions capable of direct interaction with the dendrimer frame work. For those metal ions which have weak or no interaction with the dendrimer, the metal-displacement method is preferred. Crooks and co-workers [Zhao 1999 (b)] have used this method to synthesize silver nanoparticles inside G₆-PAMAM dendrimers. Ag(I) did not exhibit strong interaction with the PAMAM dendrimer. The authors observed that G₆-PAMAM dendrimer encapsulated Cu nanoparticles (Cu@PAMAM) can react with Ag(I) ions according to equation 1.1.



The silver nanoparticles thus formed are encapsulated inside the PAMAM dendrimer. Spectral evidence for the exchange process was obtained by UV-Vis spectroscopy and this is shown in Figure 1.9. Spectrum 1 corresponds to the absorption of Cu@PAMAM. Upon adding Ag(I), a new

peak centered around 400 nm emerges, which corresponds to the plasmon resonance of silver nanoparticles. Intensity of the Ag plasmon absorption was found to increase with time (spectra 2-4) indicating the progressive formation of Ag nanoparticles at the expense of Cu nanoparticles.

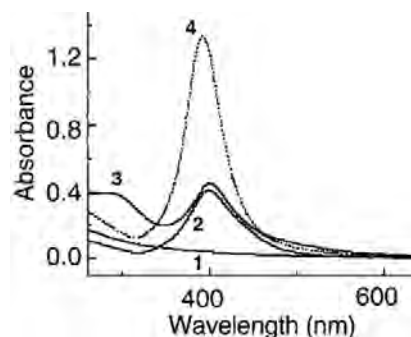
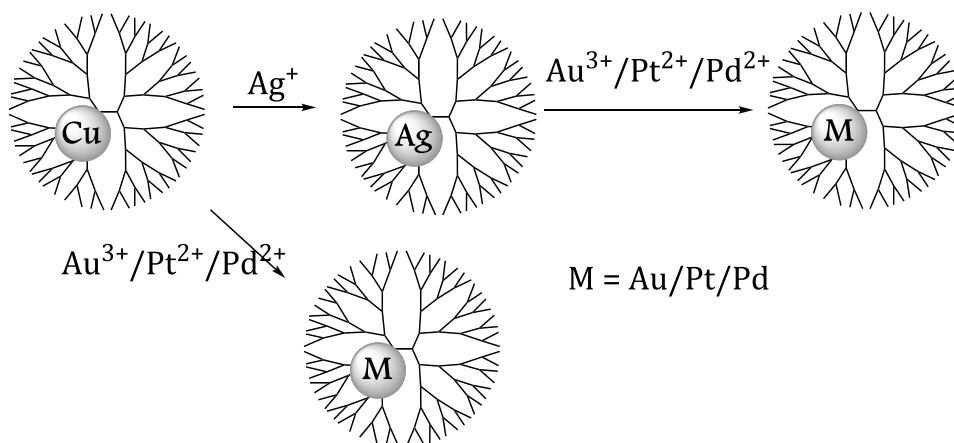


Figure 1.9 Absorption changes during the addition of Ag(I) into a solution of G₆-PAMAM dendrimer encapsulated copper nanoparticles.

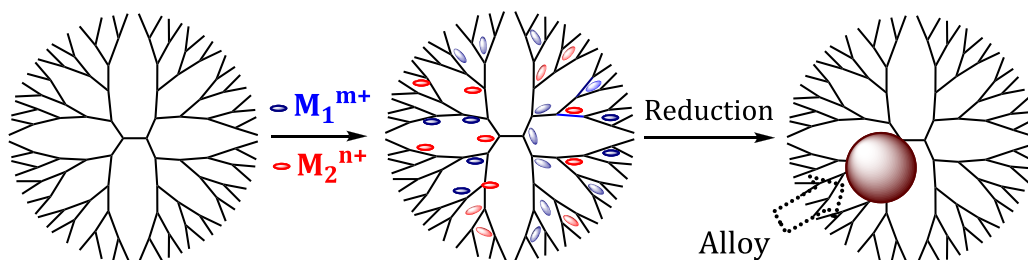
The metal-displacement method was found to be effective for the synthesis of other noble metal nanoparticles such as Au, Pt and Pd inside PAMAM dendrimers as the standard potential (E°) of the corresponding half reactions for these metals are more positive than that of Cu(II)/Cu couple. This is shown in Scheme 1.5.



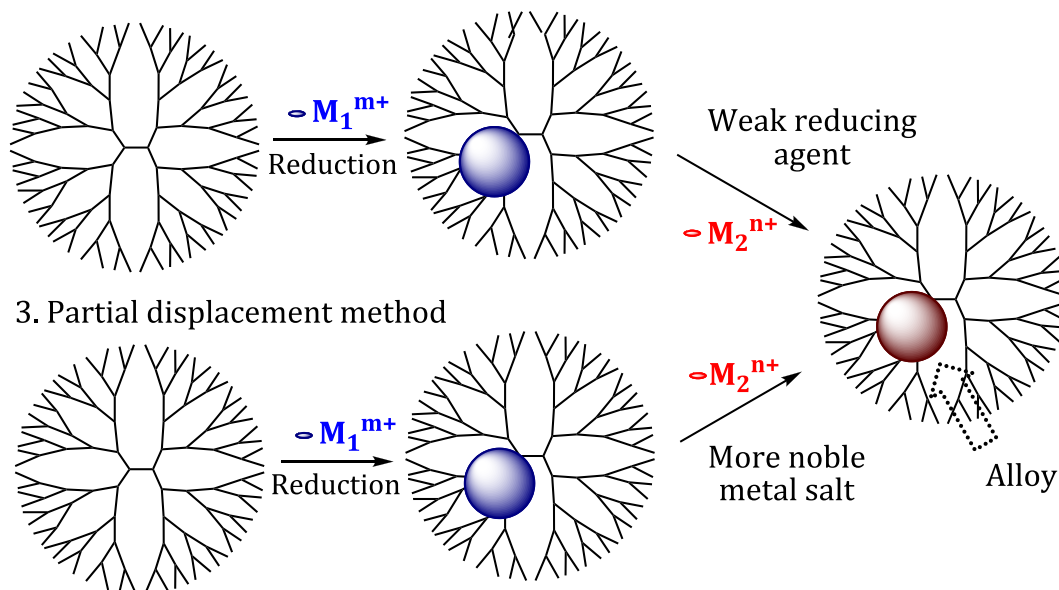
Scheme 1.5 Synthesis of DENs of noble metals through metal-displacement reactions.

Dendrimer encapsulated bi-metallic nanoparticles (alloy nanoparticles) were also synthesized by Crooks and co-workers [Scott 2003]. The different approaches employed are shown in scheme 1.6. In the co-complexation approach, both metal ions are simultaneously loaded inside the dendrimer and reduced, whereas in the sequential method a step-wise loading and reduction approach is used. In the partial displacement method which is a modification of the complete displacement approach, an initially formed DEN is allowed to react with less than stoichiometric amounts of the more reducible metal ion [Chung 2003 (a); Scott 2003; Li 2008; Myers 2009].

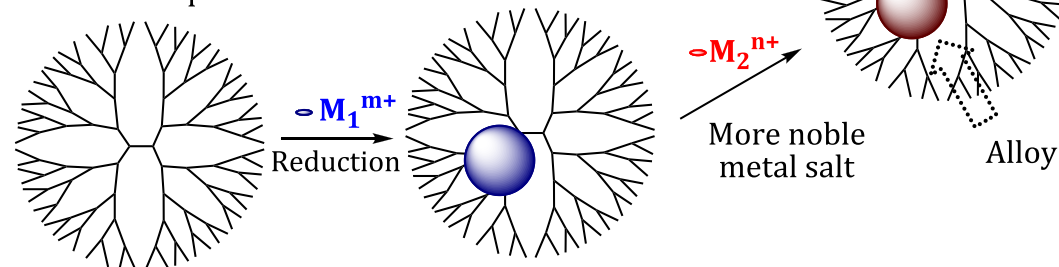
1. Co-complexation method



2. Sequential method



3. Partial displacement method

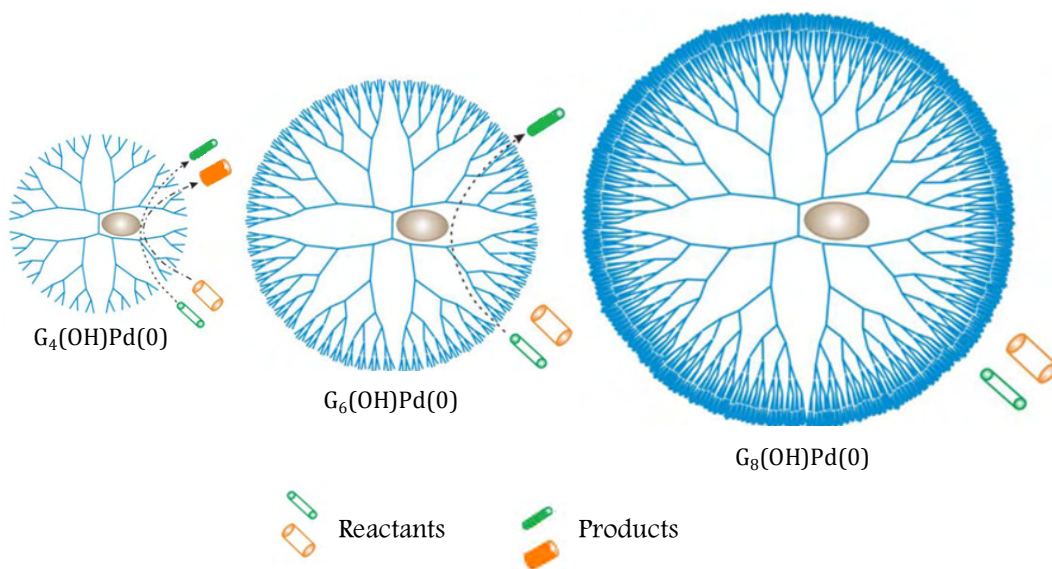


Scheme 1.6 Different approaches for the synthesis of bimetallic DENs.

The most important application of DENs is in the field of catalysis, owing to the following reasons. Besides controlling the solubility of the DEN for homogenous catalysis, the dendrimer back bone can act as handle for immobilization of the metal nanoparticle for heterogeneous catalysis. Since the nanoparticle surface is not completely passivated, the vacant metal surface can act as active site for catalysis. Also, the dendrimer frame work can provide substrate/product selectivity in the reaction owing to steric crowding. The use of DEN for hydrogenation and C-C bond forming reactions under different conditions has been extensively studied [Zhao 1999 (a); Rahim 2001]. DENs also found application as heterogeneous electrocatalysts for the reduction of oxygen [Chung 2003 (b)]. The metal nanoparticle in DEN can be effectively transferred onto solid supports and the resulting supported catalysts, which do not contain dendrimer also finds application as hydrogenation catalysts [Huang 2008].

The substrate size selectivity of DEN for hydrogenation reactions has been established by Crooks and coworkers [Niu 2001]. According to them lower generation dendrimers are open structures and allow smaller and larger substrates to penetrate into the interior of the dendrimer and have contact with the encapsulated nanoparticles. As the dendrimer generation increases the steric congestion at the surface increases and hence only smaller substrates would be allowed to access the nanoparticles. When the generation number is very high even smaller substrates are not able to penetrate the surface layer (Scheme 1.7). Since the catalytic activity depends on the interaction between the substrate

and nanoparticles, no catalytic activity would be observed if the substrate fails to penetrate into the dendritic interior where the nanoparticles reside. This suggests that nanoparticles encapsulated in smaller generation dendrimers would exhibit more catalytic activity. This conclusion is also supported by the fact that the statistical average of the number of encounters between the substrate and catalyst will be more for smaller substrates and lower generation dendrimers when compared to a nanoparticle enclosed in a bigger dendrimer. Ooe *et al.* [2002] also reported similar selectivities based on substrate size for PPI dendrimer encapsulated Pd nanoparticles.



Scheme 1.7 Size selective catalysis using DEN.

The use of Pd DENs for Heck reaction was first reported by Crooks and co-workers [Yeung 2001]. Even though the reaction yield was low, this was the first attempt towards the use of DEN for catalyzing C-C bond forming reactions. Yamamoto and co-workers described the synthesis of dendrimer encapsulated Rh nanoparticles and demonstrated their use as hydrogenation catalysts for substituted alkenes and aromatic nitro

compounds [Nakamura 2008]. Astruc and co-workers reported the synthesis of dendrimer stabilized palladium nanoparticles through click chemistry and demonstrated its use as catalyst for Suzuki reaction under ambient conditions with as little as 1 ppm of the nanoparticle [Diallo 2007].

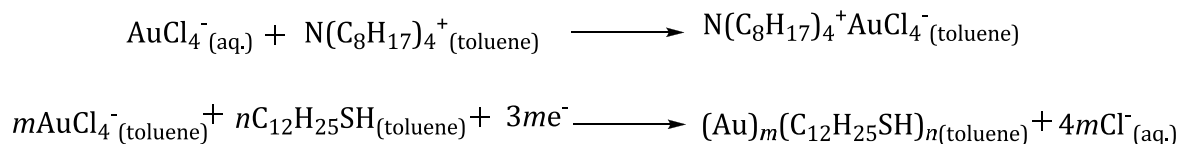
The ease of separation of catalyst from products and reactants makes heterogeneous catalysis always attractive, especially in industrial processes. But the common heterogeneous catalysts supported on alumina, silica or highly cross linked polymer supports are not very highly active, owing to the extensive surface passivation of the metal nanoparticle by the supports. Heterogeneous catalysts can be prepared using DENs by immobilizing the dendrimer template onto a solid support. Surface modification can be made out either by direct adsorption of DENs or by the initial adsorption of an empty dendrimer followed by the encapsulation of nanoparticles. Removal of the dendrimer after immobilization is also possible, but sometimes this may lead to the aggregation of nanoparticles. Crooks and co-workers have reported the grafting of Pt/Pd DEN on a gold surface, where the amine terminated DEN was reacted with mercaptoundecanoic acid self-assembled monolayer on gold surfaces and studied their electrocatalytic activity for oxygen reduction [Ye 2004].

1.3.2.2 Nanoparticle-Cored Dendrimers (NCDs)

Nanoparticle-cored dendrimers are organic-inorganic hybrid core-shell nanostructures, where a metal particle core is surrounded by

dendrons connected radially to the core. Even though both NCD and DEN are dendrimer-metal nanocomposites, the major difference between them is that in the former, the metal nanoparticle is stabilized against aggregation through weak, indirect encapsulating interactions whereas for the latter stabilization is through direct bonding interactions between the metal nanoparticle and the dendrons. This direct bonding between the metal nanoparticle and the dendrons makes NCDs superior to DENs in terms of stability. This thesis deals with the synthesis, characterization and application oriented studies of a new class of NCD. In order to put our work in the proper perspective a detailed description of the work done in this area is provided herein [Shon 2007].

The two-phase synthesis of monolayer protected clusters (MPC) of gold reported by Brust and co-workers [1994] was a breakthrough in the synthesis of metal nanoparticles. In the first step of the synthesis, a Au(III) salt is phase transferred from aqueous to organic layer with the aid of a phase transfer catalyst such as tetra-*n*-octylammonium bromide (TOAB). The phase transferred Au(III) was then reduced using NaBH₄ in the presence of an alkanethiol. During the reaction Au(III) ions are reduced to gold atoms which undergo nucleation and growth leading to the formation of clusters of gold atoms. The alkanethiols get attached to the growing gold clusters leading to formation of SAM as shown in Scheme 1.8.



Scheme 1.8

Kim and co-workers [2001] reported the synthesis of thiol terminated Fréchet type dendron capped gold nanoparticles by adopting the Brust procedure. Structure of the thiol capped G₃ poly(arylether) dendron used in the study is given in Figure 1.10.

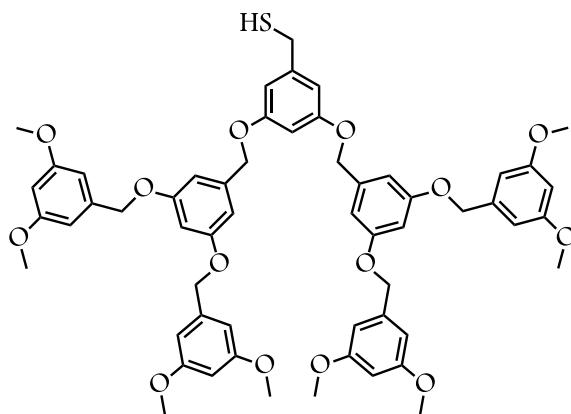


Figure 1.10

The NCDs formed were characterized by absorption spectroscopy as well as TEM analysis and they found that the ‘dendronized nanoparticles’ are more stable than the corresponding alkyl chain protected nanoparticles. The authors claimed formation of nearly monodisperse gold nanoparticles especially when G₂ dendron was employed as the ligand.

Torigoe and co-workers [Nakao 2002] reported the synthesis of gold-dendron nanocomposites by reacting first four generations of poly(oxymethylphenylene) (PPD) dendrons with a thiol group at the focal point with gold using the Brust method of MPC synthesis. Figure 1.11 shows the structure of the third generation dendron used as the capping ligand. The nanocomposites obtained did not show any characteristic surface plasmon absorption band. The TEM analysis, however, indicated the formation of one dimensional array of Au nanoparticles. The authors

projected potential use of this one dimensional array in nanoelectronic applications. It is to be mentioned that the reports of Kim *et al.* and Torigoe *et al.* did not attempt detailed structural characterization of the synthesized materials.

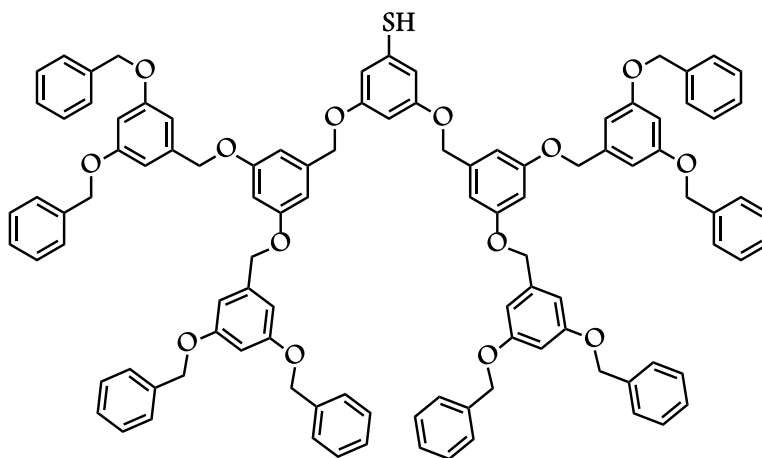
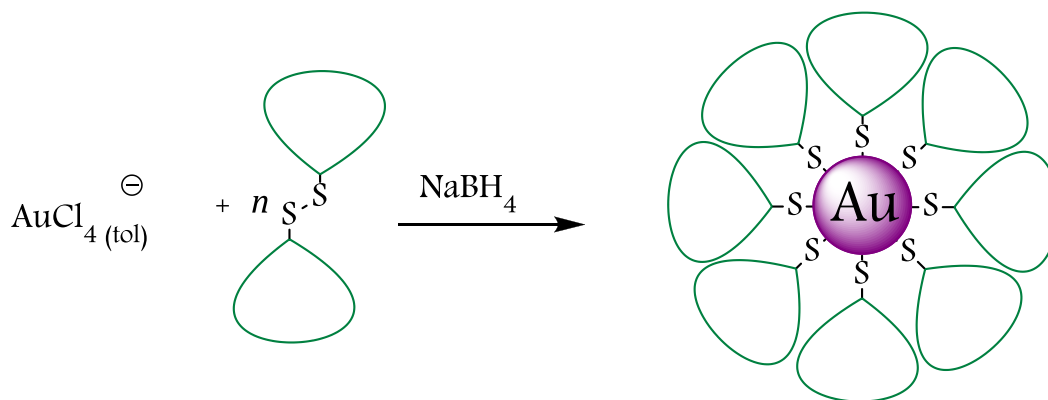


Figure 1.11 Structure of the third generation dendron thiol used in Torigoe's work.

The first systematic investigation of the synthesis and characterization of NCDs has been carried out by Fox and co-workers in 2003 [Gopidas 2003 (a)]. Instead of the alkanethiol used in the Brust synthesis, the authors employed dendron disulfides, prepared by the reaction of hexamethyldisilathiane and tetrabutylammonium fluoride with different generation Fréchet type dendritic bromides. Reduction of the phase transferred Au(III) in presence of the corresponding dendritic thiol yielded different generation gold nanoparticle-cored Fréchet dendrimers. Schematic representation of the formation of NCDs is given in Scheme 1.9.



Scheme 1.9 Synthesis of Au-NCDs using modified Brust procedure.

Structure of the fourth generation dendron disulfide employed in the study is shown in Figure 1.12.

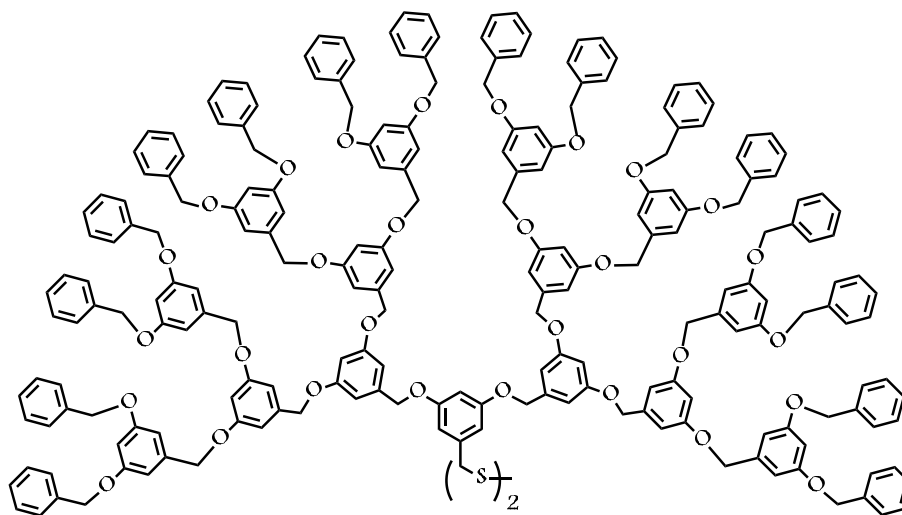


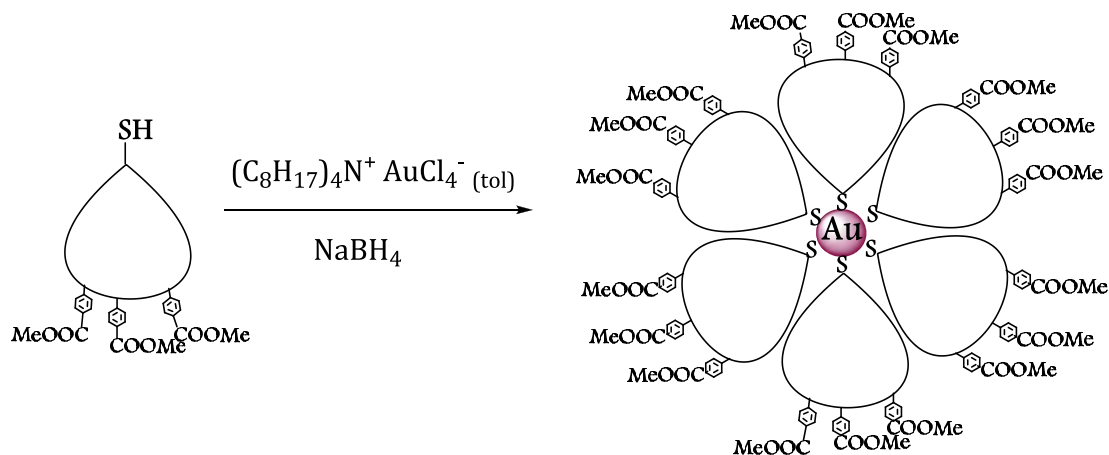
Figure 1.12 Structure of the fourth generation dendron disulfide used for the synthesis of Au-NCDs.

The authors have carried out several control experiments to show that the dendrons are chemically bonded to the gold cluster. For example, the Brust reaction was performed using G₁-G₅ dendritic bromides instead of the disulfides. The nanoparticles obtained in these experiments were unstable which agglomerated within 5 – 10 minutes, clearly indicating the

absence of a direct bonding interaction with the metal particle in the control experiments.

Formation of unstable nanoparticles in the control experiments enabled the authors to draw some conclusions regarding the course of the reaction. For larger dendritic disulfides, the sulfide group is a very small functionality when compared to the bulky arylether part and these groups are expected to react slowly with the growing metal nanoparticles. The authors explained the absence of any precipitation of the metal in terms of an initial encapsulation of the growing gold cluster within the cavities of the dendritic disulfide. The initially formed, small, TOAB stabilized gold cluster migrates into the cavities formed by the dendrons and there it finds the disulfide group with which it reacts in a very slow process. In this respect the disulfides are expected to function better than the thiols as the disulfide contains two dendritic wedges, it can form a better cavity for encapsulation along with the formation of two Au-S bonds simultaneously. During the control experiments, the encapsulation might have assisted the initial formation of nanoparticles, but further stabilization cannot be provided as the disulfide groups were absent, leading to the precipitation of the metal particles. Based on these results, the authors have formulated a four step mechanism for the formation of NCDs which include nucleation, growth, encapsulation and passivation rather than the three step Brust protocol where the encapsulation process is absent. Assuming a spherical geometry for the metal particles, the authors have calculated the number of dendrons attached to unit surface area of the gold core and it was found that the number of dendrons per

square nanometer decreases steadily with increase in dendron generation. For all NCDs reported, the occupancy per square nanometer is much lower ($0.2 - 2.0 \text{ nm}^{-2}$) than those reported for alkanethiolate (4.7 nm^{-2}) and arenethiolate ($5 - 9 \text{ nm}^{-2}$) protected MPCs. This proves the presence of large vacant metal surface available in the case of NCDs when compared to other MPCs. Later the same group has successfully synthesized water soluble NCDs, where the Fréchet type dendron wedges were decorated with peripheral carboxylate moieties as shown in Scheme 1.10 [Gopidas 2003 (b)]. Catalytically active Pd-NCDs were also synthesized in a similar manner by reducing Pd(II) in presence of thiol functionalized third generation Fréchet dendron [Gopidas 2003 (c)].



Scheme 1.10 Synthesis of Au-NCDs with peripheral ester groups.

Smith and co-workers reported the synthesis, characterization and thermal studies of gold nanoparticle-cored L-lysine based dendrimer [Love 2004]. They employed G_1 - G_3 L-lysine based dendritic disulfides (structure of G_3 disulfide is shown in Figure 1.13). Their studies showed a decrease in the size of the metal core with increase in dendron generation.

They observed a growth of the metal core upon heating the NCD in DMF, as evidenced from the increase in intensity of the surface plasmon band upon heating. Their studies showed a lower rate of particle growth for the G_3 Au whereas G_1 Au has the maximum growth rate but was lower than that of the butane thiol capped gold nanoparticles. This was explained on the basis of thick packing provided by the extensive branching present in higher generation dendrons leading to lower ripening rate.

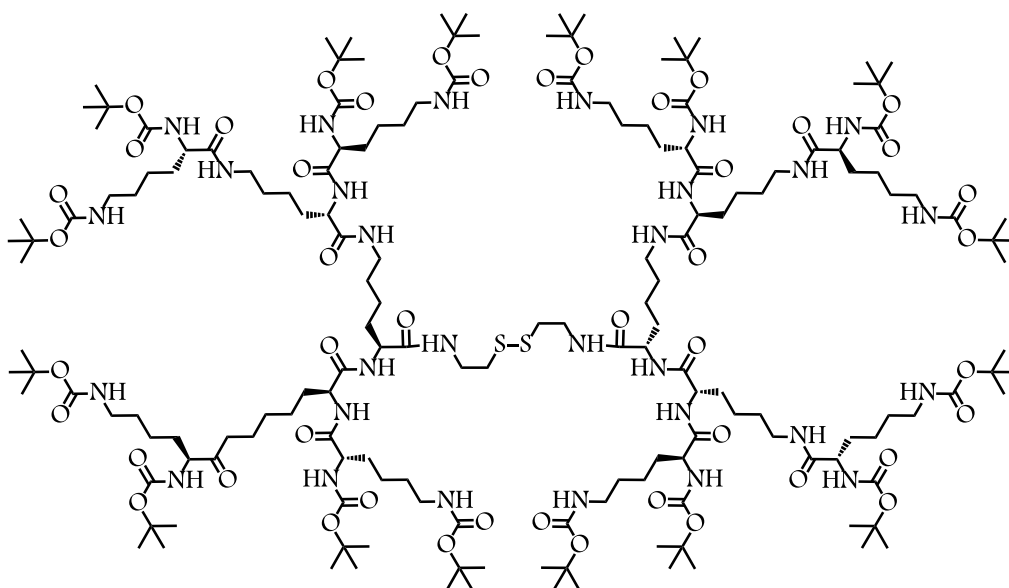


Figure 1.13 L-Lysine based G_3 dendritic disulfide.

NCDs with peripheral phenothiazine units were reported by Fujihara and co-workers [Komine 2006]. Synthesis of the NCDs involved the Brust reaction, where the phenothiazine appended dendrons (Figure 1.14) with a thiol terminated long alkyl chain self-assembled on gold surface.

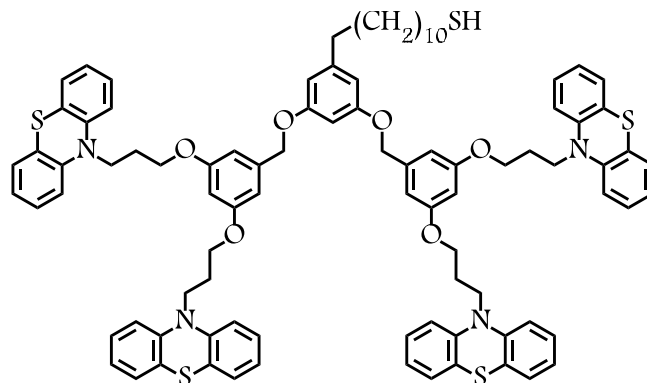


Figure 1.14 Structure of phenothiazine-terminated dendron used by Fujihara *et al.*

Zheng and co-workers reported the synthesis of gold NCDs with 4-pyridone functionalized dendrons as capping ligands (Figure 1.15) [Wang 2001]. In this case the dendrons are attached to the metal core through the weak metal-pyridone interaction. Consequently the higher generation NCDs of this group were unstable.

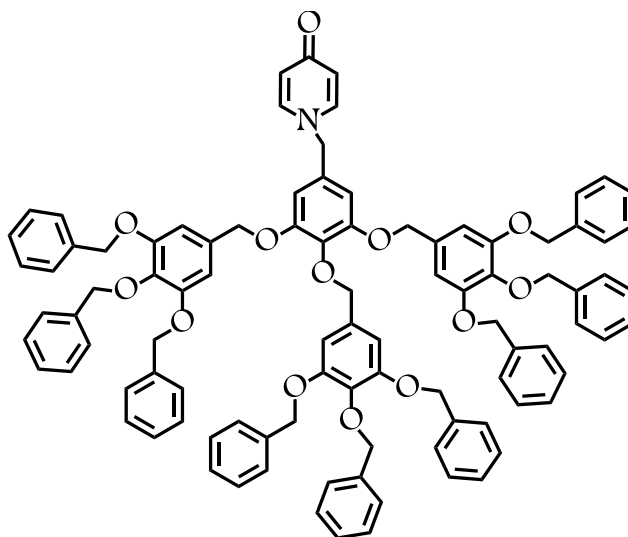
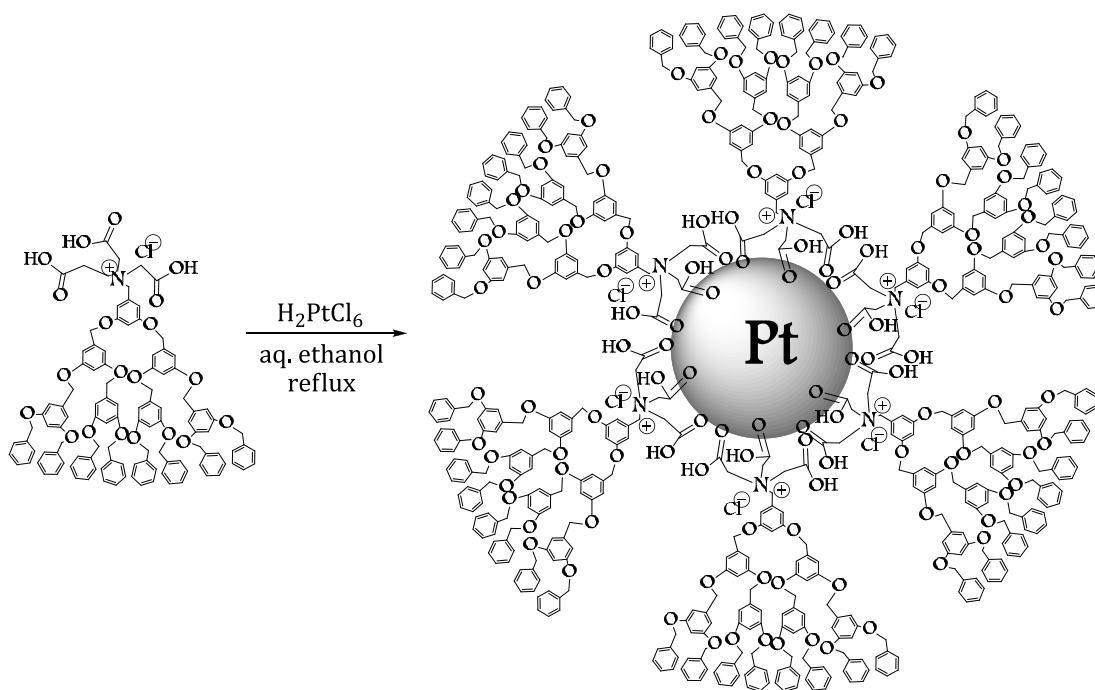


Figure 1.15 Structure of 4-pyridone functionalized dendron used by Zheng *et al.*

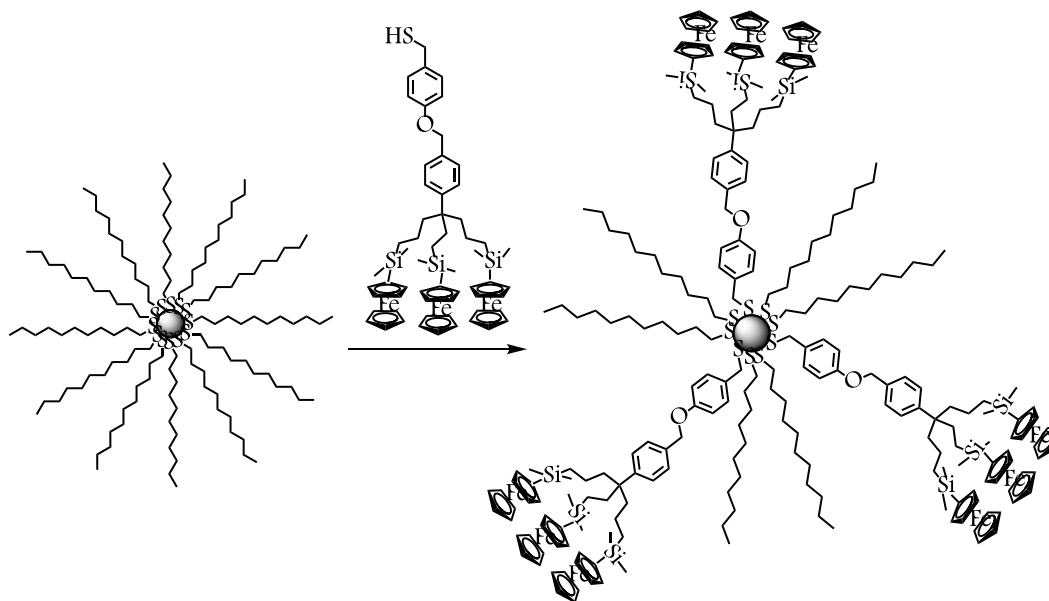
Jiang *et al.* [2004] reported the synthesis of catalytically active palladium NCDs using ester terminated dendrons. Yang and co-workers [2006] reported the synthesis of platinum NCDs with Fréchet type dendrons having trisacetic acid ammonium chloride units at the focal point (Scheme 1.11). The C=O stretching frequency of the carboxylic acid group shifts to lower wave numbers in the NCD, indicating formation of weak bonds between the dendron C=O groups and the metal core which stabilizes the NCD. The synthetic scheme is given in Scheme 1.11.



Scheme 1.11 Synthesis of Pt-NCDs using ester terminated dendrons.

NCDs can also be synthesized by ligand exchange reactions of alkanethiol protected metal nanoparticles with thiol terminated dendrons, where the incoming dendron ligands replace the alkanethiols on the metal surface. For example, Astruc and co-workers reported the ligand exchange

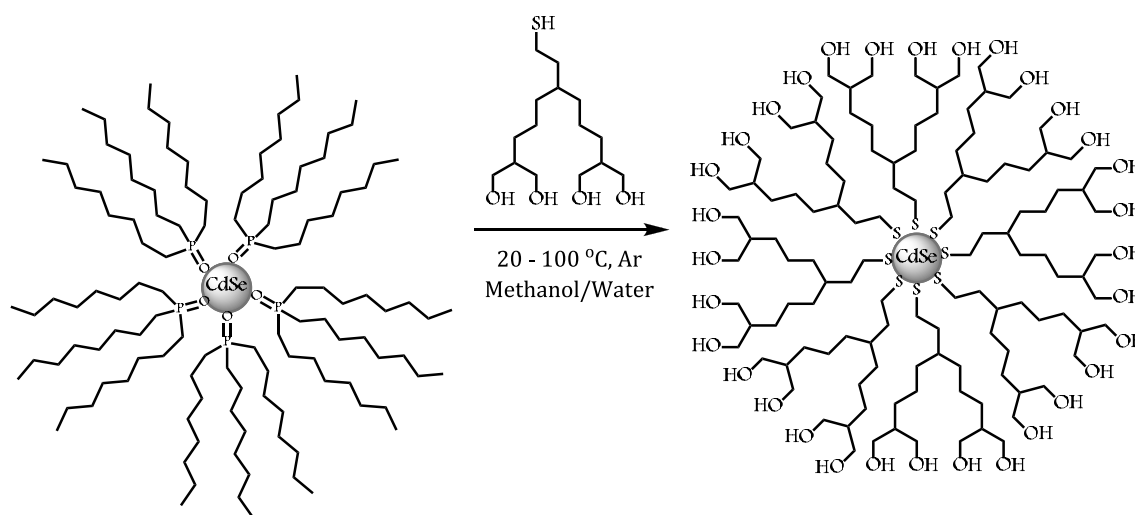
reaction of dodecanethiolate-protected gold nanoparticles with triferrocenyl thiol dendrons as shown in Scheme 1.12 [Daniel 2003].



Scheme 1.12 NCD synthesis through ligand exchange.

Complete exchange of the initially adsorbed alkanethiol is not possible by this method. In the above reaction the percentage of ligand exchange was less than 5 even in the presence of excess thiolated dendrons. In the case of higher generation dendrons, there was practically no exchange. This can be due to the lower rate of ligand exchange which in turn depends upon the chain length and steric bulk of the initial monolayer present on the nanoparticle surface. Hence this way of NCD synthesis is limited to lower generation dendrons only. Peng and co-workers showed that citrate capped gold nanoparticles can undergo ligand-exchange reaction with hydroxyl functionalized thiol dendrons to form hydrophilic gold NCDs [Wang 2002]. They were also successful in the ligand exchange of trioctylphosphine oxide (TOPO) capped CdSe

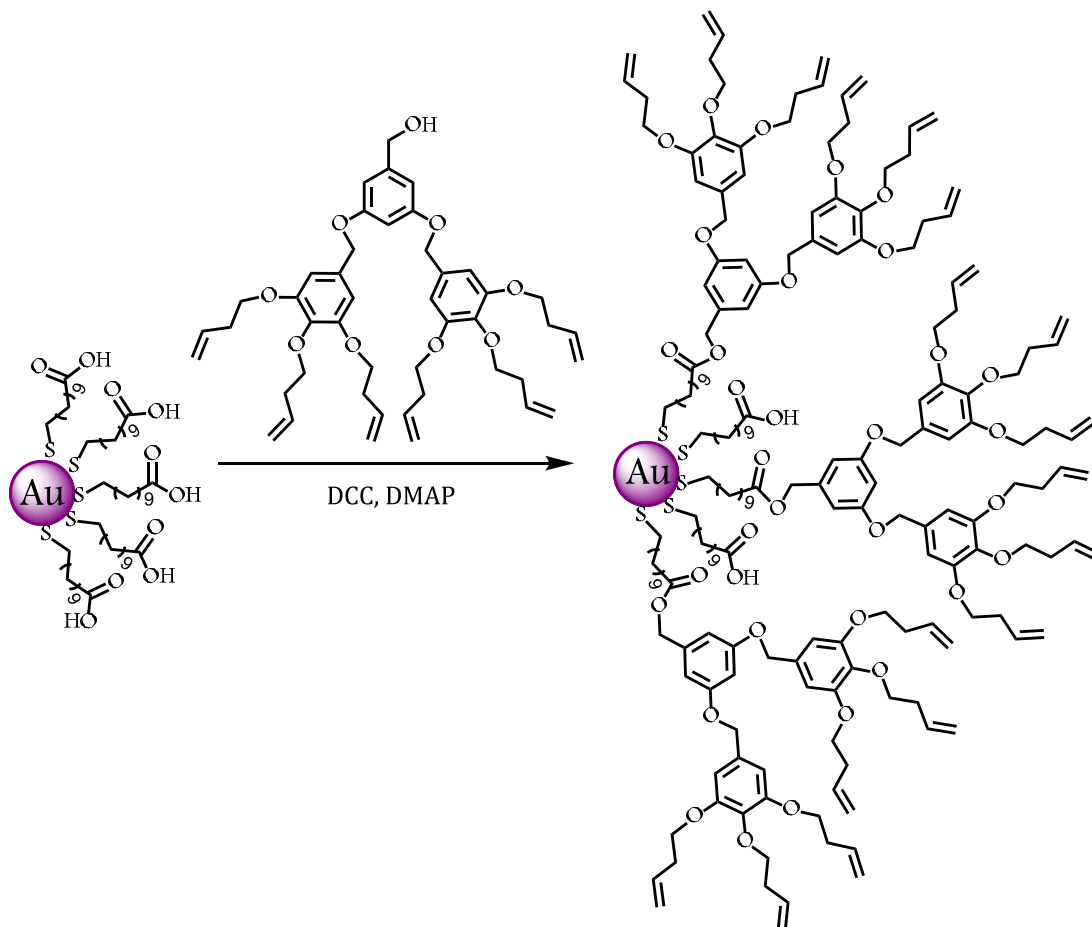
nanoparticles with the hydroxyl functionalized thiol dendrons as shown in Scheme 1.13 [Guo 2003]. The NCDs obtained in this way were found to be exceptionally stable compared to the corresponding alkanethiol protected nanoparticles.



Scheme 1.13 Synthesis of dendritic thiol capped CdSe through ligand exchange.

One major disadvantage of NCD synthesis through direct method is that it has little control over the nanoparticle size. One recent method, which is expected to overcome this difficulty, involves the synthesis of monolayer-protected nanoparticles followed by building the dendrimer architecture on the nanoparticle surface using either convergent or divergent approach. Scheme 1.14 shows the convergent synthesis of NCDs reported by Shon and co-workers accomplished by the ester coupling reaction of 11-mercaptoundecanoic acid functionalized gold nanoparticles with third generation poly(arylether) dendritic alcohol in the presence of 1,3-dicyclohexylcarbodiimide (DCC) and 4-dimethylaminopyridine

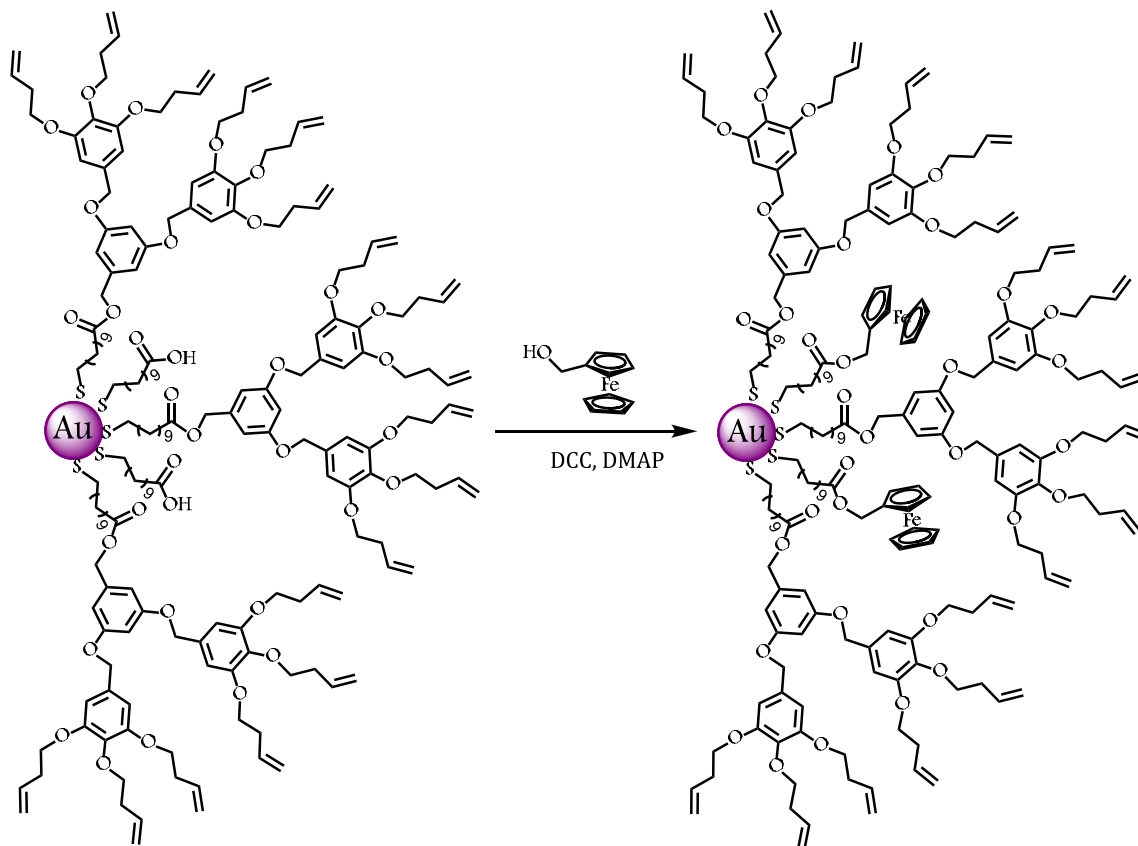
(DMAP). The resulting NCDs were characterized using FT-IR, NMR and TG studies which supported the presence of dendritic wedges on the nanoparticle surface [Choi 2005; Shon 2006; Cuttler 2007].



Scheme 1.14 NCD synthesis through secondary reaction on a self-assembled monolayer.

Shon *et al.* incorporated redox labels in the above NCDs through the coupling of ferrocene methanol molecules with the unreacted carboxylic acid groups present on the surface of the nanoparticle as shown in Scheme 1.15. Cyclic voltammetric studies of both ferrocene methanol and ferrocene incorporated NCDs exhibited well defined voltammetric peaks corresponding to the ferrocenyl groups. The peak splitting voltage of

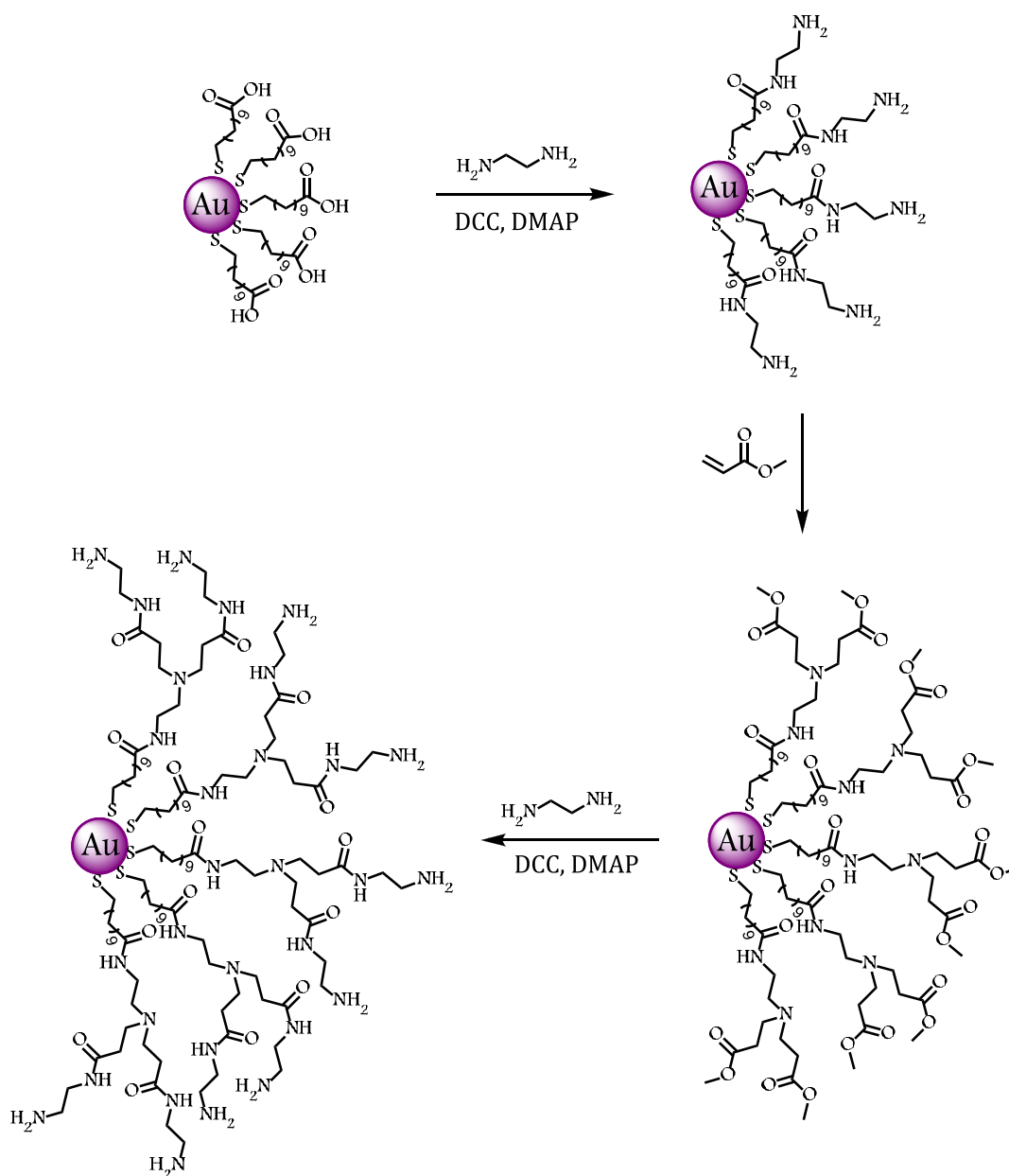
ferrocene incorporated NCD was found to be half of that of ferrocene methanol which can be due to either multi-electron transfer or adsorption of the particle to the electrode.



Scheme 1.15 Reaction of ferrocene methanol with the unreacted carboxylic acid groups attached to the metal core.

Jordan *et al.* [2001] described the synthesis of NCDs through a divergent route as shown in Scheme 1.16. Here the NCD was grown in a stepwise manner from a central nanoparticle involving the amide coupling reaction (with 1,2-diaminoethane in presence of 1,3-dicyclohexylcarbodiimide) and the Michael addition reaction of the terminal amines with methyl acrylate. All disadvantages associated with

the divergent dendrimer synthesis such as incomplete reactions at higher generations, long reaction times, poor selectivity along with need for excess reagents to force the reaction to completion etc. are also present in this NCD synthesis.



Scheme 1.16 Divergent synthesis of NCDs.

Almost all known applications of NCDs are in the area of catalysis and this requires unpassivated area of the metal surface. Alkanethiolate protected metal clusters are not catalytically active because almost all atoms on the metal cluster are passivated by metal-S bonds. NCDs prepared through place exchange or secondary reactions also would have all their surface atoms passivated by the thiolate. Hence these NCDs also would not exhibit any catalytic activity.

Metal nanoparticles are effective catalysts for several chemical transformations because of their large surface areas [Hayat 1991; Schmidt 1994; Feldheim 2002]. Since metal nanoparticles tend to lose their catalytic activity as they precipitate or aggregate, stabilizers such as polymers, ligands or surfactants are used in these preparations to prevent agglomeration and to control the particle size. This process may result, however, in strong adsorption of the stabilizers on the active sites of the metal nanoparticles leading to loss of catalytic activity. Hence there is a need for new nanoparticle technologies that provide the improved protection with minimal surface passivation. In this context, NCDs prepared through the direct route appear to be ideal candidates as metal catalysts.

Figure 1.16 is a schematic representation of an NCD prepared through the direct route. The metal cluster at the core has diameters in the range of 2 - 5 nm and hence these particles exhibit large surface area/unit volume. The number of dendrons attached to the metal core is decided by a sterically induced stoichiometry and depend upon the size of the dendron and diameter of the metal core. As we can see in Figure 1.16, only

a few atoms on the nanoparticle surface are attached to dendrons leaving most of the surface atoms unpassivated. Thus the NCD would have most of the atoms on the metal surface exposed to substrates capable of penetrating the dendritic shell. The free space or voids present on the metal surface can act as guest cavities and can function as “reaction vessels” for catalytic reactions. These features make NCDs ideally suited as nanoreactors for metal-catalyzed reactions.

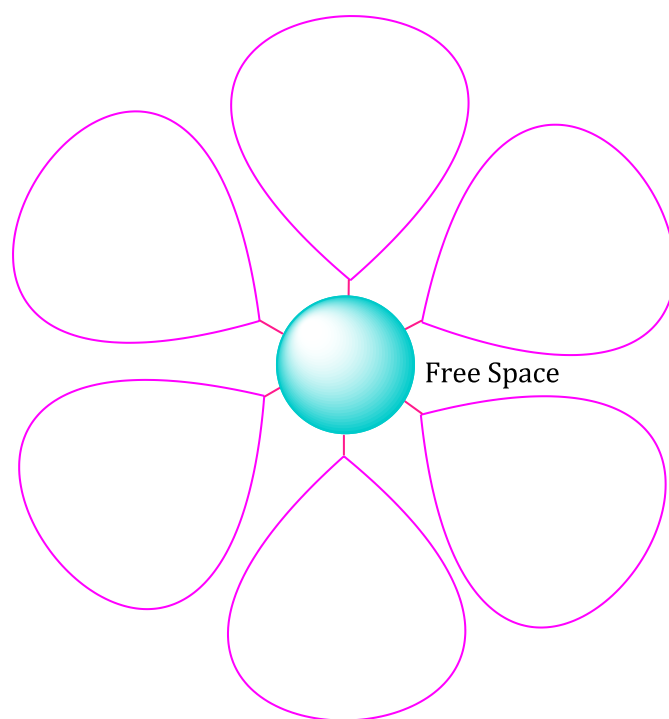
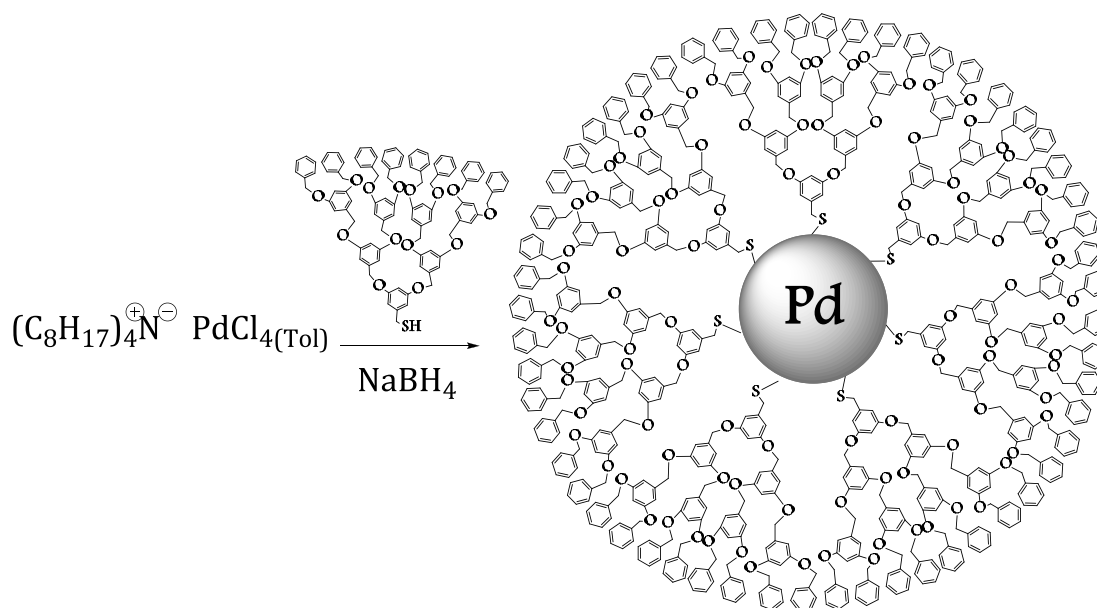


Figure 1.16

Synthesis and characterization of catalytically active NCD was first reported by Fox and co-workers [Gopidas 2003 (c)]. They synthesized a Pd-NCD by the Brust reaction as shown in Scheme 1.17. The palladium NCDs thus prepared were found to be good catalysts for different C-C bond forming reactions like Heck and Suzuki couplings. The values of the

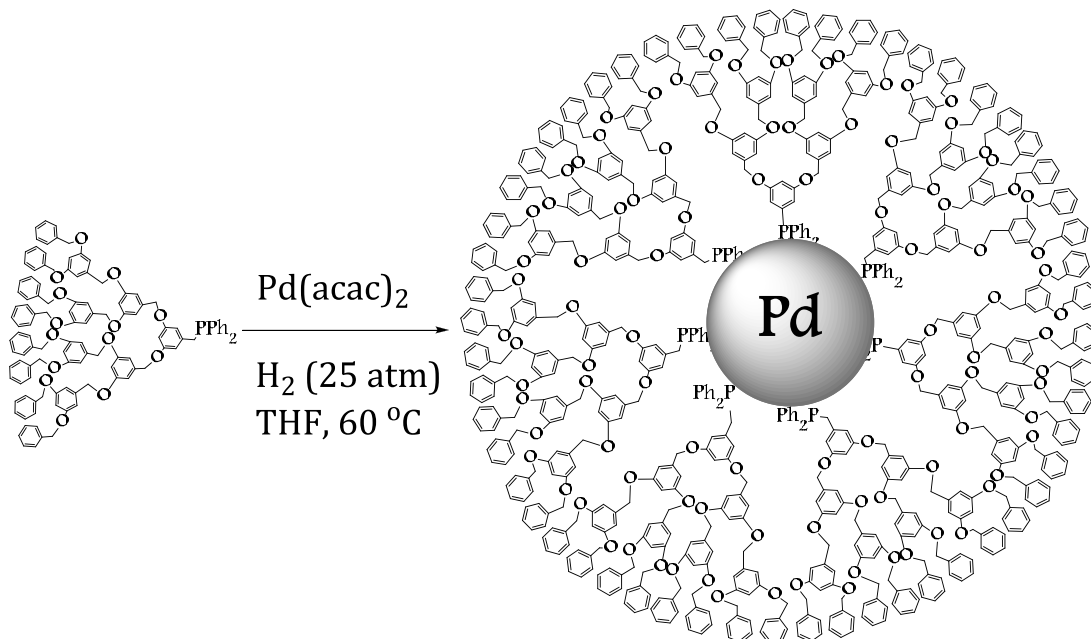
turn-over number (TON) and turn-over frequency (TOF) obtained for the NCD catalysis was found to be higher than those obtained for DEN catalysts. However, the palladium NCD reported by Fox *et al.* was found to undergo hydrogenolysis at the CH₂-S bond under hydrogenation conditions leading to decomposition of the NCD and precipitation of the Pd metal, which limits its use as a hydrogenation catalyst.



Scheme 1.17 Synthesis of Pd-NCDs stabilized by dendron thiols.

Fan and co-workers reported the synthesis of catalytically active palladium NCDs through the reduction of Pd(II) salt by hydrogen under pressure in the presence of phosphine terminated Fréchet dendrons as shown in Scheme 1.18 [Wu 2006]. These NCDs were found to be efficient catalysts for Suzuki and Stille coupling reactions. The catalyst also showed good recyclability. The authors were also successful in demonstrating the ability of this NCD as a hydrogenation catalyst, but the reaction required

high temperature and pressure. Also, the catalyst was found to be non-recyclable for hydrogenation reactions.



Scheme 1.18 Synthesis of dendritic phosphine stabilized Pd-NCDs.

NCDs can be considered as dendrimers with a metal core. A comparison of NCDs with conventional dendrimers, however, shows that there exist several differences between these two classes of compounds. During the convergent synthesis of dendrimers, the number of covalent bonds formed in the final step is known and hence the molecular weight can be calculated accurately. But in NCDs, as the final step involves the self-assembly of dendrons on the surface, which in turn depends on the available surface area, usually a distribution of molecular weights can be anticipated. In a convergent dendrimer synthesis, the number of dendrons reacting in the final step rarely exceeds four, whereas this number will be very high for NCDs depending upon the sterically induced

stoichiometry. Up to generation three, the conventional dendrimer synthesis results in the formation of open structured molecules without the so called 'dendritic properties' and a globular shape will be achieved only for higher generation dendrimers. For NCDs, assembly of the dendrons is on an almost spherical core and hence dendritic properties can be extracted from first generation itself. Also the accessibility of the guest molecules towards the interior of a conventional dendrimer decreases with increase in dendritic generation. But this trend is reversed in the case of NCDs [Gopidas 2003 (a)] mostly due to the irregularities in the self assembly of the dendron wedges on the nanoparticle surface.

NCDs can also be considered as MPCs wherein the monolayer is formed from dendrons. A comparison, however, shows several differences between NCDs and MPCs. In the case of MPCs, packing of the ligands is assumed to be uniform with the methylene groups closely packed near to the core but are free to move at the periphery. In the case of NCDs, an opposite trend is expected. Also, the number of dendritic wedges on the surface of the nanoparticle decreases as the dendron generation increases, enabling NCDs to enclose large interior void spaces, which is absent in the case of MPCs. As stated earlier, MPCs would have no catalytic activity whereas NCDs can be good catalysts [Gopidas 2003 (a)].

1.4 Origin of the Present Work

Although the Au-S bond in diatomic Au-S is very strong (100 kcal M⁻¹) [Lynch 1974], the Au-S bond in R-S-Au systems such as alkanethiolate self-assembled monolayers (SAM) of gold and Au NCDs are much weaker

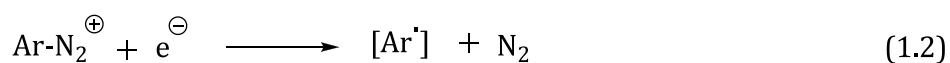
($\sim 40 \text{ kcal M}^{-1}$) [Nuzzo 1990]. In the case of alkanethiolate SAMs on gold, it has been shown that prolonged exposure to air leads to oxidation of the gold-thiolate bond, leading to formation of sulfinates and sulfonates [Schoenfish 1998]. Annealing of the SAMs at $100 \text{ }^\circ\text{C}$ or above for long periods also lead to oxidation of thiolate species to sulfonates [Delamarche 1994]. Irradiation by UV light leads to photo-oxidation of alkanethiolates which provides yet another pathway for the formation of sulfonates [Huang 1993; Rieley 1996]. The sulfinates and sulfonates thus formed have lower affinity to the gold surface and exhibit a tendency to desorb from the metal surface. It is also reported that oxidized SAMs can undergo rapid exchange reactions with thiols present in solution [Tarlov 1992; Tarlov 1993]. The gold-thiolate bond in NCDs is also expected to behave similarly, casting doubt on the long time stability of metal-thiolate NCDs. In addition, the C-S bonds in NCDs are also not very strong if the carbon is benzylic type ($\sim 53 \text{ kcal M}^{-1}$) [Lynch 1974] and hence NCDs with Metal-S-Dendron type structure may undergo cleavage at the C-S bond under certain conditions. For example, Fox and co-workers have reported that Pd-NCDs are unstable under hydrogenation reaction conditions, most probably due to hydrogenolysis of the C-S bond, which leads to precipitation of the Pd metal [Gopidas 2003 (c)]. It is, therefore, of great practical interest to develop methodologies for SAM, MPC or NCD synthesis, that avoids chemisorption of thiolate-capped ligands on the metal surface.

The primary objective of this thesis is to synthesize and study NCDs where the dendrons are linked to the metal clusters through Carbon-Metal

bonds. Our synthetic approach is based on the propensity of the aryl radical generated by the one electron reduction of diazonium salts to form covalent bonds with metal/solid surfaces [Canning 2002; Pinson 2005; Jiang 2006]. The reactions of aryl radicals, generated through the reduction of aryl diazonium salts, with different substrates is well documented in the literature [Pinson 2005] and this aspect is briefly reviewed in the following section.

1.5 Electrochemical Grafting of Aryl Groups on Electrode Surfaces

Grafting of aryl groups on to electrode surfaces through the electrochemical reduction of aryldiazonium salts was reviewed recently by Pinson and co-workers [2005]. Due to the strong electron withdrawing nature of the N_2^+ group, aryl diazonium salts can be easily reduced. Upon receiving an electron, the diazonium salt decomposes almost spontaneously to give aryl radicals and dinitrogen as shown in equation 1.2.

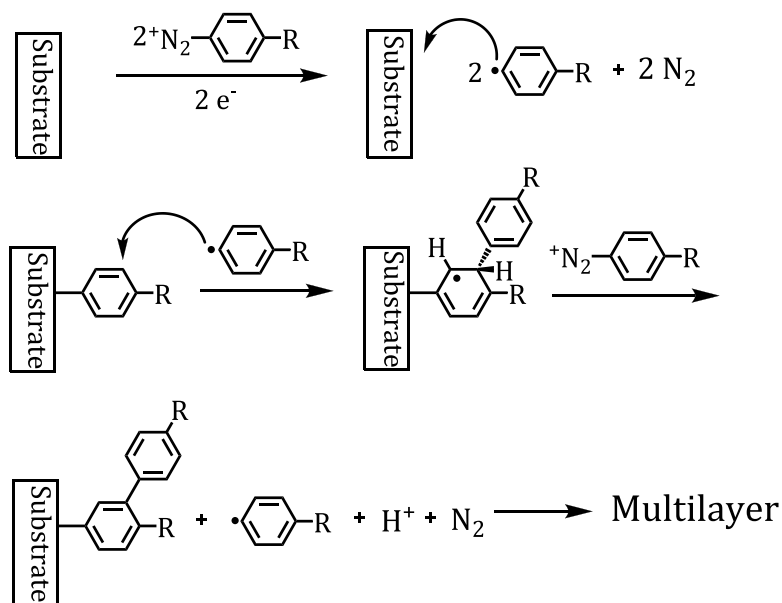


The aryl radical thus formed is very reactive and undergoes usual radical reactions. When the reduction of diazonium salt is carried out electrochemically, the concentration of the aryl radicals formed is very high at the electrode surface leading to grafting of these radicals on to the electrode surface. This reaction has been exploited for the modification of solid surfaces with mono or multi layers of organic materials. Surfaces

modified in this way include carbon (carbon fibers [Delamar 1997], carbon black [Allongue 1997], carbon nanotubes [Dyke 2003], HOPG [Liu 1995; Kariuki 2001], diamond [Wang 2004]), semiconductors (Si [de Villeneuve 1997; Allongue 2003], GaAs [Stewart 2004]) and metals (Au [Paulik 2007; Liu 2007], Pt [Bernard 2003], Fe [Shimura 2006], Zn [Bernard 2003], Cu [Hurley 2004], Pd [Stewart 2004] etc).

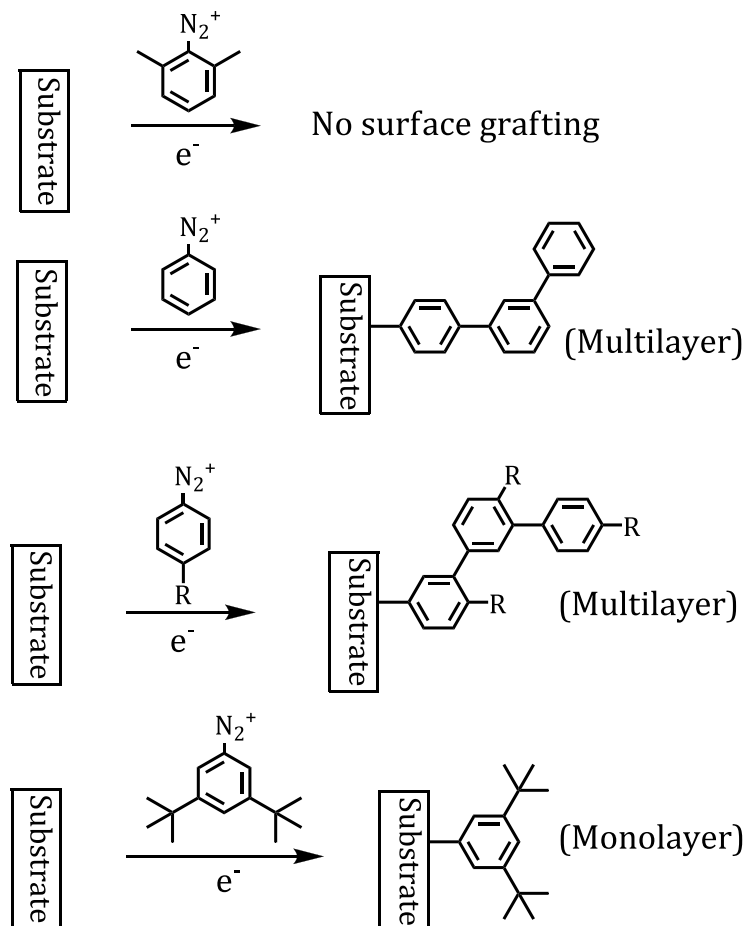
The nature of bonding between the solid (metal, electrode or semiconductor) surface and aryl residues was also discussed. Pinson *et al.* [2005] projected the ability of the organic coated surfaces to withstand ultrasonic treatment as a major evidence for the presence of a strong covalent bond between the substrate and aryl residues. The authors found that the grafted organic layer resists ultrasonic cleaning in a variety of solvents like acetonitrile, dimethylformamide, dimethyl sulfoxide, benzene, benzonitrile, acetone, methanol, ethanol, dichloromethane and chloroform for 15 minutes and it was stable for one month under ambient conditions [de Villeneuve 1997]. 4-Bromophenyl layers on Si surface were found to resist 40% HF for two minutes and 10 M NH₄F for one minute [Kariuki 2001; Stewart 2004; Hurley 2004; Combellas 2005]. Auger signals for aromatic layer could be obtained from 4-nitrophenyl modified carbon surfaces at 700 K under ultra high vacuum [Combellas 2008]. The fact that the organic layer could be removed only by mechanical polishing or by scratching with an AFM tip further excludes the possibility of any weak interaction (such as van der Waals or hydrogen bonding) being responsible for stabilizing the organic layer on these solid surfaces.

The reaction of the *in situ* generated aryl radicals with surfaces results in the overcoating of the surface with an organic layer, the thickness of which increases with time owing to multiple layer formation. This is shown in Scheme 1.19. The concerted electron transfer reaction and dinitrogen elimination results in the formation of the aryl radical as shown in Scheme 1.19, which can get grafted on to the electrode surface. Now, when a second aryl radical is generated it can attack either the electrode surface or the already attached phenyl ring. This latter reaction results in the formation of a cyclohexadienyl radical. The cyclohexadienyl radical thus formed can get aromatized by the elimination of a proton and an electron, and this is possible either through an electron transfer to the electrode followed by the loss of a proton or by the oxidation of the dienyl radical by the diazonium cation. If excess diazonium salt is present, the same reaction sequence can continue resulting ultimately in the formation of thick polyphenylene structures [Pinson 2005].



Scheme 1.19 Mechanism of multilayer formation.

Podvorica and co-workers [Combellas 2005] carried out detailed studies on the multilayering process during the reduction of diazonium salts and they observed that the position of substituents in the aryl ring is having a remarkable effect in the multilayering process (Scheme 1.20). The authors found out that if the 2 and 6 positions of the diazophenyl group are occupied by methyl groups, then grafting of the aryl group will not occur. This shows that the *ortho* positions of the initially grafted aryl ring will be sterically protected by the surface of the material upon which the ring is attached. Absence of substituents at the *meta* and *para* positions of the grafted ring can lead to multilayer formation. If the *para* position of the grafted phenyl ring is protected by a substituent, then the newly formed aryl radicals can target the *meta* position, which is free, resulting in multilayer formation. But, blocking the *meta* positions of the grafted phenyl ring with bulky substituents such as *tert*-butyl groups can lead to the formation of monolayer. In this case, even though the *para* position of the initially attached phenyl ring is free, the steric crowding provided by the bulky *meta* substituents hinders the attack of aryl radical at the *para* position, thereby leading to the formation of monolayers.



Scheme 1.20 Effect of substituent position on the surface grafting by diazonium salts.

McDermott and co-workers [Shewchuk 2009] carried out comparative studies for assessing the stabilities of diazonium and thiol derived gold surfaces. They fabricated the surface using 4-nitrobenzenethiol and 4-nitrobenzene diazonium salt to get the thiol and diazonium stabilized surfaces and these surfaces were subjected to various treatments like vigorous sonication, refluxing in different solvents and chemical displacement reaction with octanethiol. They observed a partial ligand desorption from both surfaces under the conditions of sonication and refluxing. However, the thiol modified surface was found to

undergo complete ligand displacement in presence of octanethiol, whereas for the diazo derived surface, the extent of ligand displacement was much less, showing a direct evidence for the enhanced stability of diazonium derived films over thiol monolayer analogues.

1.6 Outline of the Thesis

Work described in the present thesis involves the synthesis and characterization of gold and palladium nanoparticle-cored Fréchet type dendrimers of different generation, in which the dendrons make a direct carbon-metal linkage with the nanoparticle. Chapter 2 of the thesis describes the synthesis of gold NCDs, carried out by the reduction of $G_1 - G_4$ Fréchet type dendritic diazonium salts in presence of Au(III). The diazonium salts and NCDs thus formed were thoroughly characterized by different spectroscopic techniques like FT-IR, NMR and UV-Vis as well as TEM and TG analysis. This chapter also deals with the different control experiments carried out in order to confirm a direct interaction of the dendron with the metal nanoparticle and also to assess the stability of the NCD.

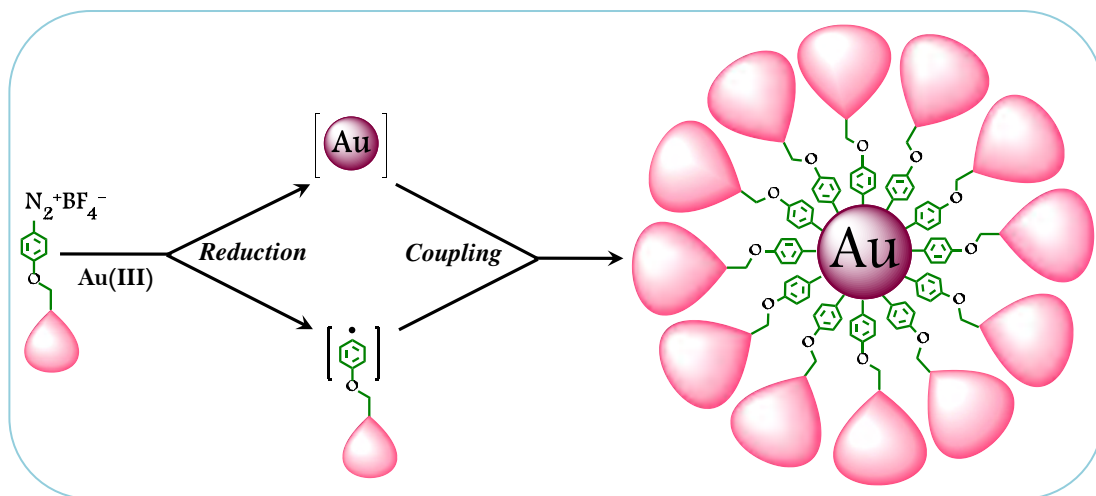
The synthetic protocols towards the preparation of Pd-NCDs is given in chapter 3, where the reduction of diazodendrons were carried out in presence of Pd(II). FT-IR, NMR, UV-Vis spectroscopies as well as TEM analysis were used to characterize the Pd-NCDs formed and the details of these studies are presented in this chapter.

The fourth chapter of the thesis deals with studies of catalytic applications of a selected Pd-NCD. Pd-NCD is found to be a highly efficient

catalyst for C-C bond forming reactions such as Suzuki, Stille, Heck, and Hiyama couplings. The catalyst also exhibited good recovery and recyclability in some of these reactions. We also observed that Pd-NCD efficiently catalyzed the chemoselective room temperature hydrogenation reactions of alkenes and alkynes. Details of these studies are presented in chapter 4 of this thesis.

Chapter 2

Synthesis and Characterization of Gold Nanoparticle-Cored Dendrimers Stabilized by Direct Carbon-Metal Bonds



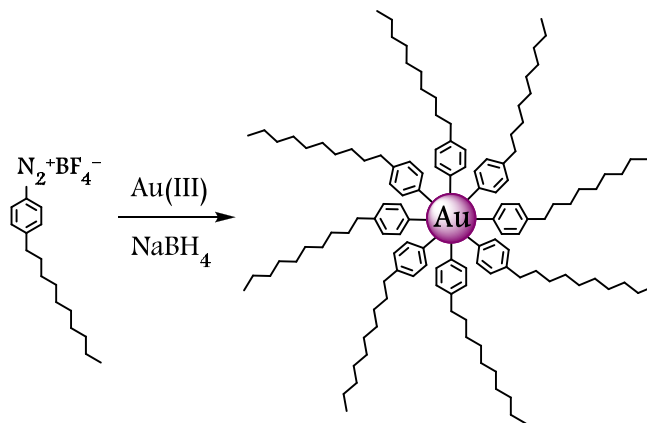
2.1 Abstract

Synthesis and characterization of gold nanoparticle-cored dendrimers (\mathbf{AuG}_n), where the dendrons are attached to the gold core through gold-carbon bonds, are described. Synthesis of these materials involved the simultaneous reduction of Au(III) and a Fréchet-type dendron with a diazonium group at the focal point, in an organic solvent such as toluene. The proposed reaction mechanism involves formation of an intermediate dendron radical by the reduction of diazodendron, which gets grafted onto the growing metal cluster thereby arresting its growth and leading to the formation of the NCD. Thus a physical structure of these materials can be envisaged as a nanometer-sized gold cluster at the core surrounded by a shell of poly(arylether) dendrons which are connected radially to the core. The NCDs and diazodendrons were characterized by IR, UV and NMR techniques. TEM studies indicated the presence of almost spherical, polydisperse metal particles with an average core diameter of 4.7 to 5.5 nm for the different generations. All NCDs exhibited the characteristic plasmon absorption of gold nanoparticles at 520 nm. Average number of dendrons per NCD in \mathbf{AuG}_n was calculated using results from TGA and TEM studies. The results indicated a decrease in the number of attached dendrons around the NCD with increase in dendrimer generation. Multiple layering of the dendrons was proposed as possible reason for the high dendron/NCD value.

2.2 Introduction

Nanoparticle-cored dendrimers (NCDs) are organic-inorganic hybrid molecular systems consisting of a nanometer sized metal cluster at the core to which dendrons of different generations are attached through their focal point. The past decade has witnessed the emergence of various attempts towards the synthesis of these core-shell hybrid materials and most of these approaches have relied on the interaction of the metal core with dendrons functionalized with a heteroatom at their focal point [Shon 2007]. Examples in this regard include the thiol stabilized NCDs reported by Fox and co-workers [Gopidas 2003 (a,b,c)] and the pyridone stabilized NCDs synthesized by Zheng and co-workers [Wang 2001.] A detailed description of the various approaches for NCD synthesis and applications of NCDs is presented in chapter 1 of this thesis. In most of the NCDs the metal-heteroatom bond is not very strong and as a result decomposition of the NCD occurs under certain reaction conditions. For example, the Pd-NCD synthesized by Fox *et al.* decomposed in the presence of hydrogen [Gopidas 2003 (c)]. These studies showed the need for developing new synthetic strategies for the preparation of NCDs with a stable core-shell stabilization which should avoid the conventional metal-heteroatom interactions. One way of achieving this goal is by making use of the reaction of phenyl radicals with surfaces to form a direct linkage with carbon. A detailed account of these reactions is presented in chapter 1. Recently Mirkalaf *et al.* [2006] made use of this reaction to synthesize monolayer protected clusters (MPC) of gold where the organic moieties are linked to the gold cluster through metal-carbon bonds. They achieved

this direct metal-carbon bonding by the simultaneous reduction of *p*-decylbenzene diazoniumfluoroborate and Au(III) using NaBH₄ as shown in Scheme 2.1.



Scheme 2.1 Synthesis of gold nanoparticles with metal-carbon bond.

A similar reaction with Pt(II) resulted in the formation of carbon-metal bond stabilized Pt MPCs. Later Chen and co-workers reported the first synthesis of titanium nanoparticles stabilized by carbon-metal bonding through the same synthetic approach [Ghosh 2008 (a)]. Chen *et al.* were successful in extending this methodology for the synthesis of palladium and ruthenium nanoparticles possessing direct metal-carbon linkages [Ghosh 2008 (b,c)]. In all these reports, the characterization techniques used were IR, NMR, UV-visible absorption spectroscopies and TEM analysis.

In this chapter we report the synthesis and characterization of Au-NCDs of generations 1-4 (abbreviated as **AuG_n** where 'n' stands for the generation number), wherein the dendrons are linked to the gold surface through metal-carbon bonds. The synthesis is based on the propensity of the aryl radical generated by the one electron reduction of diazonium salts

to form covalent bonds with metal/solid surfaces. Here we show that reduction of HAuCl_4 , phase-transferred into toluene in the presence of diazonium salt-capped Fréchet-type dendrons (G_1 - G_4) results in the formation of AuG_n with carbon-gold covalent bonds. Idealized structures of the third and fourth generation NCDs are shown in Figure 2.1.

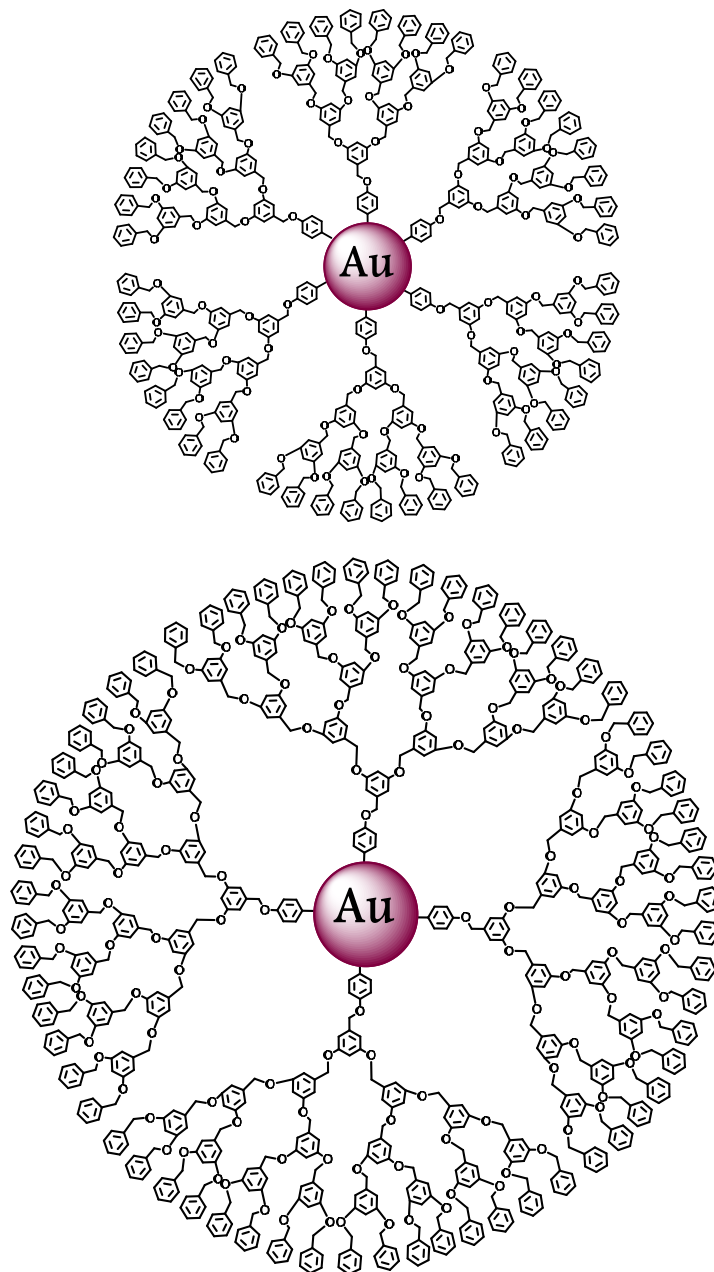


Figure 2.1 Idealized structures of AuG_3 (top) and AuG_4 (bottom).

2.3 Results and Discussions

2.3.1 Syntheses

Structures of the G_1 – G_4 poly(arylether) dendritic bromides used as starting materials for the synthesis of diazodendrons are shown in Figure 2.2. The dendritic bromides were reported previously by Fréchet and co-workers and we adopted the reported procedures for synthesizing these bromides [Hawker 1990; Wooley 1991; Kwock 1991; Percec 2006]. The synthesized compounds were thoroughly characterized and their NMR spectra were compared with those reported by Fréchet and co-workers to establish identity of the compounds.

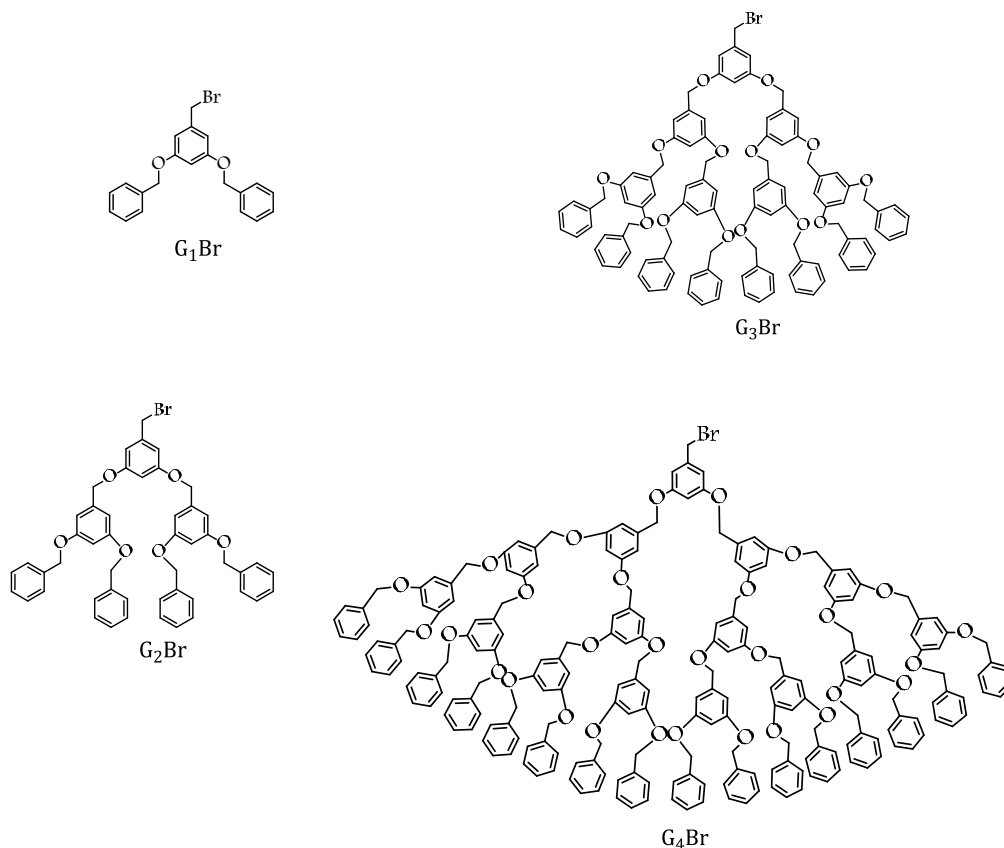
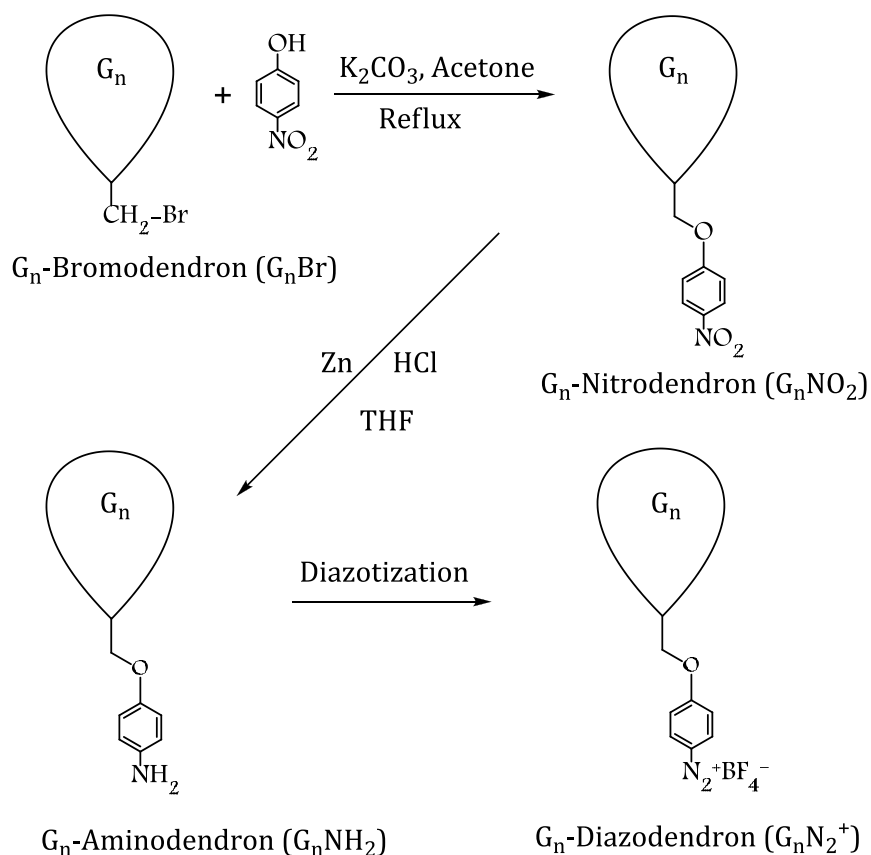


Figure 2.2 Structures of G_1 – G_4 dendritic bromides.

The dendritic bromides ($G_n\text{-Br}$) were converted to corresponding diazodendrons ($G_n\text{N}_2^+$) by the three-step reactions shown in Scheme 2.2. The synthetic scheme involves reaction of $G_n\text{-Br}$ with *p*-nitrophenol to get the nitrodendrons ($G_n\text{-NO}_2$) followed by their reduction to the aminodendrons ($G_n\text{NH}_2$), which upon diazotization gave the corresponding diazodendrons ($G_n\text{N}_2^+$) as shown in Scheme 2.2.



Scheme 2.2 Synthesis of diazodendrons ($G_n\text{N}_2^+$) (balloon represents the dendron).

2.3.1.a Synthesis and characterization of nitrodendrons ($G_n\text{NO}_2$)

The nitrodendrons were prepared through reaction of the corresponding diazodendrons with *p*-nitrophenol in dry acetone in the presence of anhydrous potassium carbonate as base. Progress of the

reaction was monitored by TLC. After completion of the reaction the mixture was filtered and the residue was washed several times with dichloromethane (DCM). The combined organic layer was washed with water to remove any unreacted *p*-nitrophenol present in the reaction mixture. The organic layer upon concentration gave the crude nitrodendron. For lower generations (G_1 and G_2) further purification was carried out by crystallization from dichloromethane-hexane mixture. For higher generation dendrons (G_3 and G_4), purification was achieved by repeated dissolution in DCM and reprecipitation by addition of ether. Finally the solids were collected and dried under vacuum. The structures of G_2 and G_3 nitrodendrons are given in Figure 2.3.

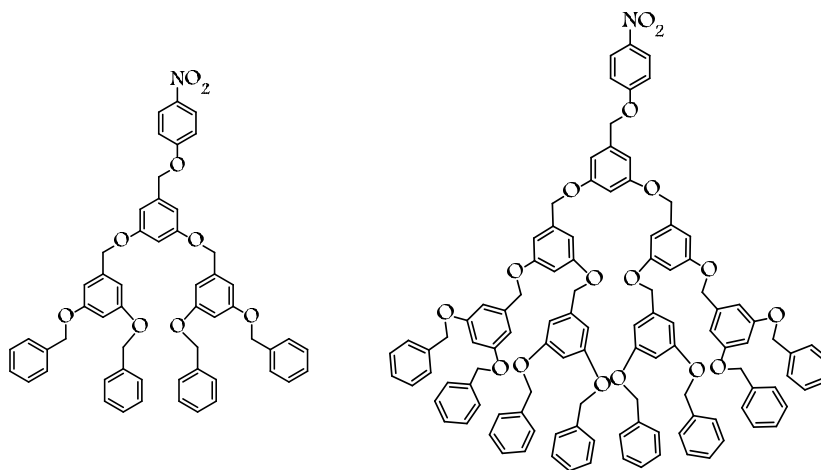


Figure 2.3 Structures of G_2 (left) and G_3 (right) nitrodendrons.

G_1 and G_2 nitrodendrons were pale yellow crystals whereas the higher generation nitrodendrons were white glassy solids. All the nitrodendrons were characterized by ^1H and ^{13}C NMR spectroscopy as well as high resolution mass (HRMS) analysis. The ^1H NMR spectra of the nitrodendrons, for example, were featured by the characteristic doublets corresponding to the ring protons of the *p*-nitrophenoxy group resonating

at 6.9 (2H) and 8 (2H) ppm as shown in Figure 2.4. As the dendron generation increases the relative contribution of these protons to the total number of protons in the dendron decreases leading to a decrease in the intensity of these protons. The ^{13}C NMR spectra of the nitrodendrons showed the signal due to the nitro group-bearing carbon at 163 ppm, the intensity of which also decreased with increase in the dendrimer generation. HRMS analysis of G_1 and G_2 gave good results whereas HRMS could not be obtained for G_3 and G_4 nitrodendrons.

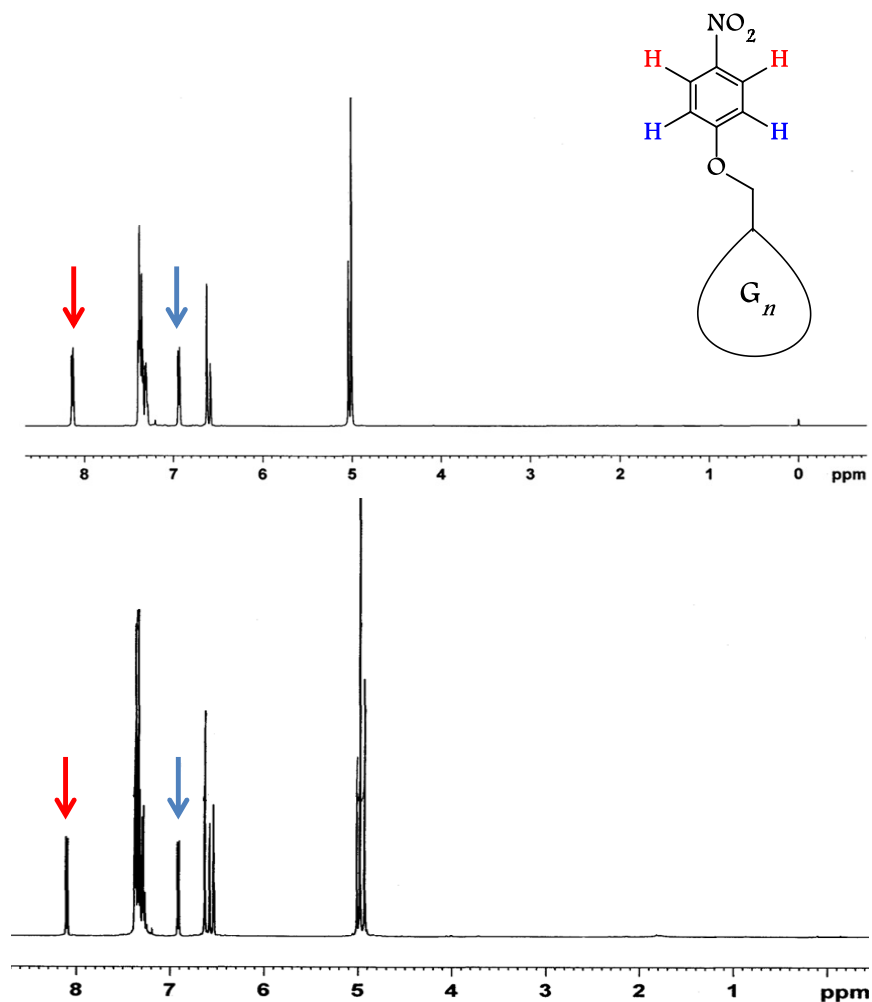


Figure 2.4 ^1H NMR spectra of G_1 (top) and G_2 (bottom) nitrodendrons.

2.3.1.b Synthesis and characterization of aminodendrons (G_nNH_2)

G_1 - G_4 aminodendrons were prepared by the reduction of corresponding nitrodendrons using zinc and conc. HCl. After removing the metal residue the reaction mixture was neutralized and the aminodendron was extracted into DCM and purified by precipitation using ether. G_1 and G_2 aminodendrons were pale red solids whereas G_3 and G_4 derivatives were glassy solids. Figure 2.5 shows the structures of second and third generation aminodendrons and all these molecules were characterized by usual spectroscopic techniques. In the 1H NMR spectra of aminodendrons protons of *p*-aminophenoxy ring appeared as merged with the dendritic proton signals which makes these spectra distinctly different from those of nitrodendrons. Similar changes were observed in the ^{13}C NMR spectra also. For the nitrodendrons, the ring carbon atom attached to the nitro group resonated at a high δ value (163 ppm). ^{13}C NMR spectra of the aminodendrons did not show this peak, indicating that the conversion of nitro to amine increased the electron density around the adjacent carbon making it to resonate at a lower δ value. The aminodendrons were also characterized by FT-IR studies and all of them were featured by the characteristic $-NH_2$ stretching bands at ~ 3440 and 3360 cm^{-1} . The intensities of these bands were also found to decrease with increase in dendron generation owing to the proportional increase in the dendron mass.

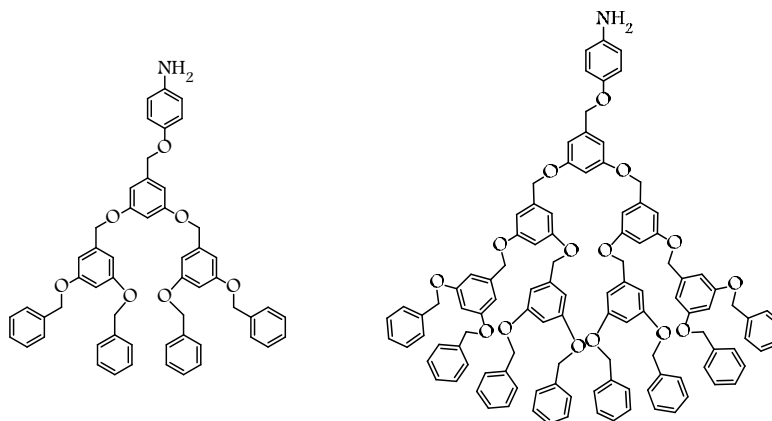


Figure 2.5 Structures of G₂ (left) and G₃ (right) aminodendrons.

2.3.1.c Synthesis and characterization of diazodendrons (G_nN₂⁺)

The aminodendrons were diazotized to obtain the diazodendrons. For diazotization of G₁ and G₂ aminodendrons, the amines were suspended in a 1:1 mixture of acetic acid and propionic acid followed by the slow addition of sodium nitrite at -10 °C. In order to isolate the diazodendrons as the corresponding fluoroborates, aqueous fluoroboric acid was added and the diazodendrons were precipitated by the addition of water. This synthetic approach, however, failed in the case of G₃ and G₄ diazodendrons, probably due to the poor dispersing nature of the starting aminodendrons in the aqueous solvent mixture used. In order to overcome this difficulty, the syntheses of G₃ and G₄ diazodendrons were performed in an organic medium (dichloromethane-tetrahydrofuran mixture) using *t*-butylnitrite and fluoroboric acid at -10 °C. After the reaction, excess diethyl ether was added to precipitate the product, which was further washed with ether and dried. The structures of G₂ and G₃ diazodendrons are shown in Figure 2.6.

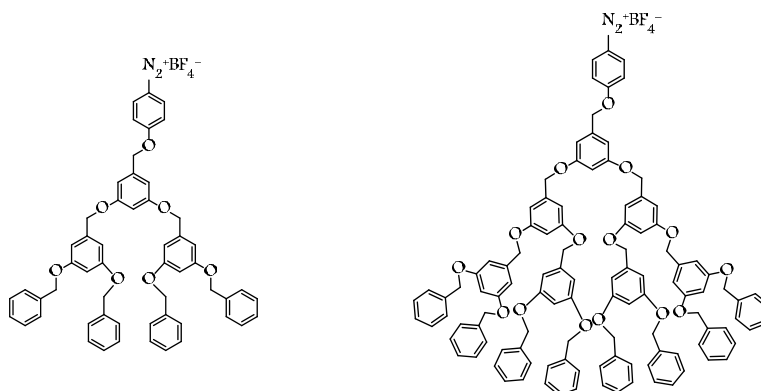


Figure 2.6 Structures of G₂ (left) and G₃ (right) diazodendrons.

The G₁ and G₂ diazodendrons were dark red powders, freely soluble in DCM and THF. G₃ and G₄ salts were dark red glassy solids, slightly soluble in toluene but freely soluble in DCM and THF. The diazodendrons were stable for about a week at room temperature. These were characterized by FT-IR, ¹H and ¹³C NMR. For example, IR spectra of the diazodendrons exhibited the characteristic diazonium stretching peak at 2245 cm⁻¹ [Mirkhalaf 2006; Ghosh 2008 (a,b,c)]. ¹H NMR spectra of these salts exhibited proton signals at δ 8.2 and 7.0 (2H each), attributable to protons of the phenyl group attached to the diazo moiety. The ¹³C NMR spectra exhibited a peak at δ 168 ppm for the phenyl carbon to which the diazo group is attached. The contribution due to the diazophenyl group to the total mass of the diazodendron decreases with dendron generation and as a result the intensities of the FT-IR, ¹H and ¹³C NMR signals due to the diazophenyl group decreases with increase in dendron generation. A detailed discussion regarding the comparison of the IR and NMR signals of

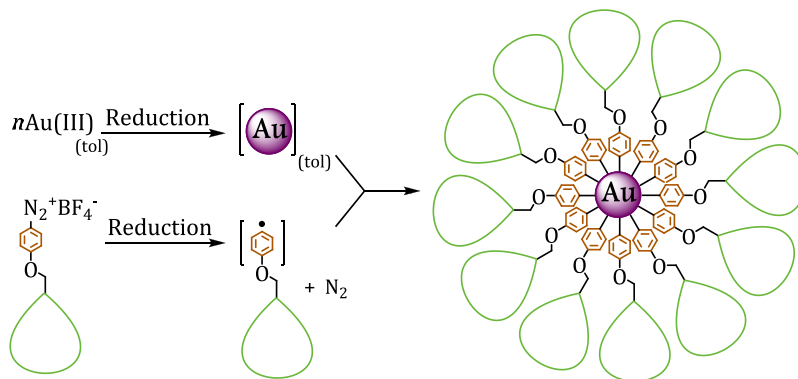
the diazodendrons with that of the NCDs is presented later in section 2.3.2.

2.3.1.d Synthesis of AuG_n

Gold NCDs with carbon-metal bonds ($\text{AuG}_1 - \text{AuG}_4$) were prepared by reducing HAuCl_4 phase-transferred into toluene in the presence of the diazodendrons. The diazonium salt (0.25 mmol) solution (in 20 mL toluene:DCM (9:1)) was stirred for 1.5 h with aq. HAuCl_4 (0.125 mmol in 5 mL water). TOAB (0.18 mmol) was added and stirring continued for 1 h. For G_1 and G_2 diazonium salts, the reduction was carried out using aq. NaBH_4 (1.9 mmol in 15 mL water) under ice-cold conditions, whereas for G_3 and G_4 diazonium salts the reduction was carried out by methanolic NaBH_4 (1.9 mmol in 15 mL methanol) at $-30\text{ }^\circ\text{C}$. For G_1 and G_2 , reaction mixture was stirred for 24 h and for G_3 and G_4 stirring was done for 48 h. After the reaction time, the mixture was extracted twice with 0.5 M H_2SO_4 , 0.5 M Na_2CO_3 and finally with water. The organic layer was dried and the solid was taken in ethanol (50 mL) and sonicated for 30 min. It was allowed to settle and ethanol was decanted. Sonication with ethanol and decantation were continued till the ethanol layer was colorless. The ethanol was decanted and product dried in air and then in vacuum for 2 days.

Based on literature reports [Mirkhalaf 2006; Ghosh 2008 (a,b,c)], the following mechanism is proposed for formation of AuG_n . Au(III) is reduced to give Au atoms, which undergo nucleation and growth to form small clusters. The dendritic diazonium salt upon receiving an electron from the reducing agent decomposes into nitrogen and dendron with

phenyl radical [Canning 2002; Dyke 2003; Allongue 2003; Bernard 2003; Wang 2004; Pinson 2005] at the focal point. At some stage of the Au cluster growth, the dendron radicals get attached to the gold surface, thereby arresting their growth and leading to formation of the Au-NCDs. A plausible mechanism for the formation of Au-NCD is shown in Scheme 2.3.



Scheme 2.3 Mechanism of **AuG_n** formation.

AuG_n thus prepared were black powders, stable in the solid form and in solution, freely soluble in DCM, chloroform, THF and toluene and insoluble in methanol, ethanol and ether. For example, a solution of **AuG₂** in toluene was observed for nearly one year and no decomposition or precipitation was observed. Dilute solutions of all the NCDs exhibited a deep wine-red color. We observed that the NCDs incorporate a small percentage of TOAB (used as the phase-transfer agent). NCDs can be chromatographed over silica gel without undergoing decomposition and this procedure also could not remove the TOAB. Soxhlet extraction using ethanol also could not remove the residual TOAB.

The NCDs synthesized were analyzed by IR, UV and NMR spectroscopy. Information about the size of the Au core is obtained using

transmission electron microscopy (TEM). Information about the organic contents in the NCD samples is obtained by thermo gravimetric analysis (TGA).

2.3.2 Characterization of Diazodendrons and AuG_n

2.3.2.1 FT-IR Spectra

In the case of NCDs reported previously, FT-IR spectra of the NCDs and precursor disulfide dendrons were nearly identical [Gopidas 2003 (a,b,c)]. In the present case IR spectra of the precursor diazodendrons were different from those of NCDs and hence the IR spectra could be used to check the completion of the reaction. In Figure 2.7, the FT-IR spectra of the diazodendrons are compared with those of corresponding NCDs. FT-IR spectra of the diazodendrons clearly showed the vibrational stretching of diazo group at 2245 cm⁻¹ [Mirkhalaf 2006; Ghosh 2008 (a,b,c)]. The intensity of this peak was found to decrease with increase in the dendron generation owing to a decrease in the contribution of this group to the total size of the dendron with an increase in the dendron generation.

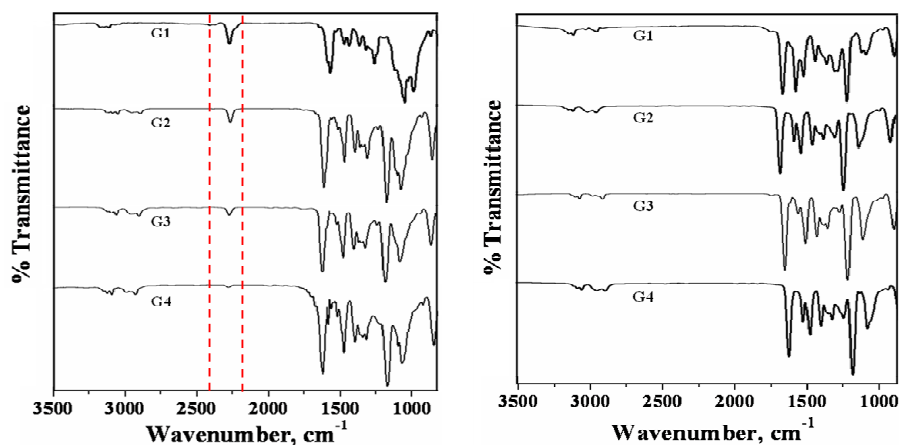


Figure 2.7 FT-IR spectra of diazo dendrons (left panel) and AuG_n (right panel).

The diazo group decomposes during the reaction and hence this peak is absent in the IR spectra of NCDs. This shows the absence of any diazo precursor in the NCDs as well as the possible formation of any azo functionality during the reduction of the diazo group. IR spectra of the diazodendrons and NCDs were featured by methylene C-H stretching modes at $\nu_s = 2870$, $\nu_{as} = 2927$ cm^{-1} and aromatic C-H vibration modes at $\nu_s = 3030$ and $\nu_{as} = 3061$ cm^{-1} .

2.3.2.2 ^1H and ^{13}C NMR Spectra

In Figure 2.8 ^1H NMR spectra of diazodendrons and the corresponding NCDs are compared. Signals at δ 8.2 and 7.0 (shown by arrows) characterize the protons of the diazophenyl group (in G_3 and G_4 diazodendrons, the peak at δ 7.0 is very small and merged with the bigger peak at δ 7.3). The intensities of these peaks were found to decrease with the increase in the dendron generation. In the ^1H NMR of AuG_n the diazophenyl proton signals have vanished. In AuG_1 and AuG_2 , the ^1H NMR signals exhibited considerable broadening. For higher generation NCDs line broadening was found to be negligible. Broadening of the NMR peaks due to fast spin-spin relaxation of atoms close to a metal core or size-dependent spin-spin relaxation clearly supports the metal core-organic shell type structure of AuG_n [Terrill 1995; Badia 1996; Hostetler 1998; Mirkhalaf 2006; Ghosh 2008 (a,b,c)]. The signals seen at $\delta < 3$ ppm in the ^1H NMR of AuG_n are assigned to protons of TOAB, which is present as an impurity (vide supra).

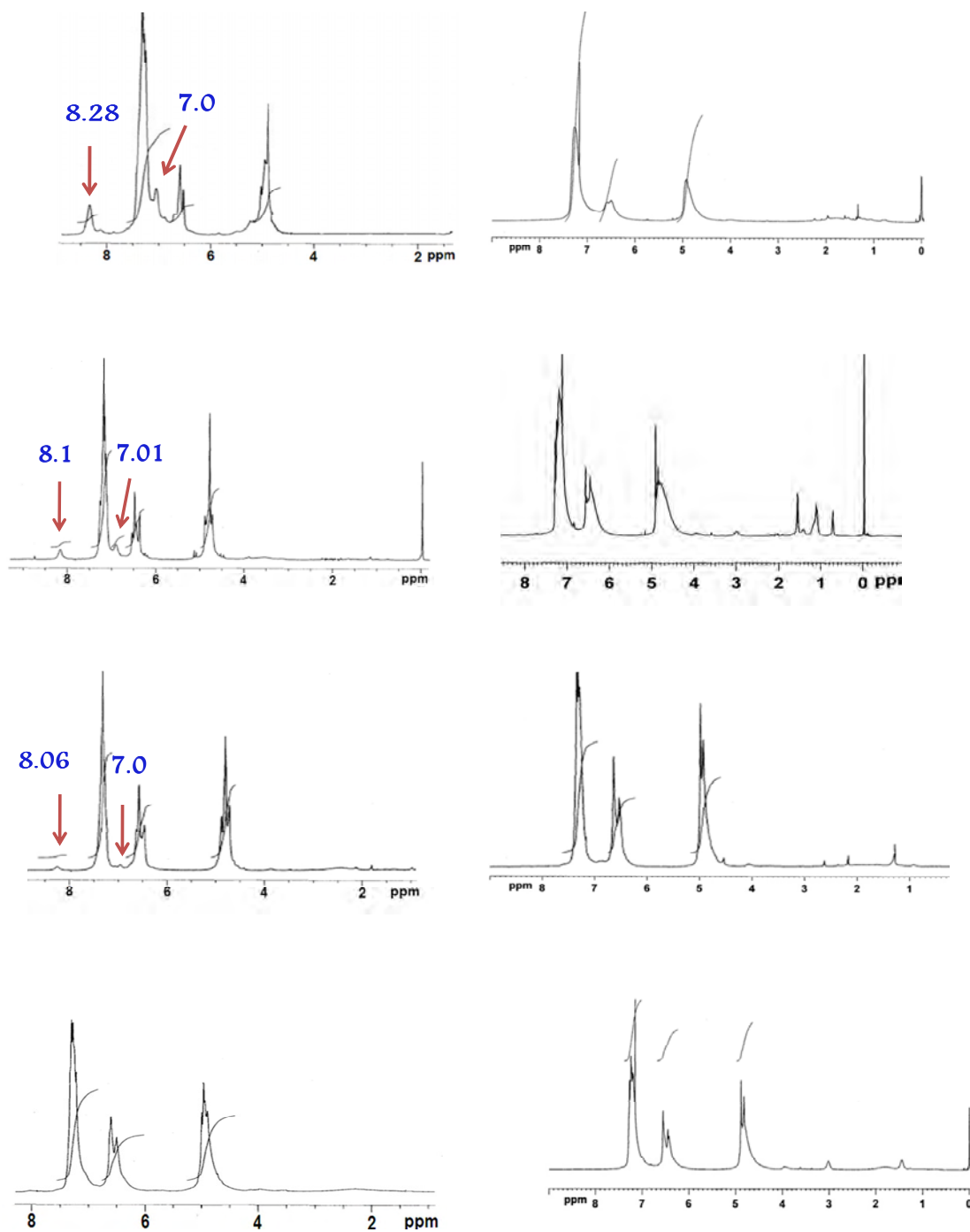


Figure 2.8 ^1H NMR spectra of $\text{G}_1\text{-G}_4$ diazodendrons (left) and $\text{AuG}_1\text{-G}_4$ (right) in CDCl_3 .

Figure 2.9 compares the ^{13}C NMR of $\text{G}_1\text{-G}_4$ diazodendrons and the corresponding NCDs. In the case of the diazodendrons, signals at δ 168, 135 and 118 ppm are identified as belonging to the diazo-bearing phenyl.

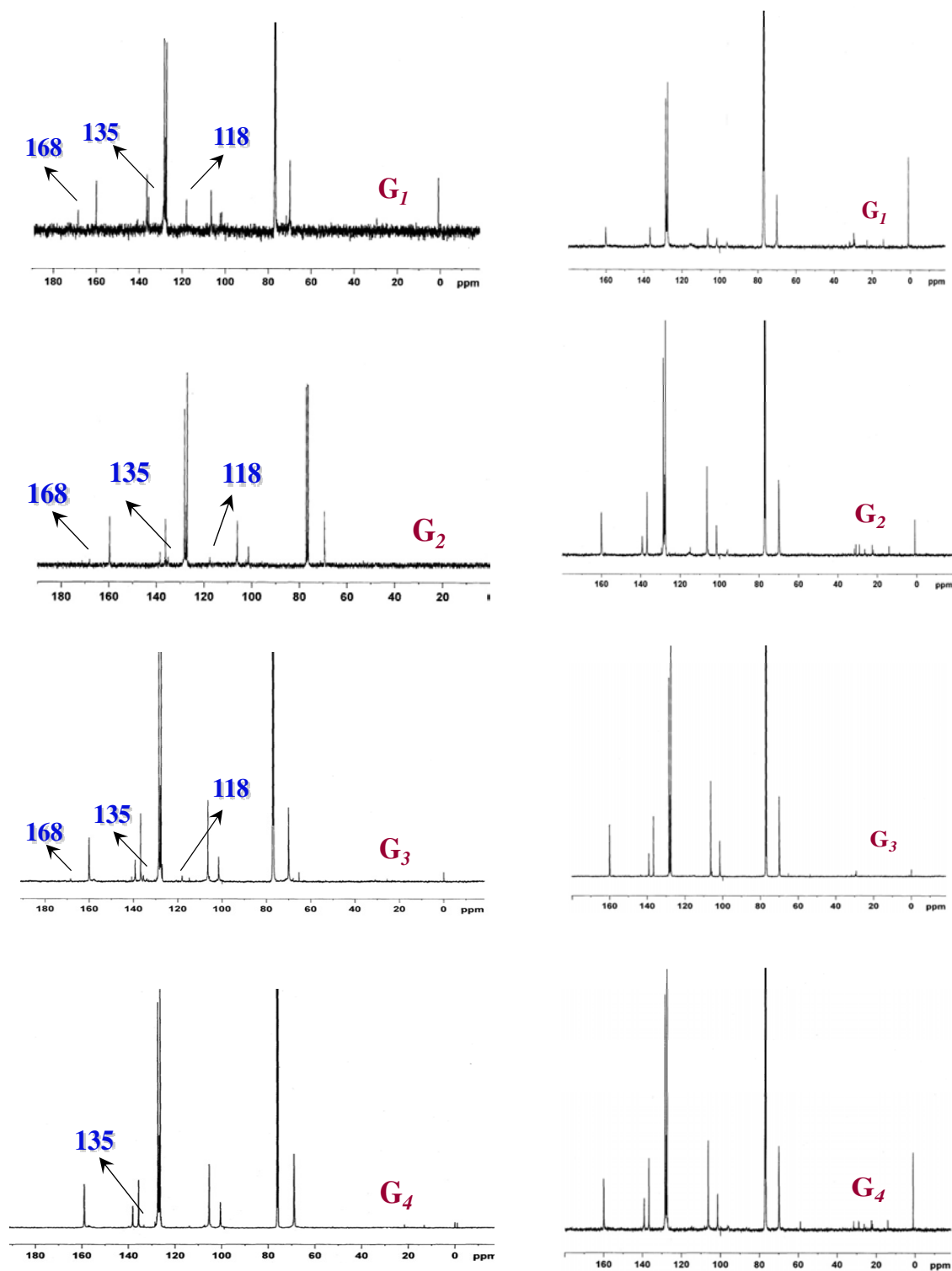


Figure 2.9 ^{13}C NMR spectra of G_1 - G_4 diazodendrons (left) and AuG_1 - G_4 (right) in CDCl_3 .

For the higher generation dendrons the diazophenyl group constitutes only a small fraction of the total dendron size and hence the signals corresponding to this group are very small. In the ^{13}C NMR of AuG_n the above peaks are not seen. Similar observations were made previously for MPCs and it was suggested that the signals due to the carbon atoms on the phenyl ring linked directly to the metal have broadened so much that they are indistinguishable from the background [Mirkhalaf 2006; Ghosh 2008 (a,b,c)]. Absence of these peaks also suggests complete removal of the diazo group during the reduction reaction. It can be concluded that ^1H and ^{13}C NMR spectra provide strong evidence that the dendron is directly linked to the metal core through the phenyl ring at its focal point.

2.3.2.3 Absorption Spectroscopy

When light wave strikes a nanocrystal with a size lower than the wavelength of the incident beam, there will be a coherent excitation of the free electrons in the conduction band of the particle leading to an in phase oscillation termed as surface plasmon resonance (SPR). The electric field of the incident light beam induces a polarization of free electrons with respect to the cationic lattice of the nanoparticle resulting in the formation of a net charge difference at the nanoparticle surface, which in turn acts as the restoring force. In this way, a dipolar oscillation of electrons is created with a certain frequency. The surface plasmon resonance is a dipolar excitation of the entire particle between the negatively charged free electrons and its positively charged lattice. The energy of the surface plasmon resonance depends on both the free electron density and the

dielectric medium surrounding the nanoparticle. For noble metal nanoparticles, the plasmon resonance frequency lies in the visible region of the electromagnetic spectrum imparting characteristic colors. Hence, UV-visible spectroscopy is very useful tool for characterizing noble metal nanoparticles. The first explanation for the characteristic red color of colloidal gold nanoparticles was proposed by Mie by solving Maxwell's equation for an electromagnetic light wave interacting with small metallic spheres. According to Mie theory, the plasmon band of spherical particles can be attributed to the dipole oscillations of free electrons of the conduction band [Mulvaney 1996; Alvarez 1997; Ghosh 2007; Cao 2008].

The absorption spectra of the present gold NCDs **AuG₁** - **AuG₄** recorded in DCM are shown in Figure 2.10, and all of them are featured by the characteristic gold SPR band centered on 520 nm. The SPR band maximum and width are dependent on the metal and also on the particle size, shape, medium dielectric constant and temperature. In the present case, the presence of SPR band around 520 nm indicates the formation of nanoparticles having diameter in the 3-6 nm range. The intensity of the SPR band did not show any regular dependence on generation. Also the band maxima and intensity did not exhibit any solvent dependence.

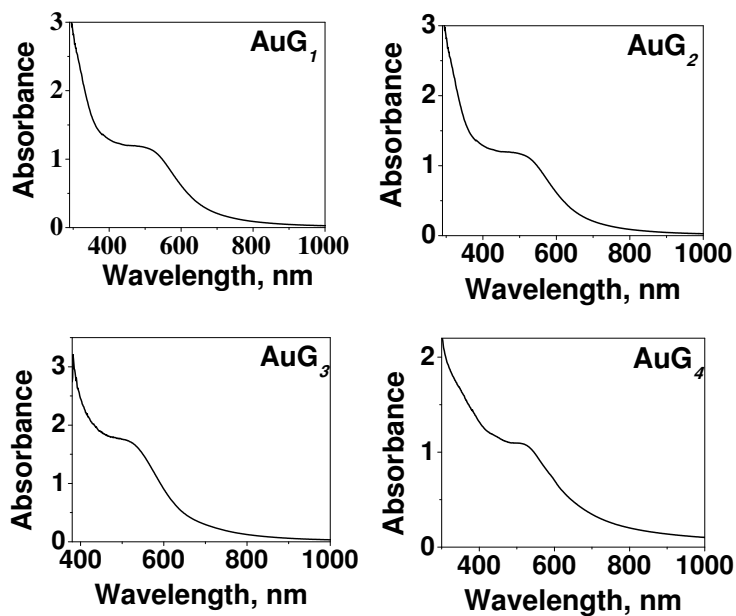


Figure 2.10 UV-Visible spectra of **AuG₁-G₄** in CH₂Cl₂.

2.3.2.4 Transmission Electron Microscopic (TEM) Studies

TEM is a microscopic technique whereby a beam of electrons is transmitted through an ultra thin specimen. An image is formed from the interaction of the electrons transmitted through the specimen. The image is magnified and focused on to an imaging device such a fluorescent screen or a photographic film or detected by a sensor device such as CCD camera. TEMs are capable of imaging at a significantly higher resolution than optical microscopes owing to the small de Broglie wavelength of electrons. This enables the user to examine fine details even as small as a single column of atoms, which is tens of thousand times smaller than the smallest available object in a light microscope [Niemantsverdriet 2000; Cao, 2008].

TEM images of **AuG₁ - AuG₄** are shown in Figure 2.8. The images were taken by drop casting the NCD solution in DCM. Corresponding core

size histograms are also given in Figure 2.11. The TEM images show dispersed metal particles, with non-uniform size of about 4-6 nm. There is no regular change in the size of the particle with increase in the dendron generation. TEM shows only the image of the gold core. In the case of several alkanethiolate MPCs, the core-core separation corresponds to the length of the alkyl chain [Hostetler 1998]. In the present case, occurrences of relatively identical core-core separations were rare in the TEM images and hence thickness of the dendritic shell could not be estimated.

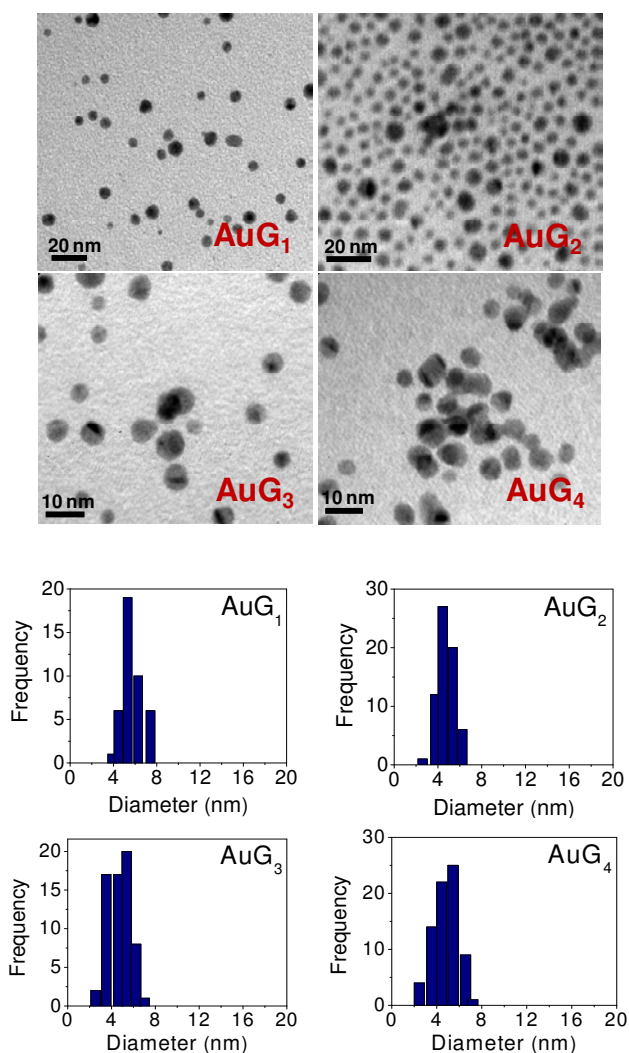


Figure 2.11 TEM images and core size histograms of **AuG₁-G₄** drop casted from CH₂Cl₂.

2.3.2.5 Energy Dispersive X-ray Analysis (EDX)

Interaction of an electron beam with an atom can give rise to its characteristic X-ray emission when the incident electron ejects a bound electron from an atomic orbital. The core-ionized atom thus formed is highly unstable and one mode of its decay occurs when the initial core hole is filled with an electron from a higher shell. The energy gain in this process is used to emit an X-ray photon characteristic of the emitting atom. The most convenient way to analyze the emitted X-rays is with an energy dispersive X-ray detector which is a solid state device with a semiconductor material. Through photoelectric effect, an incident X-ray photon is converted into an electron with kinetic energy $E_{X-ray} - E_{BE}$, where E_{BE} is the binding energy of the photoelectron. The photoelectron dissipates its kinetic energy by creating electron-hole pairs in the semiconductor. Application of a voltage over the detector results in a current, the pulse height (measured in counts) of which will depend upon the number of electron-hole pairs. Thus the pulse height is a measure of the kinetic energy of the photoelectron and hence the energy of the incident X-ray photon. A plot of pulse height against the electron energy gives the spectrum which is characteristic of the elemental composition of the sample [Niemantsverdriet 2000].

In order to get a clear picture about the elemental composition of the NCDs, we obtained the energy dispersive X-ray (EDX) spectrum of **AuG_n**, which allows us to determine the elemental composition of these

nanoclusters. The EDX spectrum obtained is given in Figure 2.12, which shows the presence of elements C, O, Au and Cu (from the grid).

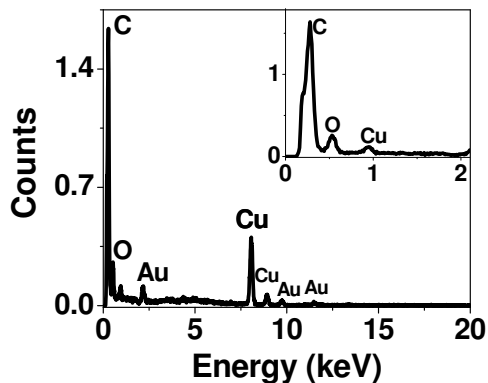


Figure 2.12 EDX spectrum of AuG_3 (inset shows the expanded low energy region).

The NMR studies of AuG_n indicated that they contained small amounts of TOAB as an impurity. There are reports which suggested that phase transfer catalysts such as TOAB are capable of stabilizing metal nanoparticles [Fink 1998; He 1999]. Hence it may be argued that the nanoparticles are stabilized by TOAB and not by the metal-carbon bonds in the present case. This argument can be rejected on two counts. The amount of TOAB present is very small as is evident from the ^1H NMR spectra of AuG_n (Figures 2.8 and 2.9) and at these low concentrations TOAB will not be able to protect the metal nanoclusters from aggregation. If TOAB were present in considerable quantity close to the metal surface, the EDX spectrum would show peaks corresponding to N and Br. The EDX spectrum of AuG_3 , (Figure 2.12) did not show any peaks corresponding to these atoms. The N peak at 0.392 keV may not be observable in the present case because of the very strong carbon signal, which could obscure any small peaks in this region. The signals due to Br, if present,

should be observed at 1.48, 11.36 and 11.90 keV [Fink 1998]. Since no peaks are observed in these regions, we believe that TOAB is not present on the surface of the Au cluster. We propose that the small amount of TOAB present in the NCDs is not present on the metal surface and is entrapped in cavities in the dendritic shell.

We have carried out an additional experiment to show that Au nanoparticles in the present case are not stabilized by TOAB. Gittins and Caruso [2001] have shown that gold nanoparticles, if protected by TOAB in an organic solvent such as toluene, can be phase-transferred into aqueous solutions using a 0.1 M aqueous solution of 4-dimethylaminopyridine (DMAP). Solutions of **AuG_n** in toluene were stirred with aqueous solutions of DMAP for several hours and we did not observe partitioning of gold into the aqueous phase, which confirms that the gold nanoparticles are present as covalently linked to dendrons and not as TOAB protected particles.

2.3.2.6 Thermal Studies

Progressive heating of NCDs led to the volatilization of the organic shell leaving a residue of gold. TGA is therefore a very useful technique to estimate the organic content of organic-inorganic hybrid materials. Figure 2.13 shows the thermograms of **AuG₂** and **AuG₃**. For **AuG_n**, the volatilization started around 250 °C and occurred in a single step. The high decomposition temperatures suggested that the thermal stabilities of these materials are similar to C₁₆-coated MPCs [Terrill 1995; Badia 1996; Hostetler 1998].

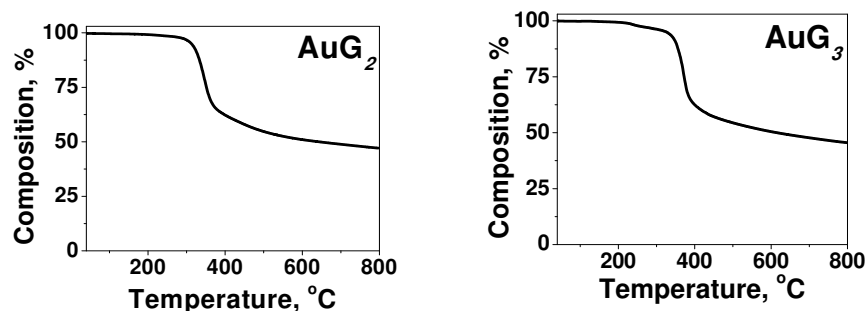


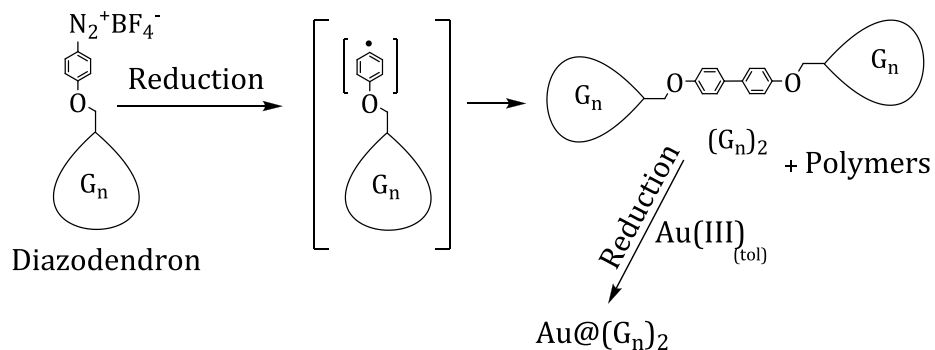
Figure 2.13 Thermograms of **AuG₂** and **AuG₃**.

2.3.3 Control Experiments

IR spectra of **AuG_n** did not show the peak due to the diazo group and NMR spectra of **AuG_n** did not exhibit peaks due to the phenyl group that was attached to the diazo moiety and these aspects are projected as major evidence for the formation of metal-carbon bonds in **AuG_n**. It may be argued that the dendron radical produced can undergo radical-radical coupling leading to dimeric products or addition to other dendrons leading to formation of polymeric products, and the Au nanoparticles formed are stabilized by encapsulation within these structures. We have carried out control experiments as shown in Scheme 2.4 to rule out this possibility.

The diazodendrons were first reduced using NaBH₄ in the absence of HAuCl₄. After stirring the reaction mixture overnight, the products were isolated. In the case of G₁ and G₂ diazodendrons, dimers (G_n)₂ arising out of radical-radical coupling (Scheme 2.4) were identified as major products using ¹H NMR, ¹³C NMR and FAB mass spectra. In the case of higher generation dendrons, products could not be identified clearly. Products of the above reaction, along with TOAB was then used to phase-

transfer Au(III) into toluene. The mixture was then reduced using NaBH₄ to obtain the gold nanoparticles, which we designate here as **Au@(*G_n)₂***.



Scheme 2.4 Mechanism of formation of dendritic dimers (*G_n)₂ and synthesis of Au nanoparticles in presence of dendritic dimers **Au@(*G_n)₂***.*

Figures 2.14 and 2.15 are the ¹H and ¹³C NMR spectra of (*G_n)₂ and **Au@(*G_n)₂***. The nanoparticles thus obtained exhibited absorption spectra and color similar to **AuG_n**, but they exhibited several differences.*

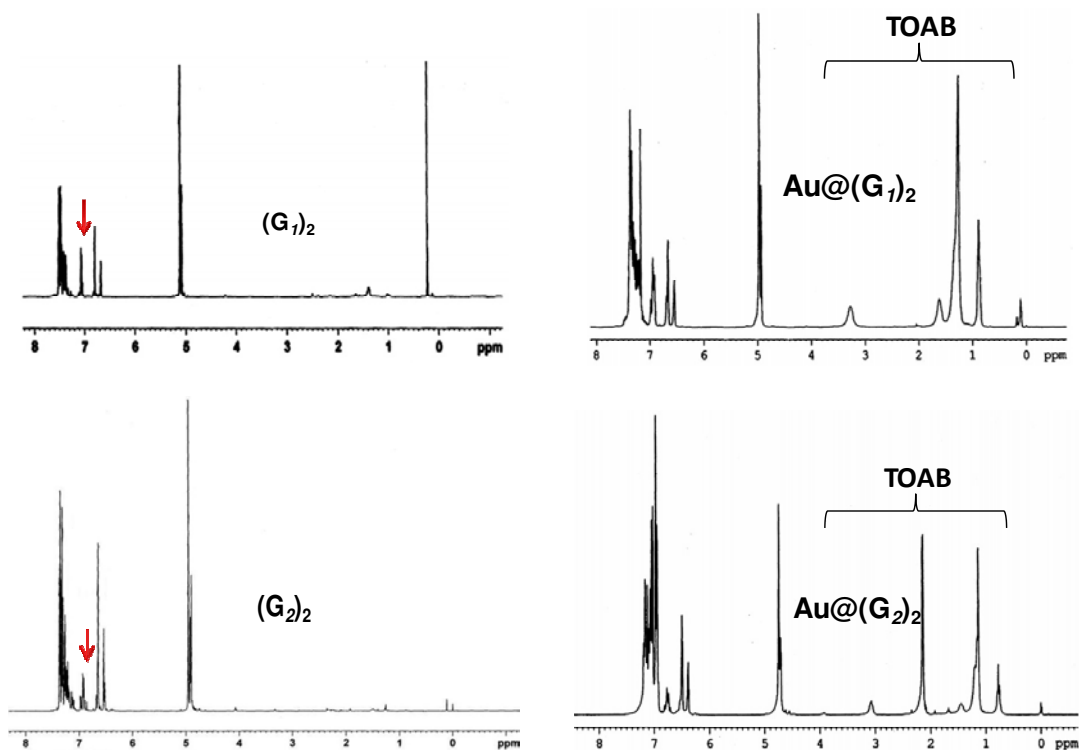


Figure 2.14 ¹H spectra of (*G_n)₂ (left) and **Au@(*G_n)₂*** (right) in CDCl₃.*

NMR spectra of $(G_1)_2$ and $(G_2)_2$ exhibited sharp peaks and the peaks due to the biphenyl group (^1H and ^{13}C) are identified by arrows. NMR spectra of $\text{Au}@(\text{G}_1)_2$ and $\text{Au}@(\text{G}_2)_2$ also exhibited these sharp peaks in addition to the peaks due to TOAB. Since all the NMR peaks in $(G_n)_2$ are also present in $\text{Au}@(\text{G}_n)_2$ we can safely suggest that the Au nanoparticle in this case is encapsulated in the dendrimer and not chemically attached to it. These NMR spectra are in sharp contrast to the NMR spectra of AuG_n shown in Figures 2.8 and 2.9, where we see considerable broadening of the ^1H NMR signals and absence of ^{13}C signals due to the phenyl group at the focal point which is covalently linked to the gold cluster.

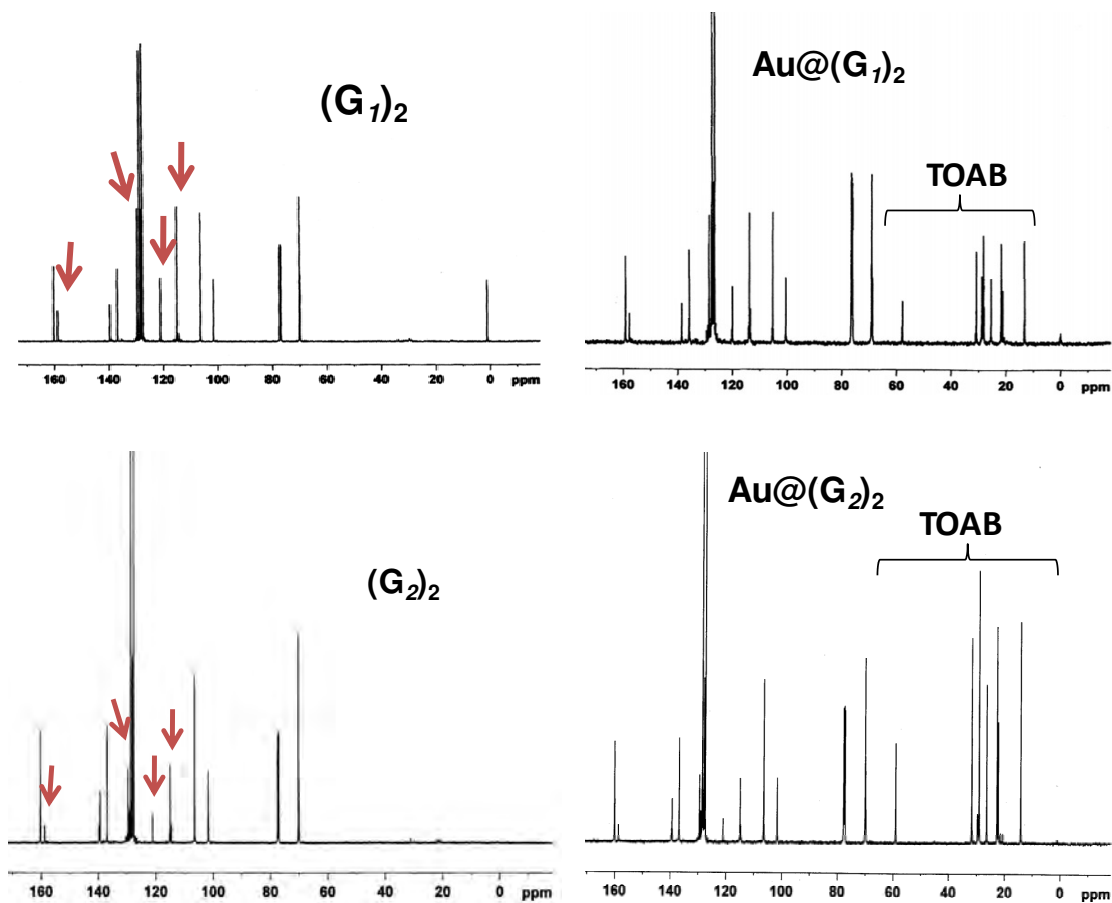


Figure 2.15 ^{13}C NMR spectra of $(G_1)_2$ (left) and $\text{Au}@(\text{G}_n)_2$ (right) in CDCl_3 .

The **Au@(G_n)₂** thus prepared were not very stable. Solutions of these materials in toluene or DCM when kept for long time periods became colourless with precipitation of the metal. Precipitation occurred within a few minutes in the case of **Au@(G_1)₂**, but other systems were stable for 1-2 days. We also observed that the gold nanoparticles in **Au@(G_n)₂** could be extracted into aqueous phase using DMAP. These control experiments clearly show that the dendrons are attached covalently to the Au clusters in **Au G_n** whereas in **Au@(G_n)₂**, the Au clusters are physically entrapped in the dendritic structure.

2.3.4 Stability of Au G_n

There are several studies dealing with the labile nature of metal-sulfur bonds in MPCs [Tarlov 1992; Huang 1993; Tarlov 1993; Delamarche 1994; Rieley 1996; Schoenfish 1998]. Scott *et al.* has recently studied the decomposition of dithiolate-protected MPCs by oxygen using ¹H NMR [Hou 2009]. They observed that bubbling oxygen for 2 h resulted in the development of ¹H NMR signals corresponding to free ligands. This was attributed to oxidation of the dithiolate ligand and its subsequent removal from the metal surface. The **Au G_n** we report here are not oxidized under similar conditions. ¹H NMR of **Au G_n** did not exhibit any change even after bubbling oxygen for 4 h.

2.3.5 Structure of Au G_n

Table 2.1 summarizes the TEM, TGA and absorption spectral data for **Au G_n** . Information from the TGA and TEM can be combined to obtain useful information about the actual structure of **Au G_n** . From the TEM size

distributions one can obtain the average core diameter (D) of the nanoparticles. The average number of gold atoms in a cluster can then be calculated using the following equation [Gopidas 2003 (a); Yang 2002].

$$N_{\text{Au}} = d (\pi/6) D^3 \quad (2.1)$$

In equation (2.1) d is the density of gold (59 atoms/nm³). Since the atomic weight of Au is 197, the weight of the gold core is given by

$$W_{\text{Au}} = N_{\text{Au}} \times 197 \quad (2.2)$$

The value thus obtained can be equated to the percentage weight of Au obtained from TGA, to obtain the total weight of the NCD. Weight due to the organic core in the NCD can be calculated and since we know the molecular weight of the dendron, we can calculate the average number of dendrons per NCD for each **AuG_n**. The values obtained are shown in Table 2.1 and also plotted in Figure 2.16. The results show that as the dendrimer generation increases, the number of dendrons attached to the gold core decreases. This is a generally expected trend and arises due to steric factors. The number of dendron units that can be attached to a metal core is decided by the steric requirements of the dendron unit and this is termed sterically induced stoichiometry (SIS) [Tomalia 1990; Swanson 2007]. As we proceed from one generation to the next higher generation, the molecular mass and size of dendron nearly doubles. Because of this size increase the number of dendrons that can be accommodated on the metal core decrease drastically as we go from **AuG₁** to **AuG₄**. If the metal cluster size remains same, the number of G₁ dendron units present in **AuG₁** will be approximately twice the number of G₂ dendrons present in

AuG₂. This logic seems to work in the case of **AuG₂ → AuG₄**, but the number of dendrons/NCD is much higher in the case of **AuG₁** (Table 2.1). Also, a comparison of the present results with previous literature reports shows that the number of dendrons attached to the gold core in the present NCDs is very high [Gopidas 2003 (a,b)].

Table 2.1 Optical and structural parameters of **AuG_n**.

NCD	λ_{\max}	Particle size		No. of dendrons/NCD
	(nm)	(nm)	% Au	
AuG₁	518	5.5	45	3161
AuG₂	520	4.7	48	845
AuG₃	523	5.4	54	475
AuG₄	522	4.9	48	229

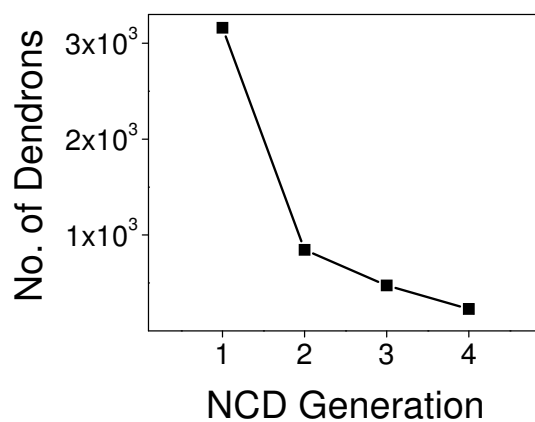
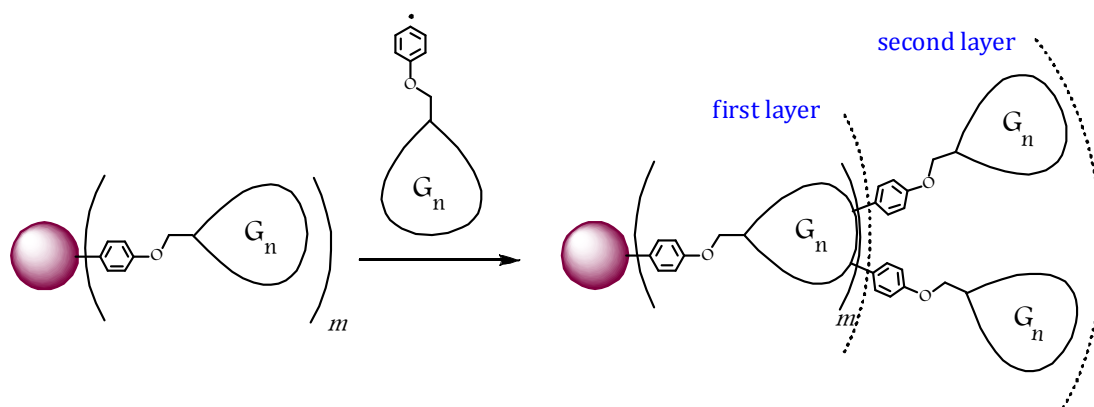


Figure 2.16 Plot of average number of dendrons against NCD generation.

We attribute the large dendron/NCD ratio to multiple layering of dendrons on NCD surface. It has been shown that multiple organic layers can form on metal surfaces during electrografting of aryl diazonium salts [Pinson 2005]. The aryl radical formed in the decomposition of the diazodendron is expected to be highly reactive and these can attack the first grafted dendron as shown in Scheme 2.5. In Scheme 2.5, we have shown the addition of two dendrons to a dendron in the first layer, but actual number depends on the availability of dendron radicals and steric factors.



Scheme 2.5 Schematic of possible dendron layering in **AuG_n**.

Because of the very high reactivity of aryl radicals, grafting of aryl groups through the diazonium route generally do not yield monolayers as against self-assembly of thiols on Au surfaces. The mechanism responsible for the multiple layering has been established by the groups of Podvorica and McDermott [Kariuki 1999; 2001; Anariba 2003; Combellas 2005; 2008; 2009; Adenier 2006; Shewchuk 2009]. The reaction involves the addition of the aryl radical on to a phenyl group of the first layer to get a cyclohexadienyl-type adduct which is rearomatized by electron exchange

with another diazonium salt (see chapter 1 for details). We expect the same mechanism to operate here as well. In the case of NCDs in general, SIS would lead to a reduction in the number of dendrons attached onto the gold cluster and a corresponding increase in the volume of the void space available on the metal surface. For the **AuG_n** reported here all the dendrons in the NCD are not connected to the metal core. As a result the void space available on the metal surface cannot be correlated directly to the dendron number.

2.4 Conclusion

We have shown that simultaneous reduction of diazo-functionalized Fréchet-type dendron and H₂AuCl₄, taken in an organic medium, leads to the formation of Au nanoparticle-cored dendrimers. Au-NCDs of generations 1-4 were thus prepared and characterized. Our studies showed that the Au-NCDs consisted of a gold core of ~ 5 nm diameter to which the dendrons of generations 1-4 are connected radially using gold-carbon bonds. These materials were stable almost indefinitely indicating the stabilization of the gold cluster through covalent bonds and not by encapsulation in dendron cavities. The NCDs exhibited a wine-red color and characterized by the plasmon absorption band of gold clusters around 520 nm. IR, ¹H and ¹³C NMR spectra suggested that the dendrons are linked to the Au core through the phenyl ring at the focal point of the dendron. Using the information from TGA and TEM studies we calculated the average number of dendrons attached to the metal core. The results suggested that the number of dendrons/NCD decreased with increase in

the dendron generation. The large dendron/NCD value could be due to multiple layering of dendrons.

2.5 Experimental

2.5.1 Materials and Methods

3,5-dihydroxybenzoic acid, benzyl bromide, carbon tetrabromide, triphenylphosphine, 18-crown-6, tetraoctylammonium bromide (TOAB), K_2CO_3 , $HAuCl_4$, $LiAlH_4$, $NaBH_4$, HBF_4 and *t*-butyl nitrite were purchased from Aldrich and used as received. Solvents such as acetone, toluene and dichloromethane (DCM) were obtained from MERCK and used as received. Dry tetrahydrofuran (THF) used for the synthesis was freshly distilled from sodium benzophenone ketyl. For the UV-Vis spectra, spectroscopic solvents from MERCK were used.

Melting points were determined on a Mel-Temp II melting point apparatus and are uncorrected. 1H NMR data were obtained from a 300 MHz Bruker Avance DPX spectrometer. ^{13}C NMR spectra were recorded using a 500 MHz Bruker Avance DPX spectrometer. FT-IR spectra were recorded on a Shimadzu IR Prestige 21 spectrometer. High-resolution mass spectra were obtained by using a JOEL JMS600 mass spectrometer. Absorption spectra were obtained using a Shimadzu 3101PC UV/Vis-NIR scanning spectrophotometer. TGA experiments were performed using a Perkin Elmer Pyris Diamond TG/DTA analyzer. TEM images of the particles were obtained with a 100 kV FEI-Tecnai 30G²S-Twin transmission electron microscope equipped with an EDAX energy-dispersive X-ray analysis system. Samples of TEM were prepared by drop-

casting one drop of a ~ 1 mg/mL **AuG_n** solution in DCM onto standard carbon-coated copper grids (300 mesh) and drying in air for 30 min.

2.5.2 Synthesis of AuG₁

2.5.2.a Synthesis of G₁NO₂

4-Nitrophenol (2.2 g, 16 mmol) and G₁Br (5.0 g, 13 mmol) were dissolved in dry acetone (30 mL) taken in a 100 mL 2-neck RB flask containing anhydrous K₂CO₃ (3.6 g, 26 mmol) and the reaction mixture was refluxed overnight under dry conditions. Acetone was evaporated and the residue was partitioned between water and DCM. Organic layer was collected and concentrated. Pale yellow crystals, yield = 5.65 g (98%), mp = 94 – 96 °C. IR (KBr) ν_{\max} (cm⁻¹) = 3063.56, 3030.71, 2963.36, 2904.47, 1595.12, 1510.45, 1448.52, 1376.25, 1336.54, 1289.25, 1261.25, 1161.15, 1053.13, 802.32, 736.28, 696.32, 632.21, 465.07. ¹H NMR (300 MHz, TMS, CDCl₃, δ): 5.05 – 5.09 (m, 6H), 6.62 – 6.67 (m, 3H), 6.98 – 7.0 (d, 2H), 7.32 – 7.44 (m, 10H), 8.17 – 8.19 (d, 2H) ppm. ¹³C NMR (75 MHz, TMS, CDCl₃, δ): 70.08, 70.39, 101.76, 106.27, 114.31, 114.81, 125.81, 127.42, 128.0, 128.54, 136.55, 137.87, 141.61, 160.24, 163.46 ppm. HRMS (FAB, m/z): Calcd for C₂₇H₂₃NO₅, 441.48; found, 442.

2.5.2.b Synthesis of G₁NH₂

G₁NO₂ (2.0 g, 4.5 mmol) was dissolved in THF (5 mL) and made into a suspension with zinc powder. Conc. HCl (10 mL) was added to it drop wise and the reaction mixture was heated at 60 °C, for 4 h. It was then neutralized and extracted with water. Organic layer was collected and

concentrated. Yield = 1.5 g (80%). IR (KBr) ν_{\max} (cm^{-1}) = 3445.21, 3366.26, 3060.27, 3030.48, 2901.16, 1595.32, 1510.23, 1498.56, 1450.22, 1376.34, 1294.28, 1163.26, 908.48, 822.29, 736.85, 694.21, 521.10. ^1H NMR (300 MHz, TMS, CDCl_3 , δ): 4.79 – 4.90 (m, 8H), 6.44 – 6.57 (m, 5H), 7.20 – 7.28 (m, 12H) ppm. ^{13}C NMR (125 MHz, TMS, CDCl_3 , δ): 70.79, 101.23, 101.53, 106.31, 115.98, 116.64, 127.10, 127.85, 128.52, 136.62, 139.22, 139.57, 139.96, 152.08, 160.02 ppm. HRMS (FAB, m/z): Calcd for $\text{C}_{27}\text{H}_{25}\text{NO}_3$, 411.49; found, 412.32.

2.5.2.c Synthesis of $\text{G}_1\text{N}_2^+\text{BF}_4^-$

G_1NH_2 (500.0 mg, 1.22 mmol) was dissolved in acetic acid-propionic acid mixture (1:1, 10 mL) and HBF_4 (10 mL) was added to it. The reaction mixture was stirred at $-10\text{ }^\circ\text{C}$ followed by the addition of NaNO_2 (420.0 mg, 6 mmol). Temperature was allowed to rise to $10\text{ }^\circ\text{C}$ and distilled water was added to precipitate the product, which was filtered, washed with water and dried. Yield = 400.0 mg (65%). IR (KBr) ν_{\max} (cm^{-1}) = 3084.18, 3062.21, 3030.87, 2885.23, 2237.43, 1595.13, 1577.77, 1493.26, 1450.47, 1382.26, 1338.60, 1282.66, 1217.08, 1149.57, 1083.99, 1062.78, 1026.13, 910.40, 839.03, 804.32, 742.39, 698.23, 648.08, 607.58, 518.85, 487.99, 460.99, 408.91. ^1H NMR (300 MHz, TMS, CDCl_3 , δ): 4.92 – 5.09 (m, 6H), 6.51 – 6.69 (m, 3H), 7.26 – 7.4 (m, 12H), 8.33 (s, 2H) ppm. ^{13}C NMR (125 MHz, TMS, CDCl_3 , δ): 70.0, 101.68, 102.31, 106.62, 118.08, 127.47, 127.96, 128.51, 135.73, 136.36, 136.52, 160.13, 168.49 ppm.

2.5.2.d Synthesis of **AuG₁**

To a stirred solution of $G_1N_2^+BF_4^-$ (132.0 mg, 0.26 mmol) in toluene, an aqueous solution of $HAuCl_4$ (44.0 mg, 0.13 mmol) was added followed by tetra-*n*-octylammonium bromide (106.0 mg, 0.19 mmol). Stirring was continued until the aqueous phase became colorless. Organic phase was separated and washed twice with water. Simultaneous reduction of diazonium salt and Au(III) was effected by the addition of 15 mL aqueous $NaBH_4$ (74 mg, 2 mmol) while the reaction mixture was stirred for 5 h at room temperature. Organic phase was separated and washed twice with 0.5 M H_2SO_4 , 0.5 M Na_2CO_3 and finally with water. Toluene was evaporated and the residue obtained was sonicated several times with ethanol until the alcohol layer become colorless. Further purification was carried out by column chromatography (silica gel). **AuG₁** nanoparticle band was eluted using methanol. IR (KBr) ν_{max} (cm^{-1}) = 3084.18, 3061.03, 3030.17, 2872.01, 1597.06, 1506.41, 1452.40, 1375.25, 1294.24, 1242.16, 1219.01, 1157.29, 1058.92, 1026.13, 908.47, 831.32, 736.81, 698.23, 632.65, 522.71, 459.06. 1H NMR (500 MHz, TMS, $CDCl_3$, δ): 4.997 (broad), 6.37 – 6.57 (broad), 7.25 – 7.35 (broad) ppm. ^{13}C NMR (125 MHz, TMS, $CDCl_3$, δ): 70.09, 101.56, 106.13, 127.53, 127.99, 128.56, 136.71, 160.15 ppm.

2.5.3 Synthesis of **AuG₂**

2.5.3.a Synthesis of G_2NO_2

4-Nitrophenol (216.0 mg, 1.6 mmol) and G_2Br (1.0 g, 1.2 mmol) were dissolved in dry acetone (10 mL) taken in a 100 mL 2-neck RB flask containing anhydrous K_2CO_3 (350.0 mg, 2.5 mmol) and the reaction

mixture was refluxed overnight under dry conditions. Acetone was evaporated and the residue was partitioned between water and DCM. Organic layer was collected and concentrated. White powder, yield = 1.05 g (98%), mp = 120 – 125 °C. IR (KBr) ν_{\max} (cm⁻¹) = 3062.96, 3030.17, 2962.66, 2906.73, 2866.22, 1595.13, 1510.26, 1448.54, 1375.26, 1336.67, 1296.16, 1261.45, 1161.15, 1053.13, 802.39, 736.81, 696.30, 632.65, 499.56, 464.84. ¹H NMR (300 MHz, TMS, CDCl₃, δ): 4.86 – 4.94 (m, 14H), 6.47 – 6.56 (m, 9H), 6.83 – 6.86 (d, 2H), 7.21 – 7.31 (m, 20H), 8.02 – 8.05 (d, 2H) ppm. ¹³C NMR (125 MHz, TMS, CDCl₃, δ): 69.91, 70.35, 101.40, 101.77, 106.31, 114.79, 125.82, 127.98, 128.54, 136.64, 137.85, 139, 141.59, 160.12, 163.43 ppm. HRMS (FAB, m/z) Calcd for C₅₅H₄₇NO₉, 865.96; found, 866.58.

2.5.3.b Synthesis of G₂NH₂

G₂NO₂ (2.0 g, 2.3 mmol) was dissolved in THF (10 mL) and made into a suspension with zinc powder (8.0 g). Conc. HCl (30 mL) was added to it drop wise and the reaction mixture was heated at 60 °C, for 4 h. It was then neutralized and extracted with water. Organic layer was collected and concentrated. Yield = 1.6 g (85%). IR (KBr) ν_{\max} (cm⁻¹) = 3446.79, 3367.71, 3086.11, 3061.03, 3030.17, 2904.80, 2864.29, 1595.13, 1510.26, 1498.69, 1450.47, 1375.25, 1323.17, 1294.24, 1230.58, 1163.08, 1058.99, 908.47, 827.46, 736.81, 696.30, 634.58, 514.99, 482.20. ¹H NMR (300 MHz, CDCl₃): δ = 4.82 – 4.93 (m, 14H), 6.49 – 6.71 (m, 12H), 7.22 – 7.31 (m, 21H). ¹³C NMR (125 MHz, CDCl₃): δ = 69.89, 70.56, 101.23, 101.53, 106.31, 115.98, 116.64, 127.10, 127.94, 128.52, 136.72, 139.22, 139.57, 139.96,

152.07, 160.09. HRMS (FAB, m/z) Calcd for C₅₅H₄₉NO₇, 835.98; found, 836.79.

2.5.3.c Synthesis of G₂N₂⁺BF₄⁻

G₂NH₂ (500.0 mg, 0.6 mmol) was dissolved in acetic acid-propionic acid mixture (1:1, 10 mL) and HBF₄ (10 mL) was added to it. The reaction mixture was stirred at -10 °C followed by the addition of NaNO₂ (200.0 mg, 2.9 mmol). Temperature was allowed to rise to 10 °C and distilled water was added to precipitate the product, which was filtered, washed with water and dried. Yield = 300.0 mg (54%). IR (KBr) ν_{\max} (cm⁻¹) = 3030.15, 2931.80, 2873.94, 2245.14, 1595.13, 1494.83, 1450.47, 1375.25, 1340.53, 1290.28, 1215.15, 1157.29, 1056.29, 910.40, 835.18, 738.74, 698.23, 632.65, 522.71, 459.06. ¹H NMR (300 MHz, TMS, CDCl₃, δ): 4.76 – 4.93 (m, 14H), 6.23 – 6.58 (m, 9H), 7.14 – 7.3 (m, 22H), 8.2 (s, 2H) ppm. ¹³C NMR (75 MHz, TMS, CDCl₃, δ): 69.64, 70.04, 101.52, 102.42, 106.37, 118.06, 127.45, 127.88, 128.46, 135.68, 136.69, 139.05, 160.03, 168.48 ppm.

2.5.3.d Synthesis of AuG₂

To a stirred solution of G₂N₂⁺BF₄⁻ (100.0 mg, 0.1 mmol) in toluene, an aqueous solution of HAuCl₄ (20.0 mg, 0.05 mmol) was added followed by tetraoctylammonium bromide (44.0 mg, 0.08 mmol). Stirring was continued until the aqueous phase became colorless. Organic phase was separated and washed twice with water. 10mL aqueous NaBH₄ (28 mg, 0.75 mmol) was added to it and the reaction mixture was stirred for 5 h at room temperature. Organic phase was separated and washed twice with 0.5 M H₂SO₄, 0.5 M Na₂CO₃ and finally with water. Toluene was evaporated

and the residue obtained was sonicated several times with ethanol until the alcohol layer become colorless. Further purification was carried out by column chromatography (silica gel). Nanoparticle band was eluted using methanol. IR (KBr) ν_{\max} (cm^{-1}) = 3030.17, 2932.21, 2245.36, 1595.13, 1506.41, 1450.47, 1373.32, 1319.31, 1296.16, 1244.09, 1217.08, 1157.29, 1055.06, 833.25, 736.81, 698.21, 418.55. ^1H NMR (500 MHz, TMS, CDCl_3 , δ): 4.97 – 5.02 (broad), 6.57 – 6.65 (broad), 7.26 (broad) ppm. ^{13}C NMR (125 MHz, TMS, CDCl_3 , δ): 69.93, 70.04, 101.55, 106.30, 127.48, 127.94, 128.19, 128.52, 136.73, 139.19, 160.02 ppm.

2.5.4 Synthesis of AuG_3

2.5.4.a Synthesis of G_3NO_2

4-Nitrophenol (302.0 mg, 2.2 mmol) and G_3Br (3.0 g, 1.8 mmol) were dissolved in dry acetone (30 mL) taken in a 100 mL 2-neck RB flask containing anhydrous K_2CO_3 (400.0 mg, 2.8 mmol) and the reaction mixture was refluxed overnight under dry conditions. Acetone was evaporated and the residue was partitioned between water and DCM. Organic layer was collected and concentrated to yield G_3NO_2 as a glassy solid. Yield = 3.05 g (97%). IR (KBr) ν_{\max} (cm^{-1}) = 3061.46, 3030.57, 2952.66, 2866.22, 1596.13, 1510.26, 1448.54, 1375.26, 1336.67, 1296.16, 1261.45, 1161.15, 1053.13, 910.23, 802.39, 736.81, 685.30, 476.84. ^1H NMR (300 MHz, TMS, CDCl_3 , δ): 4.84 – 4.90 (m, 30H), 6.46 – 6.56 (m, 20H), 6.80 – 6.83 (d, 2H), 7.20 – 7.28 (m, 41H), 8.0 – 8.03 (d, 2H) ppm. ^{13}C NMR (125 MHz, TMS, CDCl_3 , δ): 69.88, 70.0, 70.30, 101.42, 101.47, 106.31,

114.75, 125.77, 127.47, 127.93, 128.50, 136.67, 137.85, 139.00, 139.10, 141.54, 159.99, 160.08, 163.39 ppm.

2.5.4.b Synthesis of G_3NH_2

G_3NO_2 (2.0 g, 1.2 mmol) was dissolved in THF (10 mL) and made into a suspension with zinc powder (2.0 g). Conc. HCl (12 mL) was added to it drop wise and the reaction mixture was heated at 60 °C, for 4 h. It was then neutralized and extracted with water. Organic layer was collected and concentrated to get G_3NH_2 as a glassy solid. Yield = 1.6 g (82 %). IR (KBr) ν_{max} (cm^{-1}) = 3442.17, 3362.32, 3062.96, 3030.17, 2929.87, 2912.51, 2872.01, 1595.13, 1510.26, 1496.76, 1450.47, 1373.32, 1342.46, 1321.24, 1296.16, 1230.58, 1157.29, 1055.06, 910.40, 831.32, 736.80, 696.30, 682.80, 532.65. 1H NMR (300 MHz, TMS, $CDCl_3$, δ): 4.79 – 4.90 (m, 30H), 6.47 – 6.65 (m, 22H), 7.23 – 7.29 (m, 43H) ppm. ^{13}C NMR (125 MHz, TMS, $CDCl_3$, δ): 69.90, 70.02, 101.53, 106.32, 114.33, 115.59, 115.99, 116.31, 127.50, 127.94, 128.52, 136.70, 139.15, 139.21, 140.16, 151.79, 159.98, 160.08 ppm.

2.5.4.c Synthesis of $G_3N_2^+BF_4^-$

To a solution of G_3NH_2 (210.0 mg, 0.125 mmol) in THF-DCM (1:3, 6 mL), HBf_4 (2 mL) was added and the reaction mixture was cooled to -10 °C. *t*-Butyl nitrite (25.0 mg, 0.25 mmol) was added and the reaction mixture stirred for 30 min followed by the addition of excess diethyl ether to precipitate the product, which was filtered, washed with diethyl ether and dried. Yield = 185.0 mg (83%). IR (KBr) ν_{max} (cm^{-1}) = 3062.96, 3030.17, 2995.01, 2910.58, 2872.01, 2243.21, 1593.23, 1496.76, 1444.68,

1371.39, 1342.46, 1321.26, 1294.24, 1215.15, 1157.29, 1055.06, 908.47, 833.25, 736.81, 696.30, 522.71. ^1H NMR (300 MHz, TMS, CDCl_3 , δ): 4.84 – 4.99 (m, 30H), 6.5 – 6.66 (m, 20H), 7.27 – 7.37 (m, 43H), 8.21 (s, 2H) ppm. ^{13}C NMR (125 MHz, TMS, CDCl_3 , δ): 70.01, 101.53, 105.77, 106.39, 114.87, 118.07, 126.96, 127.50, 127.94, 128.20, 128.52, 129.34, 135.50, 136.73, 139.21, 140.83, 157.92, 160.09, 168.50 ppm.

2.5.4.d Synthesis of **AuG₃**

To a stirred solution of $\text{G}_3\text{N}_2^+\text{BF}_4^-$ (400.0 mg, 0.22 mmol) in toluene, an aqueous solution of HAuCl_4 (38.0 mg, 0.11 mmol) was added followed by tetraoctylammonium bromide (92.0 mg, 0.17 mmol). Stirring was continued until the aqueous phase became colorless. Organic phase was separated and washed twice with water. Simultaneous reduction of diazonium salt and Au(III) was effected by the addition of NaBH_4 (64.0 mg, 1.7 mmol) in methanol (15 mL) at $-20\text{ }^\circ\text{C}$ and the reaction mixture was stirred for 48 h at room temperature. Organic phase was separated and washed twice with 0.5 M H_2SO_4 , 0.5 M Na_2CO_3 and finally with water. Toluene was evaporated and the residue obtained was sonicated several times with ethanol until the alcohol layer become colorless. Further purification was carried out by column chromatography (silica gel). Nanoparticle band was eluted using acetone. IR (KBr) ν_{max} (cm^{-1}) = 3030.17, 2929.87, 2914.44, 2872.01, 1595.13, 1498.69, 1448.54, 1373.32, 1321.24, 1296.16, 1215.15, 1157.29, 1055.06, 910.40, 833.25, 738.74, 698.23, 632.65, 460.99. ^1H NMR (300 MHz, TMS, CDCl_3 , δ): 4.92 – 4.97 (m), 6.54 – 6.65 (m), 7.18 – 7.36 (m) ppm. ^{13}C NMR (125 MHz, TMS, CDCl_3 ,

δ): 69.93, 70.05, 101.53, 106.33, 127.52, 128.54, 136.70, 139.17, 143.47, 159.99, 160.10 ppm.

2.5.5 Synthesis of AuG₄

2.5.5.a Synthesis of G₄NO₂

4-Nitrophenol (50.0 mg, 0.36 mmol) and G₄Br (1.0 g, 0.3 mmol) were dissolved in dry acetone (10 mL) taken in a 100 mL 2-neck RB flask containing anhydrous K₂CO₃ (103.0 mg, 0.75 mmol) and the reaction mixture was refluxed overnight under dry conditions. Acetone was evaporated and the residue was partitioned between water and DCM. Organic layer was collected and concentrated to get G₄NO₂ as a glassy solid. Yield = 963.0 mg (95%). IR (KBr) ν_{\max} (cm⁻¹) = 3061.46, 3030.57, 2952.66, 2866.22, 1596.13, 1510.26, 1448.54, 1375.26, 1336.67, 1296.16, 1261.45, 1161.15, 1053.13, 910.23, 802.39, 736.81, 685.30, 476.84. ¹H NMR (300 MHz, TMS, CDCl₃, δ): 4.62 – 4.86 (m, 62H), 6.33 – 6.54 (m, 45H), 6.73 – 6.76 (d, 2H), 7.11 – 7.25 (m, 80H), 7.94 – 7.97 (d, 2H) ppm. ¹³C NMR (125 MHz, TMS, CDCl₃, δ): 69.83, 69.94, 101.46, 106.29, 114.68, 125.72, 127.45, 127.88, 128.46, 136.66, 137.81, 139.10, 141.48, 159.96, 160.04, 163.33.

2.5.5.b Synthesis of G₄NH₂

G₄NO₂ (750.0 mg, 0.22 mmol) was dissolved in THF (5 mL) and made into a suspension with zinc powder (1.4 g). Conc. HCl (3 mL) was added to it drop wise and the reaction mixture was heated at 60 °C, for 4 h. It was then neutralized and extracted with water. Organic layer was

collected and concentrated to get a glassy solid. Yield = 595.0 mg (80%). IR (KBr) ν_{\max} (cm^{-1}) = 3445.29, 3365.89, 3062.96, 3030.17, 2929.87, 2872.01, 1595.13, 1510.26, 1496.76, 1450.47, 1373.32, 1340.53, 1321.24, 1296.16, 1215.15, 1157.29, 1053.13, 910.40, 831.32, 736.81, 696.30. ^1H NMR (300 MHz, TMS, CDCl_3 , δ): 4.9 – 4.96 (m, 62H), 6.5 – 6.63 (m, 47H), 7.09 – 7.35 (m, 82H) ppm. ^{13}C NMR (125 MHz, TMS, CDCl_3 , δ): 69.85, 69.95, 101.49, 106.29, 115.91, 127.07, 127.23, 127.64, 127.90, 128.17, 128.35, 128.49, 136.69, 136.81, 139.14, 139.27, 159.95, 160.04 ppm.

2.5.5.c Synthesis of $\text{G}_4\text{N}_2^+\text{BF}_4^-$

To a solution of G_4NH_2 (250.0 mg, 0.074 mmol) in THF-DCM (1:3, 6 mL), HBF_4 (2 mL) was added and the reaction mixture was cooled to -10°C . *t*-Butyl nitrite (25.0 mg, 0.25 mmol) was added and the reaction mixture stirred for 30 min followed by the addition of excess diethyl ether to precipitate the product, which was filtered, washed with diethyl ether and dried. Yield = 213.0 mg (83%). IR (KBr) ν_{\max} (cm^{-1}) = 3086.11, 3030.17, 2872.01, 2235.50, 1662.64, 1595.13, 1537.27, 1496.76, 1450.47, 1373.32, 1321.24, 1296.16, 115.36, 1053.13, 910.40, 835.18, 746.45, 698.23, 632.65, 520.78, 484.13, 460.99. ^1H NMR (300 MHz, TMS, CDCl_3 , δ): 4.86 – 4.96 (m, 62H), 6.50 – 6.61 (m, 45H), 7.23 – 7.32 (m, 82H), 8.08 (b, 2H) ppm. ^{13}C NMR (125 MHz, TMS, CDCl_3 , δ): 67.31, 69.62, 69.34, 100.55, 107.29, 107.67, 124.60, 126.11, 126.50, 126.93, 127.19, 127.51, 127.96, 128.43, 128.71, 133.44, 135.72, 138.18, 139.93, 159.09 ppm.

2.5.5.d Synthesis of **AuG₄**

To a stirred solution of $G_4N_2^+BF_4^-$ (200.0 mg, 0.057 mmol) in toluene, an aqueous solution of $HAuCl_4$ (10.0 mg, 0.029 mmol) was added followed by tetraoctylammonium bromide (24.0 mg, 0.044 mmol). Stirring was continued until the aqueous phase became colorless. Organic phase was separated and washed twice with water. It was cooled to $-20\text{ }^\circ\text{C}$ and a solution of $NaBH_4$ (16.0 mg 0.42 mmol) in methanol (5 mL) was added and the reaction mixture was stirred for 48 h at room temperature. Organic phase was separated and washed twice with 0.5 M H_2SO_4 , 0.5 M Na_2CO_3 and finally with water. Toluene was evaporated and the residue obtained was sonicated several times with ethanol until the alcohol layer become colorless. Further purification was carried out by column chromatography (silica gel). Nanoparticle band was eluted using acetone. IR (KBr) ν_{max} (cm^{-1}) = 3061.03, 3030.17, 2927.94, 2870.08, 1595.13, 1496.76, 1452.40, 1373.32, 1321.20, 1296.16, 1263.37, 1155.36, 1053.13, 833.25, 736.81, 696.30. 1H NMR (500 MHz, TMS, $CDCl_3$, δ): 4.82 - 4.92 (m), 6.42 - 6.55 (m), 7.15 - 7.22 (m) ppm. ^{13}C NMR (125 MHz, TMS, $CDCl_3$, δ): 70.0, 101.54, 106.31, 127.49, 127.92, 128.51, 136.72, 139.17, 160.0, 160.08 ppm.

2.5.6 Control Experiments

2.5.6.a Reduction of G_1 diazodendron in the absence of Au(III)

G_1 diazodendron (0.25 mmol) was dissolved in DCM and reduced using an aqueous solution of $NaBH_4$ (1.9 mmol) under ice cold conditions. After the reaction, organic layer was extracted and washed with water,

dried and concentrated. The residue obtained was further purified by column chromatography. ^1H NMR (500 MHz, TMS, CDCl_3 , δ): 5.08 – 5.13 (m, 12H), 6.68 (s, 2H), 6.79 – 6.8 (m, 3H), 7.05 – 7.07 (m, 5H), 7.37 – 7.52 (m, 24H) ppm. ^{13}C NMR (125 MHz, TMS, CDCl_3 , δ): 69.88, 70.18, 101.61, 106.43, 114.97, 121.1, 127.68, 128.11, 128.69, 129.6, 136.89, 139.67, 158.79, 160.26 ppm. HRMS (FAB, m/z) Calcd for $\text{C}_{54}\text{H}_{46}\text{O}_6$, 790.94; found, 814.23 (M+Na).

2.5.6.b Reduction of Au(III) in presence of $(\text{G}_1)_2$

$(\text{G}_1)_2$ (0.06 mmol) was dissolved in DCM and stirred with an aqueous solution of HAuCl_4 (0.12 mmol) followed by the addition of TOAB. After stirring for 1 h at room temperature, the organic layer was separated and reduced using NaBH_4 (1.9 mmol) under ice cold conditions. The reaction mixture was then stirred at room temperature for 24 h. After the reaction time, the reaction mixture was extracted with 0.5 M H_2SO_4 , 0.5 M Na_2CO_3 and finally with water. Organic layer was collected and concentrated. The residue obtained was dried and analyzed. ^1H NMR (500 MHz, TMS, CDCl_3 , δ): 4.93 – 4.96 (m, 12H), 6.54 (s, 2H), 6.54 – 6.68 (m, 3H), 6.9 – 6.93 (m, 5H), 7.21 – 7.45 (m, 24H) ppm. ^{13}C NMR (125 MHz, TMS, CDCl_3 , δ): 13.32, 21.82, 25.49, 28.25, 28.31, 28.9, 30.89, 69.04, 69.17, 100.61, 105.44, 113.99, 120.14, 126.71, 127.15, 127.73, 128.66, 135.92, 138.72, 157.82, 159.29 ppm.

2.5.6.c Reduction of G_2 diazodendron in the absence of Au(III)

G_2 diazodendron (0.25 mmol) was reduced using NaBH_4 (1.9 mmol) under the same conditions used for the synthesis of Au NCDs. Organic

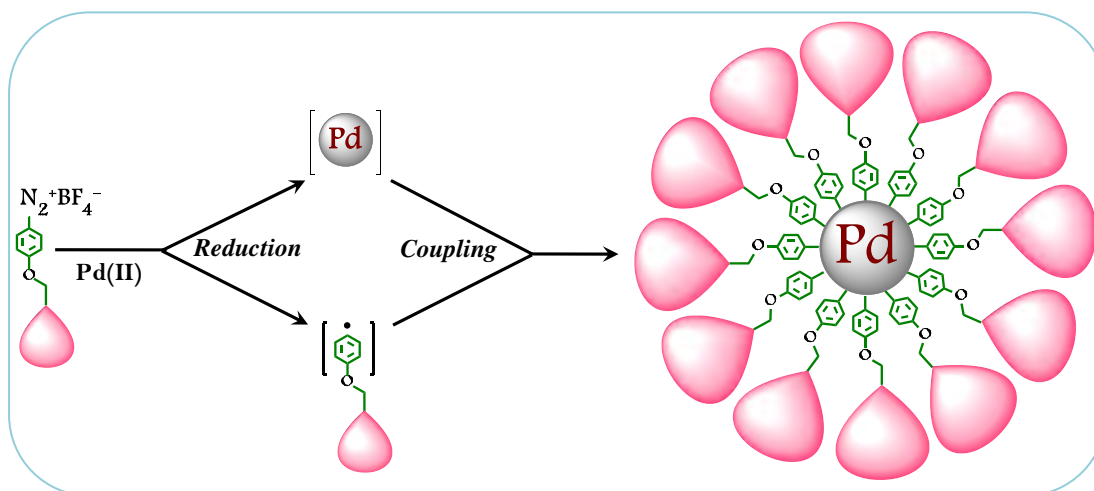
layer was separated and product isolated and purified as in 2.5.6.a. ^1H NMR (500 MHz, TMS, CDCl_3 , δ): 4.9 – 4.95 (m, 28H), 6.5 (s, 6H), 6.54 – 6.66 (m, 10H), 6.91 – 6.93 (m, 4H), 7.21 – 7.36 (m, 46H) ppm. ^{13}C NMR (125 MHz, TMS, CDCl_3 , δ): 69.9, 70.2, 101.72, 106.52, 115.01, 121.15, 127.72, 128.4, 128.73, 129.65, 136.93, 139.74, 160.2, 160.31 ppm.

2.5.6.d Reduction of Au(III) in presence of $(\text{G}_2)_2$

Reduction of HAuCl_4 (0.12 mmol) was carried out using NaBH_4 (1.9 mmol) in presence of $(\text{G}_2)_2$ (0.06 mmol) under the same conditions mentioned in 2.5.6.b. ^1H NMR (500 MHz, TMS, CDCl_3 , δ): 4.94 – 4.99 (m, 28H), 6.58 (s, 6H), 6.69 – 6.71 (m, 10H), 6.94 – 6.96 (m, 4H), 7.21 – 7.40 (m, 46H) ppm. ^{13}C NMR (125 MHz, TMS, CDCl_3 , δ): 13.32, 20.32, 21.59, 28.31, 28.06, 28.69, 30.64, 68.79, 68.88, 100.46, 105.25, 113.76, 119.87, 126.84, 127.05, 127.34, 127.86, 135.75, 138.23, 159, 159.09 ppm.

Chapter 3

Synthesis and Characterization of Palladium Nanoparticle-Cored Dendrimers Stabilized by Direct Carbon-Metal Bonds



3.1 Abstract

The synthesis and characterization of palladium NCDs of generation 1-4, where the dendron ligands are linked to the metal cluster at the core through Pd-C bonds are reported in this chapter. Synthesis of these NCDs was accomplished by the reduction of the corresponding diazodendrons in the presence of Pd(II). NCDs thus prepared were black powders freely soluble in common organic solvents and stable for several months both in solid as well as solution state. All the NCDs and precursor diazodendrons were characterized using IR, NMR and UV-visible spectroscopies. In the IR spectra of diazodendrons the characteristic diazo stretching vibration band was observed around 2230 cm^{-1} whereas this band was absent in the IR spectra of NCDs. ^1H NMR of lower generation Pd-NCDs were broadened significantly due to the presence of the metal cluster. In the ^{13}C NMR spectra signals due to the carbon atoms of the phenyl ring directly attached to the Pd cluster were absent. UV-visible spectra of NCDs did not exhibit a plasmon absorption band and consisted of a continuously decreasing absorption profile with decrease in energy. TEM analysis of the NCDs indicated the presence of nearly spherical, polydisperse metal particles with a core diameter of 2-4 nm.

3.2 Introduction

The vital position of palladium in organic synthesis makes the chemistry of palladium nanoparticles very attractive leading to extensive research which resulted in the discovery of large number of reactions catalyzed by Pd(0) complexes [Beletskaya 2000]. In several reactions catalyzed by Pd(0) complexes, formation of Pd nanoparticles during the reaction were reported [Reetz 1995; Li 2000]. Pd metal deposited on various support materials were used as catalysts for the last several decades [Yin 2007; Bergbreiter 2009]. In recent times the emphasis has shifted to the synthesis and study of Pd nanoparticles stabilized by different ligands such as polymers, dendrimers, surfactants etc for catalytic applications [Reetz 2004; Phan 2006]. Synthesis of palladium nanoparticle-cored dendrimers (Pd-NCD) for catalytic applications was first reported by Fox and co-workers [Gopidas 2003 (c)]. The synthesis, which made use of the strong affinity of thiol groups for transition metal surfaces, involved the reduction of Pd(II) in presence of thiol functionalized third generation Fréchet dendrons. The NCDs formed were thoroughly characterized by different spectroscopic techniques such as IR, NMR, and UV-visible and also by TEM. The formation of metal nanoparticles with an average core diameter of 2 nm was confirmed from TEM studies and detailed thermogravimetric analysis suggested that on the average 14 dendron ligands are linked to each palladium metal cluster.

The pioneering effort by Fox and co-workers [Gopidas 2003 (c)] was followed by the study of Fan and co-workers [Wu 2006] who reported the synthesis of palladium NCDs stabilized by dendron ligands possessing

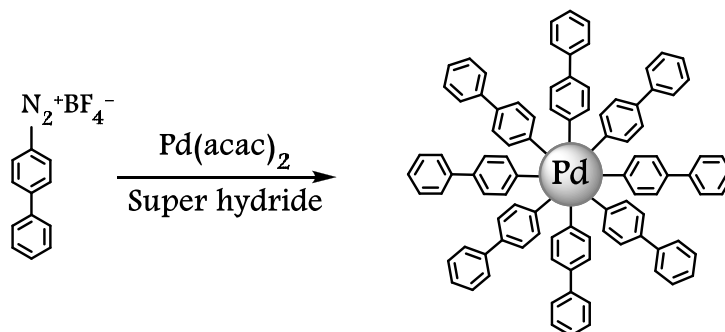
phosphine groups at the focal point. The synthetic sequence involved the reaction of different generation Fréchet type dendritic bromides with $KPPh_2$ to get the respective phosphine terminated dendrons. Reduction of $Pd(acac)_2$ in an autoclave using 25 atm hydrogen pressure at 60 °C for 18 h in presence of the phosphine-terminated dendrons resulted in the formation of dendron stabilized palladium nanoparticles as a black powder. Later the same group conducted detailed ^{31}P NMR studies and arrived at the conclusion that the phosphine dendrons might have undergone oxidation and the resulting dendron oxide may be stabilizing the palladium nanoparticles [Wu 2008]. However, a clear mechanism for the formation of the oxide could not be identified and the authors attributed trace amount of water present in the reaction medium as the possible source of oxygen. Kläui and co-workers [Glöckler 2007] earlier reported a similar oxidation of phosphine ligands during the synthesis of rhodium nanoparticles using hydrogen. The core-shell structures formed were further confirmed by TEM studies and size distribution analysis indicated that the mean particle diameter decreased with increase in the dendrimer generation. A similar trend has been reported earlier by Love *et al.* [2004] with dendrimer-stabilized metal nanoparticles.

As discussed in chapter 1, NCDs are expected to have applications in the area of catalysis. In the reports mentioned above, the authors also conducted studies to investigate the use of palladium NCDs as catalysts in different organic transformations. The thiol stabilized palladium NCDs reported by Fox and co-workers [Gopidas 2003 (c)] exhibited good catalytic activity in carbon-carbon bond forming reactions such as Heck

and Suzuki couplings under homogenous and heterogenous conditions. However, attempts to use this NCD as catalyst for hydrogenation reactions were unsuccessful. Upon exposure to hydrogen, the NCD underwent decomposition owing to the rapid hydrogenolysis of C-S bond, leading to precipitation of Pd metal. The NCDs reported by Fan and co-workers [Wu 2006; 2008] also catalyzed Suzuki and Stille coupling reactions efficiently. The stability of these nanocomposites has been further evidenced by recyclability of the NCD in the catalytic reactions. Unlike the thiol stabilized NCDs of Fox *et al.*, the palladium systems reported by Fan and co-workers was capable of catalyzing hydrogenation reactions of simple organic molecules but these reactions required elevated temperature and high hydrogen pressure. The non-recyclable nature of these catalysts for hydrogenation reactions cast doubts regarding their stability in presence of hydrogen. These reports suggest that new synthetic strategies for preparing Pd-NCDs with strong metal-ligand interactions are required for efficient catalysis. Other synthetic approaches developed for preparing palladium nanoparticles include vapour condensation, sonochemical reduction, electrochemical deposition etc. [Devenish 1996; Mizukoshi 1997; Mayer 1997; Nunomura 1998; Nemamcha 2006; Xiong 2007; Taratula 2007]. The covalent grafting of ligands on to the palladium nanoparticle surface is a recent addition to this classification [Ghosh 2008 (a)].

Chen and co-workers [Ghosh 2008 (a)] reported the first synthesis of palladium nanoparticles stabilized through a direct palladium-carbon bonding interaction. The authors achieved the desired palladium-ligand

interaction by adopting the synthetic strategy employed by Mirkhalaf *et al.* [2006] for the preparation of Au and Pt nanoparticles stabilized by metal-carbon linkages which involved the simultaneous reduction of the metal salt and 4-alkylbenzenediazonium fluoroborate. The authors synthesized the diazonium fluoroborates of 4-ethylaniline, 4-decylaniline and 4-aminobiphenyl and these were characterized by IR and NMR studies. Synthesis of nanoparticles involved the aqueous to organic phase transfer of Pd(II) using the diazonium salt followed by reduction of the organic phase with super hydride. The metal clusters thus obtained were characterized using IR and NMR spectroscopies as well as TEM analysis. A schematic illustration of the formation of biphenyl stabilized palladium nanoparticles is shown in Scheme 3.1.



Scheme 3.1 Formation of palladium nanoparticles stabilized by carbon-palladium bond.

Bond energy of Pd-S bond in thiol-stabilized Pd nanoparticles is 380 kJmol^{-1} , where as bond energy of Pd-C bond is 436 kJmol^{-1} in similar systems [Ghosh 2008 (a)]. Thus Pd nanoparticles stabilized by Pd-C bonds are expected to be much more stable compared to nanoparticles stabilized through Pd-S bonds. Based on this we anticipated that Pd nanoparticle-cored dendrimers would be ideal candidates as catalysts both in terms of

stability and efficiency. This has prompted us to synthesize Pd-NCDs of different generations and undertake a detailed study of the catalytic ability of these materials in various organic reactions.

In this chapter we describe the synthesis and characterization of Pd-NCDs of different generations stabilized by Pd-C bonds. Synthesis of the NCD was carried out by the reduction of G₁-G₄ Fréchet type diazodendrons using NaBH₄ in the presence of Pd(II). The as prepared NCDs were further purified and characterized by FT-IR, NMR and UV-Visible spectroscopic techniques as well as TEM analysis. TEM images confirmed the formation of almost spherical particles with a core diameter around 2-4 nm.

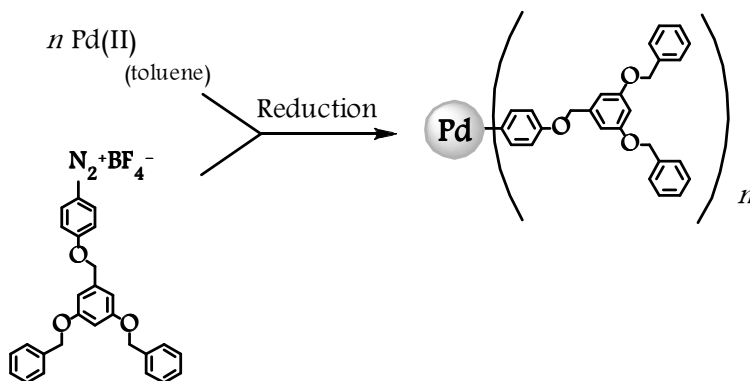
3.3 Results and Discussions

3.3.1 Syntheses

Fréchet-type dendritic bromides (G_nBr) were prepared using reported procedures [Hawker 1990; Wooley 1991; Kwock 1991; Percec 2006] and these were converted to corresponding diazonium salts as described in chapter 2 of this thesis. The bromides were treated with *p*-nitrophenol to get the respective nitrodendrons, which were reduced to get the amino derivatives. For diazotization reaction fluoroboric acid (HBF₄)/sodium nitrite was used. Diazodendrons were dark red powder, freely soluble in toluene and THF and insoluble in ethanol, methanol and diethyl ether. The diazodendrons were stable for about a week at room temperature and these were characterized by FT-IR, ¹H and ¹³C NMR. For example, IR spectra of the diazodendron exhibited the characteristic

diazonium peak at 2241 cm^{-1} [Mirkhalaf 2006; Ghosh 2008 (a,b,c)]. Detailed characterization of the diazodendron is given in section 2.3.1.c (Chapter 2).

Synthesis of Pd-NCDs of generation 1-4 (abbreviated in this chapter as **PdG_n**, where **n** varies from 1-4) was carried out as shown in Scheme 3.2. Aqueous solution of K_2PdCl_4 was stirred with a toluene solution of diazodendron followed by the addition of tetra-*n*-octylammonium bromide. After the complete transfer of Pd(II) from aqueous to organic phase, the latter was separated and reacted with sodium borohydride. Pd(II) is reduced by electron transfer from BH_4^\ominus to give Pd atoms, which undergo nucleation and growth to form small clusters. The dendritic diazonium salt upon receiving an electron from the reducing agent decomposes into nitrogen and dendron with phenyl radical [Pinson 2005; Ghosh 2008 (a)] at the focal point. At some stage of the Pd cluster growth, the dendron radicals get attached to the Pd surface, thereby arresting its growth and leading to the formation of **PdG_n**.



Scheme 3.2 Synthetic scheme for **PdG₁**.

The **PdG_n** thus prepared were black powder, stable in the solid form and in solution for several months, freely soluble in DCM, chloroform, THF

and toluene and insoluble in methanol, ethanol and ether. Dilute solutions of **PdG_n** exhibited a deep brown color. We observed that the NCDs incorporate a small percentage of TOAB (used as the phase-transfer agent) in the dendritic shell. Pd-NCDs can be chromatographed over silica gel without undergoing decomposition.

The NCDs synthesized were analyzed by IR, UV and NMR spectroscopy. Information about the size of the Pd core is obtained using transmission electron microscopy (TEM). Idealized structure of **PdG₄** is shown in Figure 3.1.

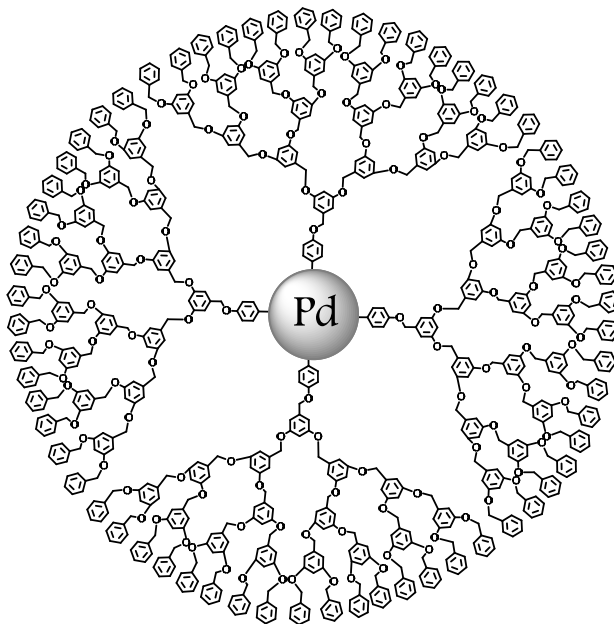


Figure 3.1 Idealized structure of **PdG₄**.

3.3.2 Characterization of PdG_n

3.3.2.1 FT-IR Spectra

In the case of Pd-NCD stabilized by Pd-S bonds, FT-IR spectra of the NCD and precursor disulfide dendron were nearly identical [Gopidas 2003 (c)]. In the present case IR spectra of the precursor diazodendrons were

different from those of the NCDs. FT-IR spectra of diazodendrons shown in Figure 3.2 clearly indicates the vibrational stretching of diazo group at $\approx 2245 \text{ cm}^{-1}$ [Mirkhalaf 2006; Ghosh 2008 (a,b,c)].

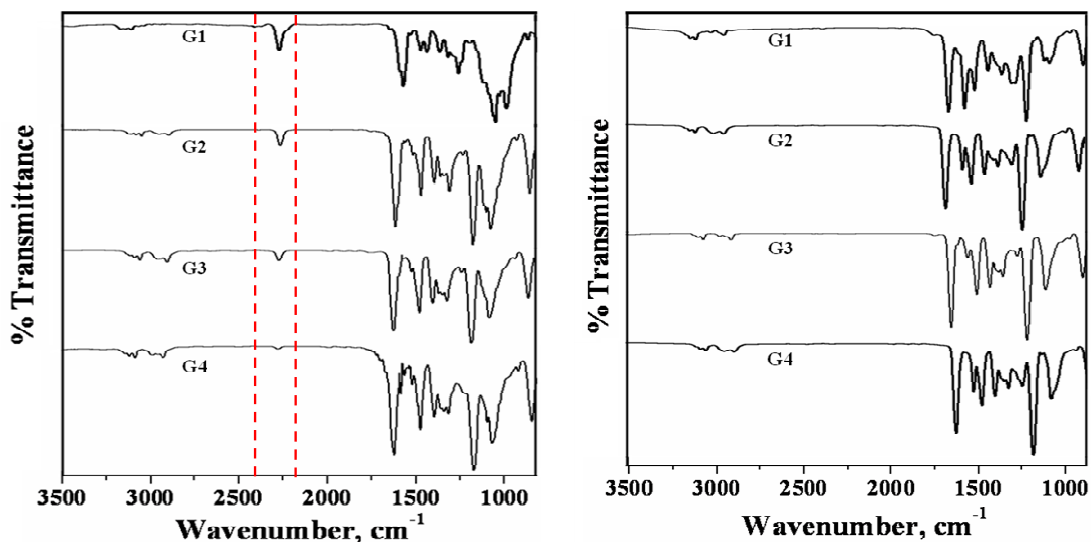


Figure 3.2 FT-IR spectra of diazodendrons and **PdG_n**.

FT-IR spectrum of **PdG_n** is also given in Figure 3.2. The diazo group decomposes during the reaction and hence this peak is absent in the IR spectrum of NCD. This also shows the absence of any diazo precursor in the NCD. IR spectra of the diazodendron and NCD were featured by methylene C-H stretching modes at $\nu_s = 2870$, $\nu_{as} = 2927 \text{ cm}^{-1}$ and aromatic C-H vibration modes at $\nu_s = 3030$ and $\nu_{as} = 3061 \text{ cm}^{-1}$.

3.3.2.2 ^1H and ^{13}C NMR Spectra

Figures 3.3 compare the ^1H NMR spectra of diazodendrons with that of the **PdG_n**. Signals at δ 8.2 and 7.0 (indicated by arrows) characterize the protons of the diazophenyl group. In the ^1H NMR spectrum of **PdG_n**, the diazophenyl proton signals have vanished and all

signals exhibited considerable broadening. The complete disappearance of these signals corresponding to the diazophenyl ring protons indicate the absence any diazodendron precursor in the Pd-NCDs. Broadening of the NMR peaks due to fast spin-spin relaxation of atoms close to a metal core or size-dependent spin-spin relaxation clearly supports the metal core-organic shell type structure of the NCD [Terrill 1995; Badia 1996; Hostetler 1998; Mirkhalaf 2006; Ghosh 2008 (a,b,c)]. The observed NMR signal broadening further confirms the presence of dendron ligands close to palladium surface [Ghosh 2008 (b)]. The signals seen at $\delta < 3$ ppm in the ^1H NMR of NCD are assigned to protons of TOAB, which is present as an impurity.

Figure 3.4 is a comparison of the ^{13}C NMR spectrum of diazodendrons and the corresponding **PdG_n**. In the case of the diazodendrons, signals at δ 168, 135, 118 and 71 ppm are identified as belonging to the diazo-bearing phenyl ring and its nearest benzyl carbon (marked by arrows in Figure 3.3). In the ^{13}C NMR spectrum of **PdG_n** the above peaks are not seen. Similar observations were made previously for MPCs and it was suggested that the signals due to the carbon atoms on the phenyl ring linked directly to the metal have broadened so much that they are indistinguishable from the background [Mirkhalaf 2006; Ghosh 2008 (a,b,c)]. Absence of these peaks also suggests complete removal of the diazo group during the reduction reaction. It can be concluded that ^1H and ^{13}C NMR spectra provide strong evidence that the dendron is directly linked to the metal core through the phenyl ring at its focal point.

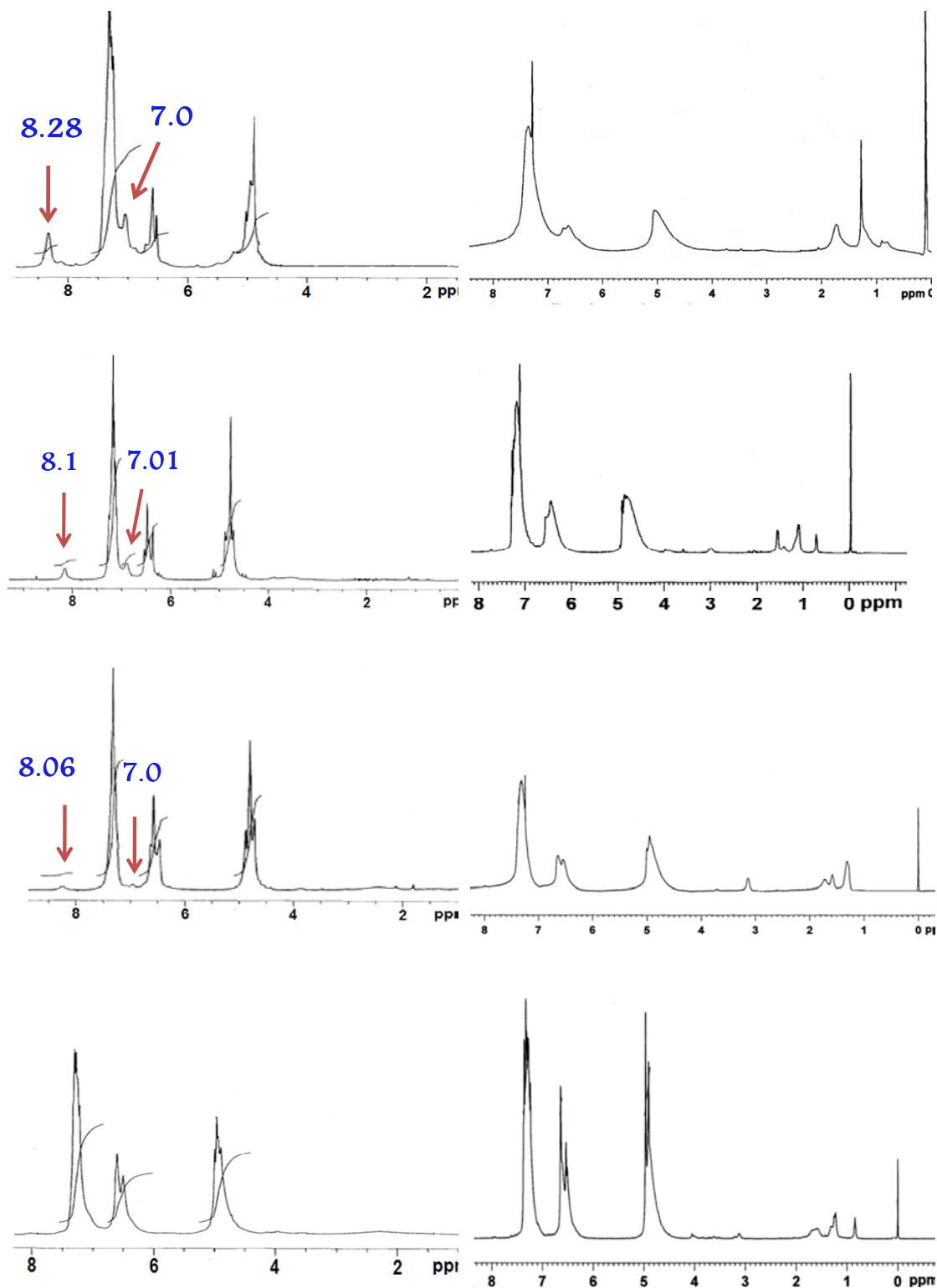


Figure 3.3 ^1H NMR spectra of diazodendrons and PdG_n in CDCl_3 .

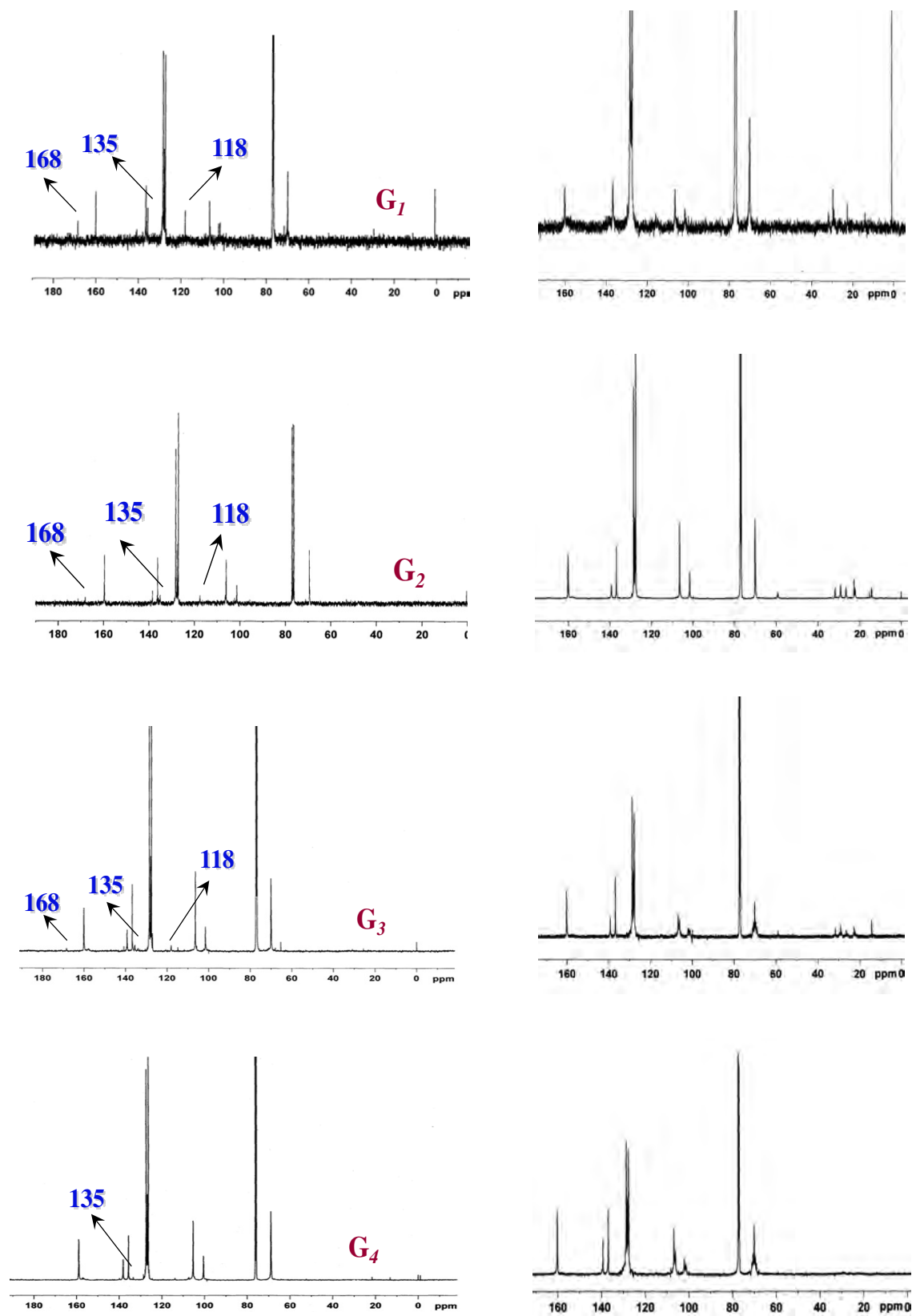


Figure 3.4 ^{13}C NMR spectra of diazodendrons and PdG_n in CDCl_3 .

3.3.2.3 Absorption Spectroscopy

UV-vis spectroscopy is very useful in characterizing metal nanoparticles. The absorption spectra of **PdG₁** and **PdG₂** in DCM are shown in Figure 3.5. The spectra show a smoothly increasing absorption at increasing energy with no characteristic surface plasmon absorption which is in accordance with the literature reports [Gopidas 2003 (c); Ghosh 2008 (a)].

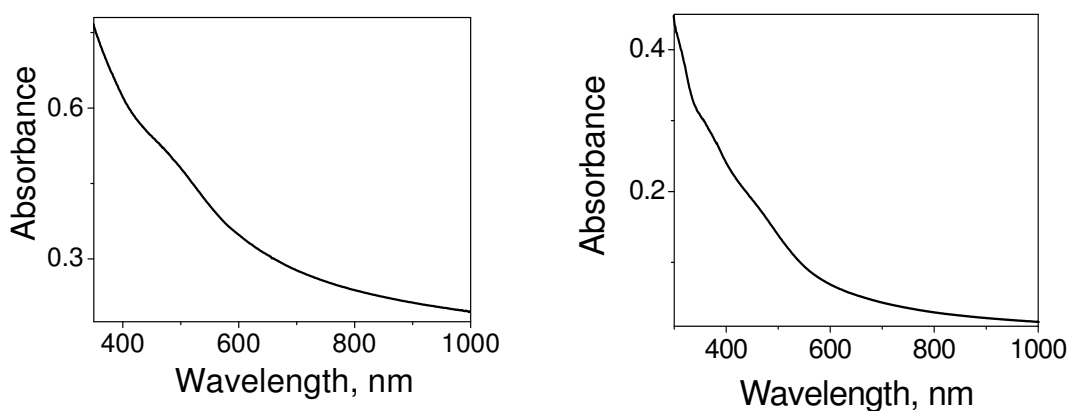


Figure 3.5 Absorption spectra of **PdG₁** and **PdG₂** in dichloromethane.

3.3.2.4 Transmission Electron Microscopic (TEM) Studies

TEM images of **PdG₁** – **PdG₄** are shown in Figure 3.6. The TEM image, taken by drop casting the NCD solution in toluene, show dispersed metal particles, with non-uniform size. TEM shows only the image of the metal core. In the case of several alkanethiolate MPCs, the core-core separation corresponds to the length of the alkyl chain. In the present case, occurrences of relatively identical core-core separations were rare in the TEM images and hence thickness of the dendritic shell could not be estimated. The core-size histograms of **PdG_n** is shown in Figure 3.6, and it indicates the formation of nearly monodisperse particles with an average

core diameter of about 2-4 nm. Unlike the earlier reports [Wu 2006; 2008], our present studies did not give any indication regarding the size dependency of the palladium metal nanocluster formation with a change in the dendrimer generation.

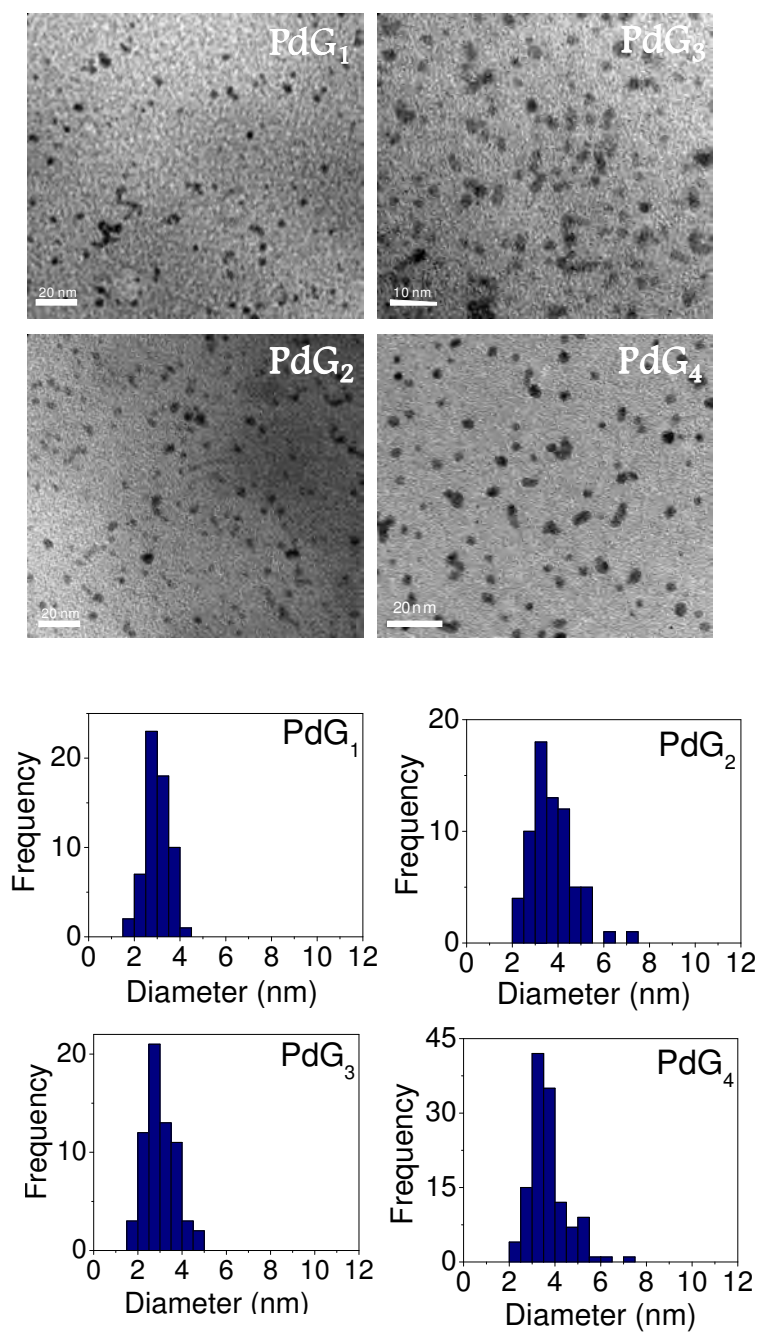


Figure 3.6 TEM images (top) and core-size histograms (bottom) for PdG_n.

3.3.3 Control Experiments

As discussed in chapter 2, we have carried out control experiments to confirm the formation of NCDs with palladium-carbon bond. The experiments described in section 2.3.3 (chapter 2) clearly show that the dendron dimers formed during the reduction of diazodendron cannot stabilize the metal nanoparticles effectively. We have attempted the reduction of Pd(II) in the absence of diazodendrons employing the same experimental conditions used for the synthesis of **PdG_n**. It has been observed that upon increasing the reaction temperature from -30 °C to room temperature, the particles aggregated rapidly to form palladium black which settled down and the solution became clear. These experiments further confirm that the stabilization of nanosized palladium can happen only through the grafting of dendron radicals under the used set of reaction conditions.

3.4 Conclusion

Our studies showed that the reduction of diazo functionalized poly(arylether) dendrons in presence of Pd(II) leads to the formation of core-shell structured palladium nanoparticle-cored dendrimers possessing nanosized Pd metal cluster as the core. These highly stable hybrid materials have been characterized by different spectroscopic as well as microscopic techniques such as NMR, FT-IR and TEM. Signal line broadening observed in NMR studies confirmed the presence of dendrons near to the metal core while TEM studies indicated the presence of nearly monodisperse metal particles with an average core diameter of 2–4 nm.

We have not observed any size change for the metal nanoclusters with increase in dendrimer generation. Unlike the previous literature reports, the better stabilization provided by the metal-carbon bonding in these NCDs are expected to increase their stability and efficiency as catalysts in organic reactions. This aspect is explored in the next chapter of this thesis.

3.5 Experimental

3.5.1 Materials and Methods

3,5-dihydroxybenzoic acid, benzyl bromide, carbon tetrabromide, triphenylphosphine, tetra-*n*-octylammonium bromide (TOAB), NaNO₂, K₂CO₃, K₂PdCl₄, LiAlH₄, NaBH₄, HBF₄, were purchased from Aldrich and used as received. Solvents such as acetone, toluene and dichloromethane (DCM) were obtained from MERCK and used as received. Dry tetrahydrofuran (THF) used for the synthesis was freshly distilled from sodium benzophenone ketyl. For the UV-vis spectra, spectroscopic solvents from MERCK were used.

Melting points were determined on a Mel-Temp II melting point apparatus and are uncorrected. ¹H NMR data were obtained from a 300 MHz Bruker Avance DPX spectrometer. ¹³C NMR spectra were recorded using a 500 MHz Bruker Avance DPX spectrometer. FTIR spectra were recorded on a Shimadzu IR Prestige 21 spectrometer. High-resolution mass spectra were obtained by using a JOEL JMS600 mass spectrometer. Absorption spectra were obtained using a Shimadzu 3101PC UV/Vis-NIR scanning spectrophotometer. TEM images of **PdG_n** were obtained with a 200 kV FEI-Tecnai 30G²S-Twin transmission electron microscope. Sample

for TEM was prepared by drop-casting one drop of a ~ 1 mg/mL solution in toluene onto standard carbon-coated copper grids (300 mesh) and drying in air for 2 days.

3.5.2 Synthesis of PdG₁

An aqueous solution of K₂PdCl₄ (448.0 mg, 1.4 mmol) was stirred with G₁N₂⁺BF₄⁻ (700.0 mg, 1.4 mmol) taken in 1:1 toluene – dichloromethane mixture (50 mL). Tetra-*n*-octylammonium bromide (1.12 g, 2.1 mmol) was added to it and stirring was continued until the aqueous phase become colorless. Organic phase was separated, washed twice with water and cooled to -30 °C. NaBH₄ (519.0 mg, 14 mmol) in methanol (20 mL) was added dropwise to the reaction mixture kept at -30 °C. The reaction mixture was stirred for 4 h at -30 °C temperature and 20 h at room temperature. Organic phase was separated and washed twice with 0.5 M H₂SO₄, 0.5 M Na₂CO₃ and finally with water. Organic layer was concentrated and the residue obtained was dried. The black powder was then dissolved in dichloromethane and stirred overnight with an aqueous solution of sodium citrate (5.0 g in 60 mL water). Further purification was carried out by column chromatography (silica gel – dichloromethane – ethylacetate – tetrahydrofuran). Nanoparticle band was eluted using tetrahydrofuran. IR (KBr) ν_{\max} (cm⁻¹) = 3084.18, 3061.03, 3030.17, 2872.01, 1597.06, 1506.41, 1452.40, 1375.25, 1294.24, 1242.16, 1219.01, 1157.29, 1058.92, 1026.13, 908.47, 831.32, 736.81, 698.23, 632.65, 522.71, 459.06. ¹H NMR (500 MHz, TMS, CDCl₃, δ): 5.06 (broad, s),

6.63 (broad, s), 7.35 (broad, s) ppm. ^{13}C NMR (125 MHz, TMS, CDCl_3 , δ): 70.17, 101.56, 106.53, 127.53, 128.05, 128.58, 136.68, 160.20 ppm.

3.5.3 Synthesis of PdG₂

An aqueous solution of K_2PdCl_4 (105.0 mg, 0.32 mmol) was stirred with $\text{G}_2\text{N}_2^+\text{BF}_4^-$ (300.0 mg, 0.32 mmol) taken in 1:1 toluene – dichloromethane mixture (30 mL). Tetra-*n*-octylammonium bromide (264.0 mg, 0.48 mmol) was added to it and stirring was continued until the aqueous phase become colorless. Organic phase was separated, washed twice with water and cooled to $-30\text{ }^\circ\text{C}$. NaBH_4 (183.0 mg, 4.8 mmol) in methanol (15 mL) was added dropwise to the reaction mixture kept at $-30\text{ }^\circ\text{C}$. The reaction mixture was stirred for 4 h at $-30\text{ }^\circ\text{C}$ temperature and 20 h at room temperature. Organic phase was separated and washed twice with 0.5 M H_2SO_4 , 0.5 M Na_2CO_3 and finally with water. Organic layer was concentrated and the residue obtained was dried. The black powder was then dissolved in dichloromethane and stirred overnight with an aqueous solution of sodium citrate (2.0 g in 30 mL water). Further purification was carried out by column chromatography (silica gel- dichloromethane-ethyl acetate). IR (KBr) ν_{max} (cm^{-1}) = 3030.17, 2932.21, 2245.36, 1595.13, 1506.41, 1450.47, 1373.32, 1319.31, 1296.16, 1244.09, 1217.08, 1157.29, 1055.06, 833.25, 736.81, 698.21, 418.55. ^1H NMR (500 MHz, TMS, CDCl_3 , δ): 4.97 – 5.02 (m, 14H), 6.57 – 6.65 (m, 10H), 7.26 (s, 23H) ppm. ^{13}C NMR (125 MHz, TMS, CDCl_3 , δ): 69.93, 70.04, 101.55, 106.30, 127.48, 127.94, 128.19, 128.52, 136.73, 139.19, 160.02 ppm.

3.5.4 Synthesis of PdG₃

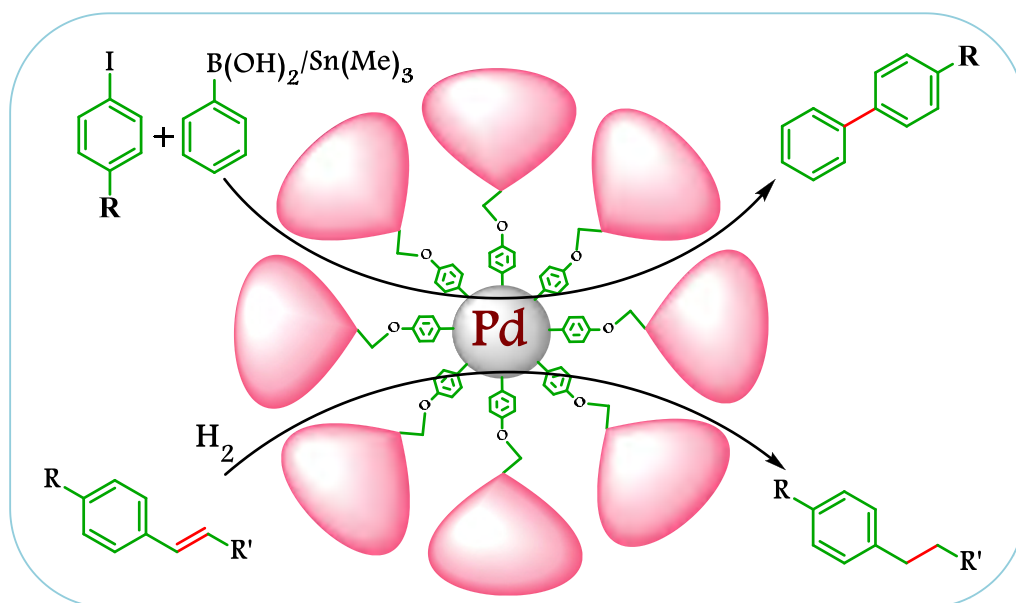
An aqueous solution of K₂PdCl₄ (110.0 mg, 0.34 mmol) was stirred with G₃N₂⁺BF₄⁻ (600.0 mg, 0.34 mmol) taken in 1:1 toluene - dichloromethane mixture (40 mL). Tetra-*n*-octylammonium bromide (276.0 mg, 0.5 mmol) was added to it and stirring was continued until the aqueous phase become colorless. Organic phase was separated, washed twice with water and cooled to -30 °C. NaBH₄ (129.0 mg, 3.4 mmol) in methanol (10 mL) was added dropwise to the reaction mixture kept at -30 °C. The reaction mixture was stirred for 4 h at -30 °C temperature and 20 h at room temperature. Organic phase was separated and washed twice with 0.5 M H₂SO₄, 0.5 M Na₂CO₃ and finally with water. Organic layer was concentrated and the residue obtained was dried. The black powder was then dissolved in dichloromethane and stirred overnight with an aqueous solution of sodium citrate (2.0 g in 30 mL water). Further purification was carried out by column chromatography (silica gel - dichloromethane - ethylacetate). Nanoparticle band was eluted using ethyl acetate. IR (KBr) ν_{\max} (cm⁻¹) = 3030.17, 2929.87, 2914.44, 2872.01, 1595.13, 1498.69, 1448.54, 1373.32, 1321.24, 1296.16, 1215.15, 1157.29, 1055.06, 910.40, 833.25, 738.74, 698.23, 632.65, 460.99. ¹H NMR (300 MHz, TMS, CDCl₃, δ): 4.951 – 5.003 (broad), 6.532 – 6.639 (broad), 7.247 – 7.311 (broad) ppm. ¹³C NMR (125 MHz, TMS, CDCl₃, δ): 69.93, 70.05, 101.53, 106.33, 127.52, 128.54, 136.70, 139.17, 143.47, 159.99, 160.10 ppm.

3.5.5 Synthesis of PdG₄

An aqueous solution of K₂PdCl₄ (34.0 mg, 0.1 mmol) was stirred with G₄N₂⁺BF₄⁻ (360.0 mg, 0.1 mmol) taken in 1:1 toluene - dichloromethane mixture (20 mL). Tetra-*n*-octylammonium bromide (85.0 mg, 0.15 mmol) was added to it and stirring was continued until the aqueous phase become colorless. Organic phase was separated, washed twice with water and cooled to -30 °C. NaBH₄ (37.8 mg, 1.0 mmol) in methanol (5 mL) was added dropwise to the reaction mixture kept at -30 °C. The reaction mixture was stirred for 4 h at -30 °C temperature and 20 h at room temperature. Organic phase was separated and washed twice with 0.5 M H₂SO₄, 0.5 M Na₂CO₃ and finally with water. Organic layer was concentrated and the residue obtained was dried. The black powder was then dissolved in dichloromethane and stirred overnight with an aqueous solution of sodium citrate (1.0 g in 20 mL water). Further purification was carried out by column chromatography (silica gel - dichloromethane - ethylacetate). Nanoparticle band was eluted using ethyl acetate. IR (KBr) ν_{\max} (cm⁻¹) = 3061.03, 3030.17, 2927.94, 2870.08, 1595.13, 1496.76, 1452.40, 1373.32, 1321.20, 1296.16, 1263.37, 1155.36, 1053.13, 833.25, 736.81, 696.30. ¹H NMR (500 MHz, TMS, CDCl₃, δ): 4.902 - 4.61 (broad), 6.506 - 6.634 (broad), 7.232 - 7.355 (broad) ppm. ¹³C NMR (125 MHz, TMS, CDCl₃, δ): 70.13, 70.66, 71.23, 101.38, 101.91, 102.10, 106.55, 106.82, 127.61, 128.58, 129.46, 136.84, 139.29, 160.19 ppm.

Chapter 4

Catalytic Applications of Palladium Nanoparticle-Cored G₁ Dendrimer



4.1 Abstract

*In this chapter an attempt is made to assess the efficiency of palladium nanoparticle-cored G₁ dendrimer (**PdG₁**) in catalyzing different organic reactions. We observed that **PdG₁** can act as a highly efficient, chemoselective room temperature catalyst for the hydrogenation of multifunctional olefins and acetylenes. Reducible functionalities like, -CHO, -CN, -NO₂ and halogen functional groups were unaffected under the reaction conditions employed. Hydrogenations catalyzed by **PdG₁** proceeded with turn-over numbers (TON) in excess of 50,000 and turn-over frequencies (TOF) as large as 14,000 h⁻¹. The catalyst also exhibited good recyclability. C-C bond forming reactions such as Suzuki, Stille, Heck and Hiyama couplings were also efficiently catalyzed by **PdG₁**. Aryl iodides and bromides were the active substrates for Suzuki reactions while aryl chlorides were unreactive. The recyclability of **PdG₁** was studied for Suzuki reaction and the recovered catalyst exhibited excellent catalytic activity in subsequent runs. **PdG₁** catalyzed Stille couplings were efficient under mild, aqueous conditions and required only short reaction times. Yields for **PdG₁** catalyzed Heck couplings, however, were low.*

4.2 Introduction

The ability of metal nanoparticles to act as the link between bulk and molecular state makes them highly applicable tools in different fields of nanoscience and nanotechnology. While the emergence of novel optical and electronic properties is responsible for the wide spread interest in noble metal nanoparticles, research in transition metal nanoparticles is driven by the need to develop active nanoparticle catalysts for various reactions. The use of metal nanoparticles for catalysis has been explored by different groups during the past decades [Aiken 1999; Shenhar 2003; Pachón 2008; Jain 2008]. In the mid 19th century, Nord and co-workers [Rampino 1941 (a,b); Kavanagh 1943] reported the hydrogenation of nitrobenzene using nanoparticle catalysts, which was followed by the reports of Parravano and co-workers [Cha 1970] on the hydrogen-atom-transfer between benzene and cyclohexane and oxygen-atom-transfer between CO and CO₂ using gold nanoparticles. Haruta *et al.* [1987; 1989; 1993] reported the oxidation of CO by O₂ at low temperature using oxide-supported gold nanoparticles which was followed by the observation of Hirai *et al.* [1978; 1979] that gold nanoparticles can catalyze hydrogenation of olefins. These reports were followed by extensive use of the catalytic activity nanoparticle in different fields. At present the main focus in this area is to improve selectivity of reactions and also to obtain a deep understanding of reaction mechanisms.

In chapter 1 of the thesis we have hypothesized that nanoparticle-cored dendrimers can be good catalysts. The metal cluster at the core has diameters in the range of 2 - 5 nm and hence these particles

exhibit large surface area/unit volume. The number of dendrons attached to the metal core is decided by a sterically induced stoichiometry as well as size of the dendron and diameter of the metal core. As we can see in Figure 1.16, only a few atoms on the nanoparticle surface are attached to dendrons leaving most of the surface atoms unpassivated. Thus the NCD would have most of the atoms on the metal surface exposed to substrates capable of penetrating the dendritic shell. The free space or voids present on the metal surface will act as guest cavities and can function as “reaction vessels” for catalytic reactions. These features make NCDs ideally suited as nanoreactors for metal-catalyzed reactions. In chapter 3 of the thesis we have described the synthesis and characterization of Pd nanoparticle-cored dendrimers **PdG₁-PdG₄**. In this chapter we have explored the catalytic activity of **PdG₁** in few reactions which are known to be catalyzed by Pd(0). The reactions studied include catalytic hydrogenations, Suzuki reactions, Stille coupling, Hiyama coupling and Heck reaction.

Catalytic hydrogenation is one of the most convenient methods for the reduction of organic compounds. It involves the addition of hydrogen to one or more unsaturated groups in the molecule or it may involve fission of a bond between atoms. These reactions are effected simply by shaking a solution of the substrate in a suitable solvent in the presence of a catalyst under an atmosphere of hydrogen. At the end of the reaction the catalyst is filtered off and the product is obtained from the filtrate, in a state of high purity. Most common unsaturated groups in organic chemistry such as >C=C<, -C≡C-, >C=O, -COOR, -C≡N, -NO₂, and aromatic/heterocyclic nuclei can be reduced catalytically under

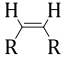
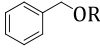
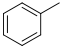
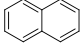
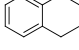
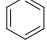
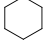
appropriate conditions. In addition, certain other groups such as allylic and benzylic hydroxyl and amino groups, carbon-halogen and carbon-sulfur single bonds readily undergo hydrogenolysis, resulting in the cleavage of the bond between the carbon and the hetero atom.

Most commonly employed catalysts for hydrogenation reactions are Pt and Pd metals. They are exceptionally active catalysts and promote the reduction of most functional groups under mild conditions, with the notable exception of $-\text{COOH}$, $-\text{COOR}$ and $-\text{CONR}_2$. The metals can be used as finely divided metals or more commonly, supported on suitable carriers such as activated carbon, alumina or barium sulfate. Supported Pt and Pd metal catalysts are very stable and can be kept for many years without appreciable loss of activity, but they are easily deactivated by many substances, particularly by compounds of divalent sulfur. Because of this reason it is necessary to use pure materials and pure solvents for hydrogenation reactions using these catalysts.

All functional groups are not hydrogenated with equal ease. Table 4.1 shows the approximate order of decreasing ease of catalytic hydrogenation of a number of common functional groups. The groups near the top of the table can be selectively reduced in the presence of groups near the bottom, but preferential reduction of groups at the bottom in presence of the more reactive groups at the top is very difficult. For example, reduction of a nitro group in the presence of a double bond may be achieved by hydrogenation over Pt or Pd, but selective reduction of the double bond without affecting the nitro group may be very difficult.

Attempts have been made in the past to modify Pd catalyst so as to improve its selectivity. Palladium adsorbed on charcoal (Pd/C) is the most widely used catalyst for hydrogenation reactions. But, Pd/C being highly active renders poor selectivity. There have been several reports in the literature regarding the use of additives with Pd/C to make it selective in reduction reactions. Sajiki and co-workers used diphenylsulphide as catalyst poison to achieve chemoselective hydrogenation using Pd/C [Mori 2006; 2008]. This enabled the authors to use the modified Pd catalyst for the reduction of olefin and acetylene functionalities without hydrogenolysis of aromatic carbonyls and halogens, benzyl esters and N-Cbz protective groups. It has also been reported that Pd/C poisoned with ethylenediamine can selectively hydrogenate alkenes and alkynes in presence of aromatic nitriles [Maegawa 2007].

Table 4.1 Ease of hydrogenation of different organic functional groups.

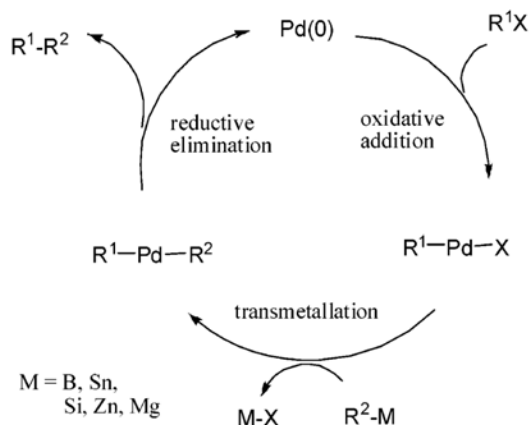
Functional group	Reduced products
R-CO-Cl	R-CHO
R-NO ₂	R-NH ₂
R-C≡C-R	
R-CHO	R-CH ₂ OH
R-CH=CH-R	R-CH ₂ -CH ₂ -R
R-CO-R	R-CHOH-R
	 + R-OH
R-C≡N	R-CH ₂ -NH ₂
	
R-CO-O-R'	R-CH ₂ OH + R'-OH
R-CO-NH-R	R-CH ₂ NH-R
	
R-CO ₂ Na [⊖]	Inert

In this chapter we have investigated the efficiency of **PdG₁** as a hydrogenation catalyst. Our studies showed that **PdG₁** can act as highly efficient chemoselective catalyst for the hydrogenation of olefins and acetylenes under room temperature conditions using a slight positive hydrogen pressure. The selectivity of **PdG₁** for hydrogenation reaction was studied using multifunctional substrates and it was found that **PdG₁** was highly selective for olefinic and acetylenic bonds in presence of other reducible functionalities like -CHO, -NO₂, -CN, and labile groups like halogens.

We have also observed that **PdG₁** can efficiently catalyze several cross coupling reactions that are catalyzed by Pd(0). Palladium catalyzed cross-coupling reactions involve assembling of the precursors on the metal surface through the formation of metal-carbon bonds. These precursors which are placed close to each other on the metal surface will undergo coupling to form a new carbon-carbon bond. These reactions begin by generating an organopalladium complex (RPdX) which will subsequently react with the nucleophile. In 1968, Heck reported the first example of these types of reactions which involve formation of styrene by the reaction of ethylene with phenylpalladium chloride [Heck 1968 (a,b,c)]. The arylpalladium precursor required for the reaction was prepared by reacting an organomercury compound with a palladium(II) salt. During the course of the reaction, the palladium(II) was reduced to palladium(0) leading to a slowing down of the reaction rate. Heck, later modified the reaction by using oxidizing additives like CuCl₂ which reoxidized the palladium(0) back to palladium(II) [Heck 1968 (d)]. In

1972, the reaction was further developed and the organopalladium complex formation was achieved by the reaction of arylhalide with palladium(0) species through an oxidative addition step and this important modification resulted in the wide spread use of palladium chemistry in organic synthesis [Heck 1972].

Negishi initiated the use of organozirconium and organoaluminium compounds in cross coupling reactions and his studies showed that organozinc compounds can act as nucleophilic coupling partners in palladium catalyzed cross coupling reactions [Negishi 1976; 1977]. Compared to other organometallic compounds, reactions with organozinc precursors are mild, highly selective and superior in terms of yield. The use of organoboron compounds in palladium catalyzed cross coupling reactions was first reported by Suzuki and co-workers in 1979 [Suzuki 1979]. The reaction required the presence of an added base, which activated the organoboron reagent as boronate intermediate and facilitated the transfer of the organic group from boron to palladium (transmetallation). The Suzuki reaction is one of the most preferred reactions in industry as it involves a more stable organoboronic acid which is non-toxic and the reaction conditions required are very mild. Other important palladium catalyzed cross coupling reactions includes Hiyama and Stille couplings. The former involves the reaction of organosilicon compounds while organotin nucleophiles are employed in the latter. Scheme 4.1 describes a general mechanism of palladium catalyzed cross coupling reactions.



Scheme 4.1 Mechanism of palladium catalyzed cross coupling reactions.

All these cross coupling reactions have been applied to the synthesis of large number of natural products and biologically active compounds of complex molecular structure. They have also found applications in the fine chemical and pharmaceutical industries. Importance of carbon-carbon bond forming reactions is reflected by the Nobel Prizes for the Grignard reaction (1912), the Diels-Alder reaction (1950), the Wittig reaction (1979) and the olefin metathesis (2005). The vital role of palladium catalysis in organic synthesis has now been recognized in the form of Nobel Prize in Chemistry (2010), being awarded to Professor Ei-ichi Negishi, Professor Arika Suzuki and Professor Richard F. Heck.

In this chapter we also describe the use of **PdG₁** as catalyst for C-C bond forming reactions. We show that **PdG₁** can act as an efficient catalyst for Suzuki and Stille reactions under mild and aqueous conditions with good recyclability of the catalyst. **PdG₁** could also be employed as catalyst for Heck and Hiyama coupling reactions. Results of these studies are presented in this chapter.

4.3 Results and Discussions

4.3.1 Catalytic Features of PdG₁

PdG₁ required for the studies was synthesized according to the procedure reported in chapter 3. Detailed studies were carried out to obtain a clear understanding of the structural aspects of **PdG₁**. Figure 4.1 shows the TEM image and corresponding core-size histogram of **PdG₁**. Figure 4.1 suggests that the palladium clusters are almost spherical with an average core diameter of 2.7 nm. The thermogram in Figure 4.1 shows that 59 % of the total weight of **PdG₁** is due to palladium metal and the organic shell constitutes the remaining 41% of the weight of **PdG₁**. Assuming spherical shape for the particles, average number of Pd atoms in a metal cluster (N_{Pd}) can be calculated using equation 4.1.

$$N_{Pd} = d(\pi/6)D^3 \quad (4.1)$$

where d is the density of Pd (68 atoms/nm³) and D is the average diameter of the cluster. This calculation gave $N_{Pd} = 700.45$, indicating that on an average **PdG₁** contain 700 Pd atoms. Atomic weight of Pd is 106.4 and hence the total weight of Pd in the cluster (W_{Pd}) can be given as

$$W_{Pd} = N_{Pd} \times 106.4 \quad (4.2)$$

This weight of palladium ($W_{Pd} = 74528$) corresponds to 59% of the weight of **PdG₁**. Using this value we can calculate the weight of the organic shell (W_{G1}), which constitute 41% of the total weight of **PdG₁**. W_{G1} when divided by the molecular weight of the G₁ dendron (395) gave the average number of dendrons attached to the palladium metal core. The above calculations

gave W_{G_1} as 51790, [Gopidas 2003 (c)] which suggested that **PdG₁** on the average contains 131 G₁ dendrons attached to the Pd core through Pd-C bonds.

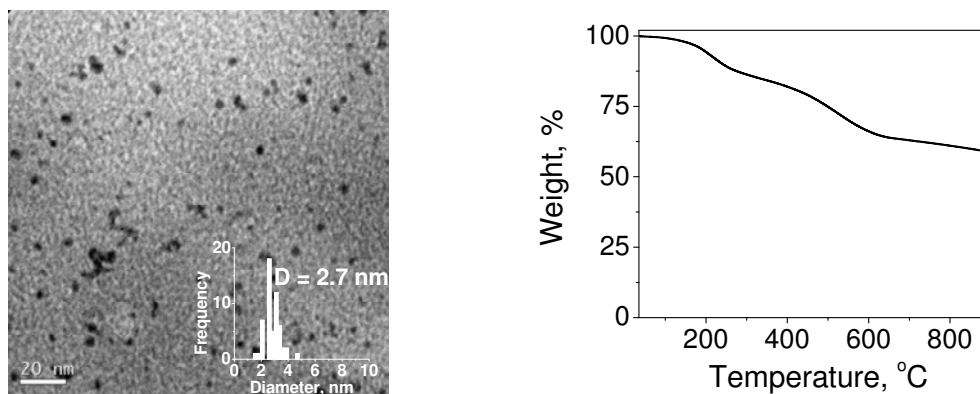


Figure 4.1 TEM image (left) and thermogram (right) of **PdG₁**.

It has been reported earlier that in a 1.6 nm spherical Pd cluster 63% of palladium atoms are present on the surface of the cluster [Chechik 2000]. If we assume that 40% of the palladium atoms in **PdG₁** are present on the surface, then 280 palladium atoms will be present on the surface of the cluster. Considering that G₁ dendrons are present on the surface of the cluster as a monolayer, then 131 palladium atoms on the surface of the cluster will be engaged in bonding interaction with the G₁ dendrons, leaving the remaining 149 binding sites (53% of total surface) on the metal surface free. In chapter 2 of this thesis we have indicated the possibility of multiple layer formation due to the high reactivity of the aryl radical. If multiple layering is actually taking place in the present case, then all the 131 G₁ ligands will not be bonded to the cluster and the actual free sites available on the cluster surface will be more than 53%. These results prompted us to propose that at least 53% of surface area on Pd

cluster is available for catalytic activity and **PdG₁** can be a good catalyst if the free metal surface is accessible to reactants. In this chapter we have investigated the ability of **PdG₁** to catalyze various reactions which include hydrogenation and C-C bond forming reactions and the results are presented in the following sections.

4.3.2 Hydrogenation Reactions Using PdG₁

The unique ability of transition metals to catalyze hydrogenation reactions has been exploited efficiently in industrial processes for a long time. Hydrogenation of organic functional groups catalyzed by transition metals can be achieved using 3 methods.

- (i) Hydrogenation using molecular hydrogen combined with homogeneous or heterogeneous catalysts, where the transition metal acts as a template on which activated hydrogen and the substrate can combine.
- (ii) Transfer hydrogenation using organic molecules to donate hydrogen. In this strategy, the transition metal facilitates the transfer of hydrogen from a donor organic molecule to the substrate. This method offers an alternative for reducing unsaturated substrates without the use of hydrogen gas and the typical examples include hydrogenation of unsaturated compounds using Pd/C-cyclohexene [Brieger 1974], Pd/C-HCOOH [Entwistle 1977].
- (iii) Transition metal – metal hydride reduction using combined reagents. Here the transition metal activates a functional group

which will undergo reduction by a metal hydride reagent. TiCl_4 - LiAlH_4 [Chum 1976] and PdCl_2 - NaBH_4 [Russel 1977] are examples of transition metal - metal hydride reagents.

Most commonly used heterogeneous hydrogenation catalysts include VIIIth group transition metals like Ru, Co, Rh, Ir, Ni, Pd or Pt. In general, heterogeneous catalysts do not favor highly selective hydrogenations and the common side reactions include isomerization, hydrogenolysis and hydrogen scrambling, especially for palladium catalyzed reductions. These shortcomings of heterogeneous systems make a preference to homogeneous catalysts wherever selective reduction is needed. Group VIII transition metal complexes like $[\text{Rh}(\text{PPh}_3)\text{Cl}]$, $[\text{HCo}(\text{CN})_5]^{3-}$, $[\text{Cr}(\text{arene})(\text{CO})_3]$ etc are frequent candidates as catalysts in homogeneous hydrogenation reactions. The observed high selectivity of homogeneous catalysts results from the fact that they contain only one type of active metal center, whereas a heterogeneous surface contains a variety of active sites differing in both electronic and steric environments [Colquhoun 1984].

Colloidal transition metal nanoparticles, particularly palladium nanoparticles, are frequent candidates as catalysts in hydrogenation reactions of organic compounds [Červený 1989; Jiang 2006; Yang 2006; Vasylyev 2006; Mori 2008; Ornelas 2008; Bhattacharjee 2009; Jurčík 2009]. Fox and co-workers [Gopidas 2003 (c)] have synthesized thiol stabilized Pd-NCDs and successfully demonstrated their ability to catalyze Suzuki and Heck cross coupling reactions. These NCDs, however, failed to catalyze hydrogenation reactions. In the presence of hydrogen,

hydrogenolysis of the C-S bonds occurred leading to decomposition of the NCD and precipitation of Palladium metal. Fan and co-workers [Wu 2006; 2008] attempted the catalytic hydrogenation of simple monofunctional organic molecules like styrene and nitrobenzene using phosphine oxide stabilized Pd-NCDs. These NCDs, even though successfully catalyzed the hydrogenation of simple organic molecules, required elevated reaction temperatures and relatively high hydrogen pressures. The authors also observed that the catalyst recovered after the first reaction cycle was inactive for further runs thereby limiting its recyclability which is a very important parameter in catalysis. In this chapter we show that **PdG₁** is a very effective catalyst for the chemoselective hydrogenation of olefinic and acetylenic bonds at room temperature and atmospheric pressure in the presence of other reducible groups like -CHO, -NO₂ and halogens.

All **PdG₁** catalyzed hydrogenation reactions described in this section were carried out at room temperature conditions. In a typical experiment the substrate (actual amount of substrate depended on its solubility in ethyl acetate and varied from 0.5 to 2.5 mM) to be reduced and 5 mg **PdG₁** were dissolved in ethyl acetate (15 mL) and the mixture was stirred under slight positive pressure of hydrogen (maintained using a hydrogen filled balloon) for 4 - 7 h. The progress of the reaction was monitored using GC-MS analysis. After the reaction, solvent was removed and the products were extracted into ether. The ether extract, containing insoluble **PdG₁** was decanted and passed through a small pad of silica to remove any suspended impurities. Ether was then removed to get pure

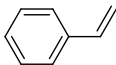
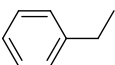
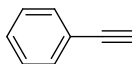
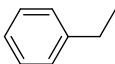
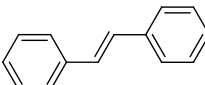
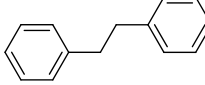
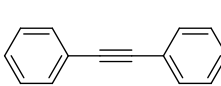
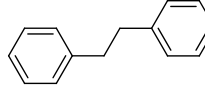
products. The efficiencies of catalytic reactions are usually evaluated in terms of 'turn-over numbers' (TON) and 'turn-over frequencies' (TOF).

$$\text{TON} = \text{Number of moles of product} / \text{Number of moles of catalyst}$$

$$\text{TOF} = \text{TON} / \text{Reaction time}$$

For calculating TON, the catalyst **PdG₁** was considered as a single molecular entity consisting of a 700 Pd atom core and a shell of 131 dendrons [Gopidas 2003 (c)]. In Table 4.2, we present the results of the hydrogenation reactions of two arylethylenes and two arylacetylenes. The olefinic/acetylenic bonds in these substrates were reduced in high yields at relatively short time periods. The aryl groups were unaffected. Yields reported in Table 4.2 are isolated yields and the products were well characterized by spectroscopic techniques.

Table 4.2 Hydrogenation reactions of monofunctional substrates catalyzed by **PdG₁**.

Entry	Substrate	Product	Yield (%)	Time (h)	TON	TOF (h ⁻¹)
A1			90	4	54545	13636
A2			92	4	58081	14520
A3			99	6	13888	2314
A4			98	6	13914	2319

We have also carried out hydrogenation reactions of multifunctional organic substrates shown in Table 4.3 using the same protocol described earlier. In addition to C=C or C≡C, these substrates contained functional groups such as CHO, NO₂, CN, COOCH₃, or halogens. All the products shown in Table 4.3 were isolated and unambiguously characterized using spectroscopic methods.

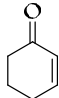
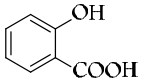
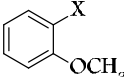
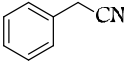
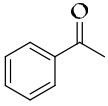
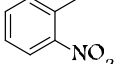
Table 4.3 Hydrogenation reactions of multifunctional substrates catalyzed by PdG₁.

Entry	Substrate	Product	Yield (%)	Time (h)	TON	TOF (h ⁻¹)
A5			81	7	20455	2922
A6			98	6	10997	1832
A7			98	7	11631	1938
A8			95	6	16190	2698
A9			98	5	15276	3055
A10			99	5	12019	2003
A11			98	5	10455	1742
A12			95	5	8588	1431
A13			94	7	8287	1183

It can be seen from Table 4.2 and 4.3 that product yields are nearly quantitative and reaction times were low compared to hydrogenation reactions of similar substrates using other palladium catalysts where the complete reduction of substrates including aromatic rings results, though under drastic conditions and longer periods [Kogan 2002]. Inspection of Table 4.3 also reveals that **PdG₁** is a very selective catalyst for the reduction of C=C and C≡C at room temperature and mild hydrogen pressure, even in presence of sensitive groups like nitro. Selective reduction of carbon-carbon multiple bonds in multifunctional organic molecules is always challenging especially in presence of groups like NO₂ and CHO which can also undergo reduction under the hydrogenation conditions [Mori 2006; 2008; Callis 2007; Maegawa 2009]. In **PdG₁** catalyzed hydrogenations, these groups remain unaffected. The TON and TOF shown in Tables 4.2 and 4.3 are very high. For entries A1 and A2 in Table 4.2, TON is > 54,000. It can be noted that even for reduction of substrate A13 in Table 4.3, involving simultaneous reduction of four C=C bonds, TON/TOF values are very high, suggesting that **PdG₁** is a very efficient hydrogenation catalyst.

In Table 4.4 we present structures of few substrates which were unaffected under the hydrogenation conditions employed. It can be seen that halogens (Cl, Br and I) and endocyclic double bonds are unaffected under the reaction conditions. At present we are unable to comment on the reasons for the observed chemoselectivity with **PdG₁** which requires reasonable understanding of the reaction mechanism.

Table 4.4 Inert functionalities towards hydrogenation catalysed by PdG₁.

Substrate	Product	Time (h)
		24
		24
 X = I, Br, Cl	no reaction	24
		24
		24
		24

Designing an efficient hydrogenation catalyst that can perform under mild reaction conditions with high chemoselectivity is still an active challenge in organic synthesis. The highly active catalytic nature of Pd/C systems make them poor in selectivity for the hydrogenation of multifunctional substrates. For example, in our control experiments with substrates A6 and A12 in Table 4.3, Pd/C (10%) did not exhibit any selectivity and gave mixtures of products arising from the reduction of nitro and olefinic groups. It is reported that the high catalytic activity of Pd/C can be lowered to some extent by the addition of suitable catalyst poisons, thereby achieving selectivity [Mori 2006; 2008; Maegawa 2009]. Examples include the use of Pd/C-ethylenediamine complex [Hattori 2001], Pd-polyethyleneimine complex [Sajiki 2008], Pd/C-diphenyl sulfide

complex [Mori 2008], Pd-fibroin complex [Kitamura 2007] etc. But, the presence of these additives may demand their separation from the final products after reaction. Thus, if chemoselective hydrogenation is desired **PdG₁** is a better choice.

We observed that most of the **PdG₁** could be recovered and reused without loss of catalytic activity. Phenylacetylene was used for the catalyst recovery study. In a typical experiment, phenylacetylene (2 mmol) and **PdG₁** (5 mg) were taken in ethyl acetate and stirred in hydrogen atmosphere for 6 h. Ethyl acetate was then removed by rotary evaporation. Ether (2 × 15 mL) was added, stirred for a few minutes and carefully decanted leaving the insoluble **PdG₁** in the flask. Fresh substrate and ethyl acetate were added and reaction repeated. We observed that the hydrogenation reactions went to completion for three cycles after which product yields decreased, most probably due to incomplete recovery of catalyst in the previous cycles. The results are summarized in Table 4.5 and Figure 4.2.

Table 4.5 Catalyst recovery studies using **PdG₁**.

Run	1 st	2 nd	3 rd	4 th
Yield of ethyl benzene (%)	92	92	91	75

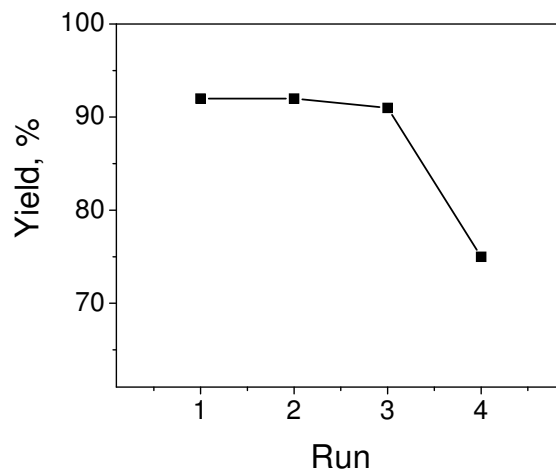
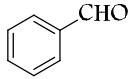
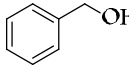
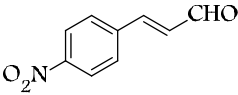
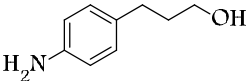


Figure 4.2 Recyclability of PdG₁ for hydrogenation reaction.

Although the use of DENs as hydrogenation catalyst has been established, there are only few reports regarding the use of Pd-NCDs for hydrogenation [Jiang 2006; Yang 2006]. In a recent report Fan and co-workers [Wu 2006; 2008] described the use of a phosphine dendrimer stabilized Pd-NCD as hydrogenation catalyst under elevated temperature and pressure conditions. This NCD, however, could not be recycled. Our observations clearly show that PdG₁ is more stable and active than other NCDs reported earlier. We have also studied the hydrogenation reactions catalyzed by PdG₁ at high hydrogen pressures and extended reaction times as shown in Table 4.6. The reactions were carried out in a Parr Hydrogenation Apparatus using a hydrogen pressure of 40 psi (2.7 atm). The results shows that groups like -NO₂ and -CHO which were unaffected at low hydrogen pressure conditions also could be reduced by increasing the hydrogen pressure. Our studies show that it is possible to use PdG₁ as a selective catalyst wherein the reaction can be controlled to the desired product by changing the reaction conditions.

Table 4.6 High pressure hydrogenation reactions catalyzed by PdG₁.

Substrate	Product	Yield	Time (h)
		100	12
		100	24

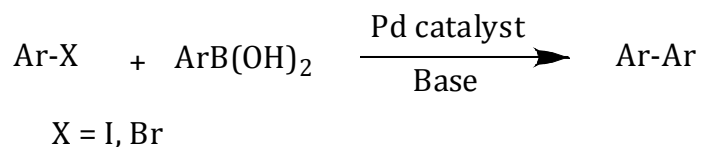
4.3.3 PdG₁ Catalyzed C-C Bond Forming Reactions

Among all the transition metal catalysts used for cross-coupling reactions in organic synthesis, palladium is the most important one owing to its remarkable ability in catalyzing C-C bond forming reactions [Köllhofer 2003; Tang 2003; Walker 2004; Kumar 2004; Schutz 2004; Shen 2005; Tsuji 1995]. A Pd(0) complex such as [Pd(PPh₃)₄] is the most commonly employed catalyst for this purpose. An alternative strategy is to employ a Pd(II) salt as precatalyst in the presence of ligands such as PPh₃ capable of reducing Pd(II) to Pd(0). Since PPh₃ is not an environmentally green reagent, [Beletskaya 2000] phosphine free conditions such as the Jeffery's protocol [Jeffery 1998; 1996] involving the use of tetraalkylammonium halides and palladacycles are also employed and these aspects have been recently reviewed by Beletskaya [2000]. Important palladium catalyzed C-C bond forming reactions include Heck, Sonogashira, Suzuki, Stille, Negishi, Hiyama, Corriu-Kumada, Tsuji-Trost and Ullmann reactions. The presence of palladium nanoparticles in some of these reactions were first suggested by Reetz *et al.* and later it has been established that nanometer sized colloidal palladium can also efficiently

catalyze C-C bond forming reactions [Bradley 1994; Reetz 1994; 1996; 2000; 2004; Beller 1996; Klingelhoefer 1997; Bars 1999; Ding 2000; Li 2000]. These reports led to a tremendous growth in the field of nanocatalysis, which resulted in the extensive use of colloidal transition metal nanoparticles as catalysts for different cross coupling reactions. Detailed studies have also been carried out to obtain a deeper insight into the mechanistic aspects of these reactions including the effect of nanoparticle size, reaction time, concentration and nature of the capping ligand on product formation process [Pathak 2000; Rahim 2001; Deshmukh 2001; Narayanan 2003; 2005 (a,b,c); Rocaboy 2002; Battistuzzi 2002; Hamill 2002; Kim 2002; Yin 2007; Bergbreiter 2009]. In the present work, ability of PdG₁ to catalyze different cross coupling reactions has been studied and the details are discussed in the following sections.

4.3.4 Suzuki Reaction

Suzuki reaction involves the coupling of an aryl boronic acid with an aryl halide in the presence of a palladium catalyst and an added base (Scheme 4.2) [Miyaura 1995; Suzuki 1999; Littke 2002].



Scheme 4.2 General scheme of Suzuki reaction.

The advent of versatile synthetic routes for boron compounds increased the wide spread use of Suzuki coupling [Astruc 2005; 2007]. We

observed that **PdG₁** can efficiently catalyze Suzuki reactions. As the reaction involve the use of a base, an attempt was made to find out the most suitable base that could be used along with **PdG₁** for the Suzuki coupling reaction. For this purpose we have studied the reaction between phenylboronic acid and 4-iodoanisole using **PdG₁** and the different bases shown in Table 4.7.

Table 4.7 Effect of base on Suzuki coupling catalyzed by **PdG₁**.

Entry	Base	Yield (%)	Time (h)
1	NaHCO ₃	94	24
2	K ₂ CO ₃	85	20
3	Na ₂ CO ₃	94	24
4	NaOH	95	3
5	K ₃ PO ₄	95	6
6	KOH	98	12
7	CH ₃ COONa	40	24
8	Et ₃ N	trace	24
9	CsF	55	24
10	CH ₃ ONa	60	20

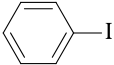
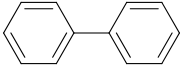
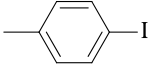
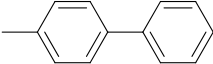
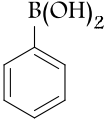
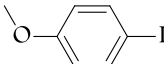
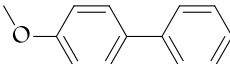
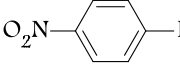
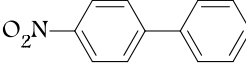
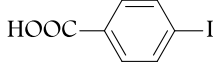


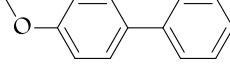
It is evident from Table 4.7 that the reaction time and yield varied significantly with the type of base employed. For example, with triethylamine, the product yield was very poor even after 24 hours. Even

though sodium hydroxide appears to be the most suitable base which catalyzes the reaction to quantitative yields in short reaction time, formation of palladium black was rather high in this reaction. We concluded that K₃PO₄ is the most suitable base for this purpose and hence we used this base to carry out all the Suzuki reactions reported here.

Tables 4.8 – 4.10 show results of the Suzuki reactions we have carried out using **PdG₁** catalyst. In a typical reaction the arylboronic acid (0.8 mmol) and the aryl halide (0.8 mmol) were dissolved in tetrahydrofuran (5 mL) taken in a dry RB flask containing 1 mg **PdG₁** and refluxed with an aqueous solution (5 mL) of K₃PO₄·3H₂O (2 mmol) for 6 h. Organic layer was separated and purified by column chromatography. In all cases the products were unambiguously characterized by ¹H NMR spectroscopy/GC-MS analysis.

Table 4.8 shows the Suzuki reaction of phenylboronic acid with different aryl halides. The aryl iodides selected for these studies included substrates possessing different electroactive groups like electron withdrawing nitro and carboxylic acid groups as well as electron donating methoxy and methyl substituents. It can be seen that regardless of the electroactive nature of substituent present on the aryl halide, all the reactions proceeded smoothly to give quantitative product yields. Aryl bromides were also found to be reactive for the Suzuki reaction using **PdG₁** catalyst.

Table 4.8 Suzuki coupling of phenylboronic acid catalyzed by PdG₁.

Entry	Substrates	Product	Yield (%)
B1			97
B2			95
B3	 		95
B4			96
B5			85
B6			89

Naphthaleneboronic acid also showed an almost similar reactivity as phenylboronic acid in the PdG₁ catalyzed Suzuki coupling. Results summarized in Table 4.9 show that the electron donating or withdrawing nature of the substituents did not influence the product yields.

Table 4.9 Suzuki coupling of 1-naphthylboronic acid catalyzed by PdG₁.

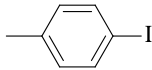
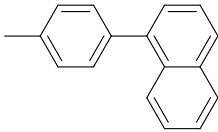
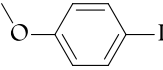
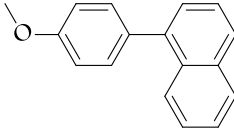
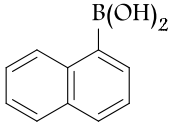
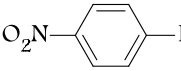
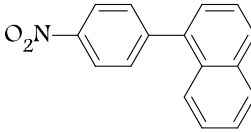
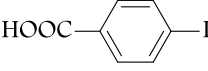
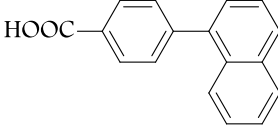

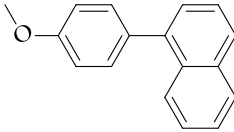
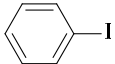
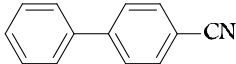
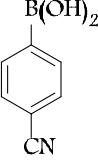
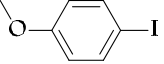
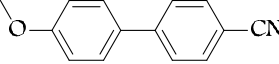
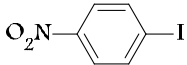
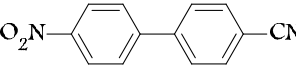
Entry	Substrates	Product	Yield (%)
B7			94
B8			93
B9	 		95
B10			88
B11			82

Table 4.10 comprises the reaction of cyanophenylboronic acid with different aryl iodides. It can be seen that the product yields obtained here are lower than those with obtained with phenyl and naphthylboronic acids. However, when nitro group was present as substituent on the aryl iodide, the yield was high. It could be noted that in all these reactions, we have not observed any oxygen interference as encountered in usual palladium catalyzed Suzuki reactions.

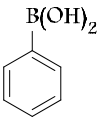
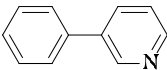
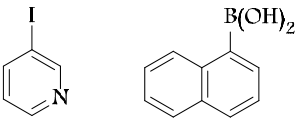
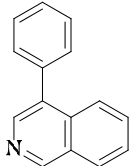
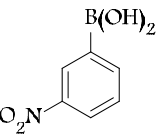
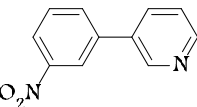
Table 4.10 Suzuki coupling of 4-cyanophenylboronic acid catalyzed by PdG₁.

Entry	Substrates	Product	Yield (%)
B12			72
B13	 		70
B14			95

4.3.4.1 Suzuki reaction using heteroaromatics

We have also studied Suzuki reactions between heteroaromatics and boronic acids using PdG₁ catalyst. We used 3-iodopyridine as the heteroaromatic component and the results obtained are shown in Table 4.11. The general procedure described earlier was adopted here also. It is evident from the studies that PdG₁ can act as good catalyst for the coupling of heteroaryl halides with different boronic acids. However, the product yields were found to be lower than those obtained with simple aryl halides. Formation of homocoupled products (coupling occurs at the position occupied by boronic acid group) was also observed in these reactions, which can be a possible reason for the low yield.

Table 4.11 Suzuki coupling of 3-iodopyridine catalysed by PdG₁.

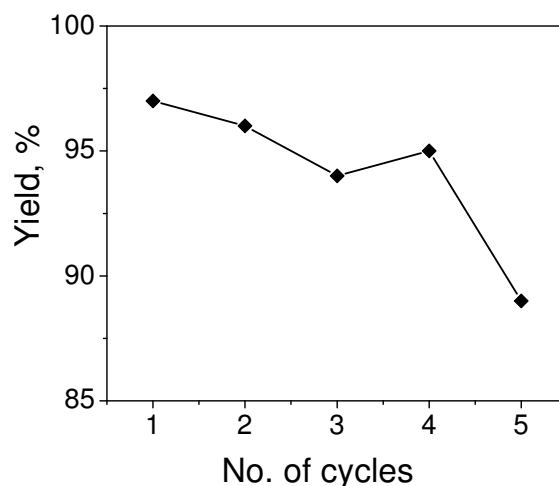
Entry	Substrates	Product	Yield (%)
B15			75
B16			61
B17			60

4.3.4.2 Recyclability of PdG₁ for Suzuki reaction

The reusability of PdG₁ in Suzuki coupling reactions was evaluated using phenylboronic acid and 4-iodoanisole as substrates. In a typical experiment 0.4 mmol each of phenylboronic acid and 4-iodoanisole were refluxed in THF containing PdG₁ (5 mg) and K₃PO₄ (1 mmol) for 6 h. THF was removed and product extracted into ether. PdG₁ being insoluble in ether adheres to the walls of the flask. Ether solution was decanted and product isolated. Fresh amounts of reactants were added to the flask containing the PdG₁ and reaction repeated. Yields of products obtained for 5 cycles are summarized in Table 4.12 and plotted in Figure 4.3. It can be noted from Table 4.12 that PdG₁ exhibited good recyclability.

Table 4.12 Catalyst recovery study of Suzuki coupling catalyzed by PdG₁.

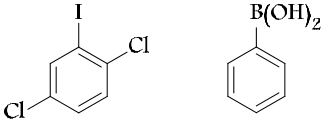
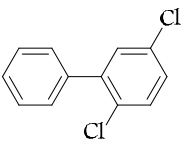
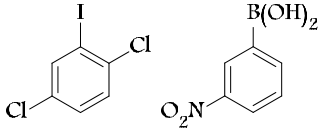
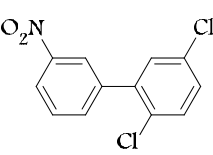
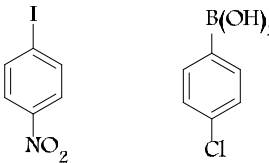
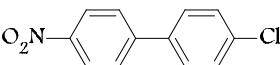
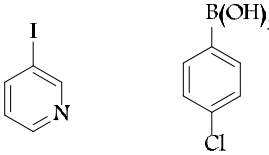
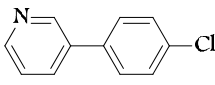
Cycle	1 st	2 nd	3 rd	4 th	5 th
Yield (%)	97	96	94	95	89

**Figure 4.3** Recyclability of PdG₁ for Suzuki coupling.

4.3.4.5 Selectivity of halides for PdG₁ catalyzed Suzuki reaction

The previously reported palladium NCDs [Wu 2006; 2008] were capable of efficiently catalyzing Suzuki reaction of aryl chlorides with boronic acids. However, we observed that PdG₁ did not catalyze Suzuki reactions between aryl chlorides and boronic acids even when the halide component contained activating substituents such as nitro and carbonyl. We observed that when the halogen component contained chloro and iodo groups, the PdG₁ catalyzed Suzuki reaction occurred only with the iodo substituents as shown in Table 4.13.

Table 4.13 Substrate selectivity for Suzuki coupling catalyzed by PdG₁.

Entry	Substrates	Product	Yield (%)
B18			75
B19			61
B20			60
B21			60

4.3.4.6 Role of capping dendrons in PdG₁ catalyzed Suzuki reaction

As mentioned in the experimental section, we have observed the formation of small amounts of palladium black in all these reactions. Formation of palladium black in these reactions can be either due to decomposition of partially protected NCDs present in the catalyst or due to Ostwald ripening. It has been reported in the literature that harsh conditions employed in nanocatalysis can induce Ostwald ripening of the nanoparticles which ultimately leads to precipitation of the metal nanoparticle [Narayanan 2003; 2005 (a,b,c); 2008]. Ostwald ripening is a cluster growth mechanism which involves detachment of atoms from

small clusters having higher surface energy followed by reattachment of these atoms to more stable larger clusters possessing lower surface energy. Thus, with time the larger cluster grows in size while the smaller ones go into solution [Imre 2000; Howard 2002]. The extend of this ripening process depends upon the nature of the capping ligands used. El-Sayed and co-workers [Li 2001; Narayanan 2003; 2005 (a,b,c); 2008] carried out systematic studies in this regard and observed that an increase in the number of capping ligands on the nanoparticle surface decreases the rate of Ostwald ripening due to the unavailability of free surfaces/defective sites on the nanoparticle surface. But, in such cases the observed catalytic activity will be less owing to the blocking of active sites on the nanoparticle surface. In the present case, the fraction of nanoparticle surface occupied by the dendron ligand is less and chances of Ostwald ripening taking place is more.

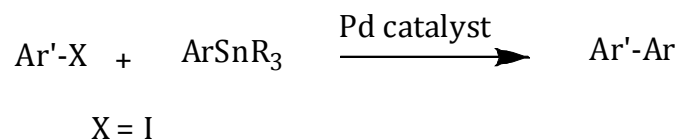
A comparative study of the rate of leaching for dendrimer stabilized and polymer stabilized palladium nanoparticles has been carried out by the groups of El-Sayed [Narayanan 2004] and de Jesús [Bernechea 2009]. Their studies indicated that even though the leaching process occurs almost equally with both the capping ligands, the possibility of the leached out metal atoms to go off from the palladium core is less for dendron ligands due to the steric congestion provided by the dendrons. As a result, a major fraction of the metal atoms will be preserved inside the dendron itself and these atoms can reattach to the parent metal core. This fact is reflected in the good recyclability of the dendrimer protected metal nanoparticles. On the other hand, polymer ligands will not be able to

provide the steric covering thus allowing the leached out atoms to get away from the initial palladium core which will reattach to growing nanoclusters leading to eventual precipitation of palladium black. The leaching followed by precipitation process results in a decrease in the amount of colloidal palladium present in the system and this will have direct consequences on the product yield for further reaction cycles.

The formation of small amounts of palladium black in the present system can be mainly due to Ostwald ripening. It was stated previously that nearly 50% of surface atoms in **PdG₁** are not linked to ligands. Pd atoms can get detached from these sites as suggested by El-Sayed and co-workers. Since the G₁ ligand is relatively small, the G₁ shell surrounding the Pd nanoparticle may not provide sufficient protection to the detached atoms. These atoms go into solution and later get attached to partially protected NCDs and eventually precipitate out. It may be noted that even in the fifth cycle, the yield of product is very high (Table 4.12), indicating that the extent of Pd black formation is very small.

4.3.5 Stille Reaction

Stille reaction involves the palladium catalyzed coupling of substituted aryl tin compounds with aryl halides leading to the formation of polyaryl compounds as shown in Scheme 4.3.



Scheme 4.3 General scheme of Stille coupling.

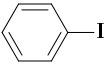
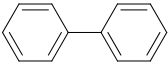

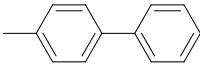
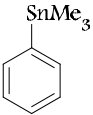
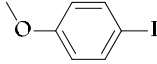
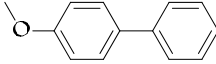
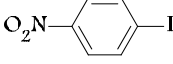
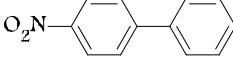
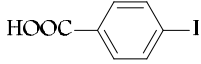

Despite the toxicity of organotin compounds, Stille coupling is considered as an important tool in organic synthesis mainly due to the availability of different organostannanes along with their compatibility with a wide variety of functional groups. A large number of unsymmetrical biaryls were synthesized using Stille coupling [Stille 1986; Dumartin 1995; Pathak 2000; Kogan 2002; Garcia-Martinez 2005; Caló 2005; Li 2006; Wu 2006; 2008].

We observed that **PdG₁** can catalyze Stille reactions between trimethylphenyltin and aryl iodides. In a typical reaction, equimolar amounts (≈ 1 mmol each) of trimethylphenyltin and aryl iodides and **PdG₁** (1 mg) were taken in THF (6 mL) and refluxed for 4 h. The reaction mixture was then worked up to get the product which was further purified by column chromatography. We have attempted the reaction with few aryl iodides in this way and the product structures and yields are given in Table 4.14. All products in Table 4.14 were well characterized by ¹H NMR spectroscopy/GC-MS analysis. Yields shown in Table 4.14 are isolated product yields.

Aryl iodide substrates used for the present studies contained both electron withdrawing and electron donating groups. It is evident from Table 4.14 that the reaction proceeded equally well with different substrates and we have not observed any influence due to the electroactive nature of the substituents present on the aryl halide substrate on **PdG₁** catalyzed Stille couplings. As with Suzuki coupling, there was no observable oxygen interference for these reactions. All the

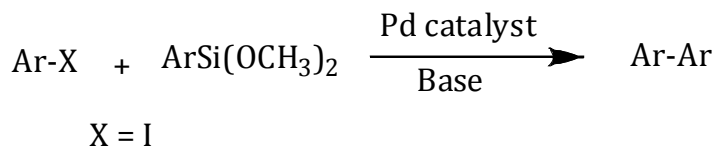
reactions were carried out under ordinary laboratory conditions without employing any special precautions like inert or dry reaction conditions.

Table 4.14 Stille coupling catalysed by PdG₁.

Entry	Substrates	Product	Yield (%)
C1			85
C2			73
C3	 		80
C4			96
C5			81

4.3.6 Hiyama Reaction

Palladium catalyzed cross coupling of organosilicon compounds with aryl halides is termed Hiyama reaction (Scheme 4.4) and this is also an important method for achieving C-C bond formation in organic synthesis.



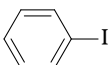
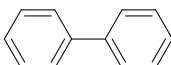
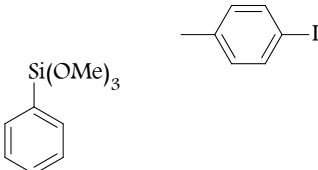
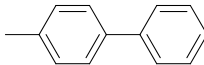
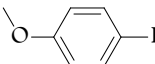
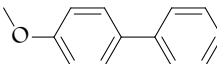
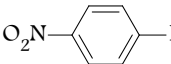
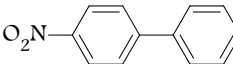
Scheme 4.4 General scheme of Hiyama coupling.

In the original report 1-iodonaphthalene was reacted with trimethylvinylsilane to produce 1-vinylnaphthalene with allylpalladium chloride dimer as catalyst and HMPA as solvent. A base or fluoride ion source is also required. The reaction possess many advantages such as low toxicity, high atom efficiency and safe handling compared with coupling reactions of organoboron, organozinc and organotin compounds [Hatanaka 1989; 1990; 1994; Gouda 1996; Pichler 1996; Hagiwara 1997; Homsí 2001; Denmark 2002; 2006; Pachón 2006].

We observed that **PdG₁** can catalyze the Hiyama reaction between phenyltrimethoxysilane and aryl iodides. In a typical experiment the silane (2 mmol), aryl iodide (1 mmol), **PdG₁** (1 mg) and a solution of tetrabutylammonium fluoride (1.0 M, 2 mL) were taken in dry THF (5 mL) and refluxed for 24 h. The reaction mixture was then worked up to get the product which was further purified by column chromatography. We have attempted the reaction with few aryl iodides in this way and the product structures and yields obtained are given in Table 4.15. All products in Table 4.15 were well characterized by ¹H NMR spectroscopy/GC-MS analysis. The isolated product yields are shown in Table 4.15 and these were low when compared to those obtained for Suzuki and Stille reactions.

We have used aryl iodides having different electroactive substituents and observed that the product yield was maximum when a nitro substituent was present on the aryl halide substrate. It could be noted that unlike Suzuki and Stille coupling, dry reaction conditions need to be maintained for the Hiyama coupling. We also observed that presence of oxygen did not interfere in the PdG₁ catalyzed Hiyama coupling reactions.

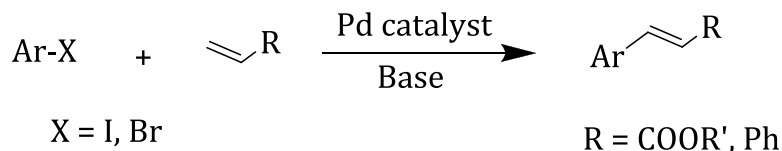
Table 4.15 Hiyama coupling catalysed by PdG₁.

Entry	Substrates	Product	Yield (%)
D1			75
D2			60
D3			61
D4			82

4.3.7 Heck Reaction

Heck reaction is one of the most important C-C bond forming reactions in organic chemistry. The reaction involves coupling of an activated alkene with an aryl/vinyl halide in the presence of a palladium catalyst and base

to give the aryl substituted alkene as shown in Scheme 4.5 [Mizoroki 1971; Heck 1972; Beletskaya 2000; Yeung 2001; de Vries 2006].



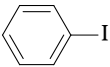
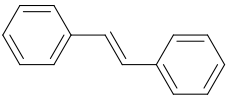
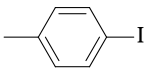
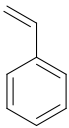
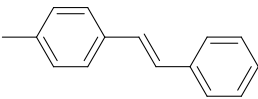
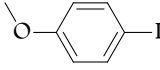
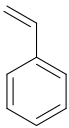
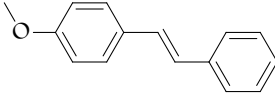
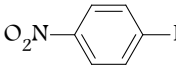
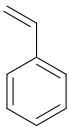
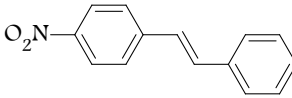
Scheme 4.5 General scheme of Heck coupling reaction.

The halide employed in the reaction can be aryl, benzyl or vinyl and the alkene must contain at least one proton. Normally an electron deficient alkene such as acrylate ester or acrylonitrile is employed. The catalyst can be tetrakis(triphenylphosphine)palladium(0), palladium chloride or palladium (II) acetate. A ligand such as triphenylphosphine or BINAP is usually employed. Bases normally used in the reaction include triethylamine, potassium carbonate and sodium acetate.

We observed that **PdG₁** can catalyze the Heck reaction between styrene and aryl iodides. Aryl iodides with electron donating and withdrawing substituents were employed in our studies. In a typical experiment styrene (4 mmol) and the aryl iodide (4 mmol) were taken in a dry RB flask containing 5 mg **PdG₁**. Triethylamine (8 mmol) and dry toluene (10 mL) were added and the reaction mixture refluxed for 24 h under argon atmosphere. Solvent was then removed using a rotavapor and the residue was chromatographed through an alumina column using hexane as eluent. Table 4.16 shows the structures of products and isolated yields of the reactions. All products in Table 4.16 were well characterized by ¹H NMR spectroscopy/GC-MS analysis. As can be seen from Table 4.16

yields are low compared with those obtained in Suzuki, Stille and Hiyama reactions. We also observed that dry reaction conditions were essential for the reaction to take place.

Table 4.16 Heck coupling catalyzed by PdG₁.

Entry	Substrates	Product	Yield (%)
E1			36
E2	 		40
E3	 		39
E4	 		49

4.4 Conclusions

The ability a palladium nanoparticle-cored dendrimer, PdG₁, to catalyze a few selected organic transformations was evaluated. We observed that PdG₁ can efficiently catalyze hydrogenation reactions of multifunctional organic molecules as well as different C-C bond forming reactions like Suzuki, Stille, Heck and Hiyama coupling. The ability of PdG₁ to catalyze chemoselective hydrogenation of multifunctional organic molecules was excellent under mild reaction conditions with good

recyclability of the catalyst. Reducible functional groups such as nitro and carbonyl remained intact while the olefinic and acetylinic bonds underwent smooth reduction with large turn over numbers and turn over frequencies. The dependence of hydrogen pressure and reaction time on the product selectivity was also studied and it was observed that on prolonged reaction time and under high hydrogen pressure, functional groups such as nitro and aldehyde also underwent reduction. This shows that, with multifunctional substrates, the reaction can be fine tuned to the desired products by changing the reaction conditions. The Suzuki coupling using **PdG₁** was studied in detail and it was observed that the reactions were selective for aryl iodides and bromides while the chlorides were inert under the conditions employed. The reactions proceeded smoothly under aqueous and mild conditions with little influence exerted by the electroactive groups present in the aryl halide substituent. The catalyst system showed good recyclability and the reactions were equally feasible with heteroaromatic systems as well. **PdG₁** catalyzed Stille coupling reactions of few substrates were also studied and the results indicated that **PdG₁** can catalyze coupling of organostannanes under aqueous and mild conditions with good yields. Heck and Hiyama couplings were also studied using **PdG₁** and aryl iodides, but product yields were low in these cases. Our idea was to develop one palladium catalyst that could be employed in all palladium catalyzed reactions. **PdG₁** seems to fulfill this role reasonably well.

4.5 Experimental

4.5.1 Materials and Methods

Phenylboronic acid, 1-naphthylboronic acid, 4-cyanophenylboronic acid, 4-iodotoluene, 4-bromoanisole, 4-iodobenzoic acid, 4-iodophenol, phenyltrimethoxy silane, tetra-*n*-butylammonium fluoride (TBAF), and K₃PO₄·3H₂O were purchased from Aldrich and used as received. Solvents such as acetone, toluene and dichloromethane (DCM) were obtained from MERCK and used as received. Dry tetrahydrofuran (THF) used for the synthesis was freshly distilled from sodium benzophenone ketyl.

Melting points were determined on a Mel-Temp II melting point apparatus and are uncorrected. ¹H NMR data were obtained from a 300 MHz Bruker Avance DPX spectrometer. ¹³C NMR spectra were recorded using a 500 MHz Bruker Avance DPX spectrometer. FT-IR spectra were recorded on a Shimadzu IR Prestige 21 spectrometer. High-resolution mass spectra were obtained by using a JOEL JMS600 mass spectrometer.

4.5.2 Reaction Conditions and Product Characterization Data for PdG₁ Catalyzed Reactions

4.5.2.1 Hydrogenation

A1: The hydrogenation was carried out using styrene (260.0 mg, 2.4 mmol). Yield = 238.0 mg (90%); ¹H NMR (500 MHz, TMS, CDCl₃, δ): 1.204 – 1.235 (t, 3H, CH₃), 2.6 – 2.645 (q, 2H, CH₂), 7.13 – 7.177 (m, 3H, aromatic), 7.237 – 7.267 (m, 2H, aromatic) ppm. ¹³C NMR (125 MHz, TMS,

CDCl₃, δ): 16.0, 29.04, 125.73, 128.03, 128.43, 144.36 ppm. GC-MS (m/z) = 106 (M⁺)

A2: The hydrogenation was carried out using phenylacetylene (255.0 mg, 2.5 mmol). Yield = 244.0 mg (92%). Product is same as in **A1**.

A3: The hydrogenation was carried out using stilbene (100.0 mg, 0.55 mmol). Yield = 99.0 mg (99 %); ¹H NMR (500 MHz, TMS, CDCl₃, δ): 2.85 (s, 4H, CH₂), 7.10 – 7.13 (m, 6H, aromatic), 7.18 – 7.22 (m, 4H, aromatic) ppm. ¹³C NMR (125 MHz, TMS, CDCl₃, δ): 37.95, 126.53, 127.63, 128.69, 130.08, 141.8 ppm. GC-MS (m/z) = 182 (M⁺)

A4: The hydrogenation was carried out using diphenylacetylene (100.0 mg, 0.56 mmol). Yield = 100.0 mg (98%). Product is same as in **A3**.

A5: The hydrogenation was carried out using cinnamaldehyde (131.0 mg, 1 mmol). Yield = 108.0 (81%); ¹H NMR (500 MHz, TMS, CDCl₃, δ): 2.636 – 2.669 (m, 2H, CH₂), 2.826 – 2.857 (t, 2H, CH₂), 7.079 – 7.114 (m, 3H, aromatic), 7.172 – 7.202 (m, 2H, aromatic), 9.682 – 9.687 (t, 1H, CHO) ppm. ¹³C NMR (125 MHz, TMS, CDCl₃, δ): 28.13, 45.27, 126.33, 128.34, 128.64, 140.41, 201.03 ppm. GC-MS (m/z) = 134 (M⁺)

A6: The hydrogenation was carried out using 1-nitro-4-styrylbenzene (100.0 mg, 0.44 mmol). Yield = 99.0 mg (98%); ¹H NMR (500 MHz, TMS, CDCl₃, δ): 2.96 – 2.99 (t, 2H, CH₂), 3.04 – 3.08 (t, 2H, CH₂), 7.14 – 7.15 (m, 2H, aromatic), 7.16 – 7.24 (m, 1H, aromatic), 7.27 – 7.31 (m, 4H, aromatic), 8.13 – 8.14 (m, 2H, aromatic) ppm. ¹³C NMR (125 MHz, TMS, CDCl₃, δ):

36.17, 36.62, 122.56, 125.28, 127.40, 128.31, 139.43, 145.42, 148.38 ppm.

GC-MS (m/z) = 227 (M⁺).

A7: The hydrogenation was carried out using 1-methoxy-4-styrylbenzene (100.0 mg, 0.48 mmol). Yield = 100.0 mg (98%); ¹H NMR (500 MHz, TMS, CDCl₃, δ): 2.78 – 2.79 (m, 4H, CH₂), 3.68 (s, 3H, OCH₃), 6.72 – 6.74 (m, 2H, aromatic), 6.99 – 7.0 (m, 2H, aromatic), 7.07 – 7.11 (m, 3H, aromatic), 7.17 – 7.2 (m, 2H, aromatic) ppm. ¹³C NMR (125 MHz, TMS, CDCl₃, δ): 37.08, 38.26, 55.28, 113.79, 125.92, 128.36, 128.53, 129.40, 133.93, 141.91, 157.89 ppm. GC-MS (m/z) = 212 (M⁺)

A8: The hydrogenation was carried out using cinnamic acid (100.0 mg, 0.68 mmol). Yield = 97.0 mg (95%); ¹H NMR (500 MHz, TMS, CDCl₃, δ): 2.593 – 2.624 (t, 2H, CH₂), 2.868 – 2.899 (t, 2H, CH₂), 7.124 – 7.15 (m, 3H, aromatic), 7.205 – 7.235 (m, 2H, aromatic) ppm. ¹³C NMR (125 MHz, TMS, CDCl₃, δ): 29.5, 34.54, 125.3, 127.19, 127.5, 139.08, 177.98 ppm. GC-MS (m/z) = 150 (M⁺)

A9: The hydrogenation was carried out using methyl cinnamate (100.0 mg, 0.62 mmol). Yield = 99.0 mg (98%); ¹H NMR (500 MHz, TMS, CDCl₃, δ): 2.49 – 2.521 (t, 2H, CH₂), 2.814 – 2.845 (t, 2H, CH₂), 3.529 (s, 3H, CH₃), 7.066 – 7.087 (m, 3H, aromatic), 7.145 – 7.175 (m, 2H, aromatic) ppm. ¹³C NMR (125 MHz, TMS, CDCl₃, δ): 30.97, 35.61, 52.09, 126.3, 128.31, 128.55, 140.56, 173.3 ppm. GC-MS (m/z) = 164 (M⁺)

A10: The hydrogenation was carried out using chalcone (100.0 mg, 0.48 mmol). Yield = 100.0 mg (99%); ¹H NMR (500 MHz, TMS, CDCl₃, δ): 2.98 – 3.01 (m, 2H, CH₂), 3.21 – 3.24 (m, 2H, CH₂), 7.13 – 7.17 (m, 1H, aromatic),

7.18 – 7.21 (m, 2H, aromatic), 7.22 – 7.24 (m, 1H, aromatic), 7.36 – 7.39 (m, 2H, aromatic), 7.4 – 7.48 (m, 2H, aromatic), 7.88 – 7.9 (m, 2H, aromatic) ppm. ¹³C NMR (125 MHz, TMS, CDCl₃, δ): 30.13, 40.47, 125.86, 126.15, 128.44, 128.54, 128.62, 133.08, 136.85, 141.3, 199.26 ppm. GC-MS (m/z) = 210 (M⁺)

A11: The hydrogenation was carried out using 1,5-diphenylpenta-2,4-dien-1-one (100.0 mg, 0.43 mmol). Yield = 99.0 mg (98%); ¹H NMR (500 MHz, TMS, CDCl₃, δ): 1.61 – 1.72 (m, 4H, CH₂), 2.56 – 2.59 (t, 2H, CH₂), 2.87 – 2.9 (t, 2H, CH₂), 7.08 – 7.1 (m, 3H, aromatic), 7.17 – 7.19 (m, 2H, aromatic), 7.34 – 7.37 (m, 2H, aromatic), 7.44 – 7.45 (m, 1H, aromatic), 7.84 – 7.86 (m, 2H, aromatic) ppm. ¹³C NMR (125 MHz, TMS, CDCl₃, δ): 22.96, 30.05, 34.76, 37.36, 124.71, 127.0, 127.28, 127.36, 127.52, 131.86, 136.04, 141.2, 199.2 ppm. GC-MS (m/z) = 238 (M⁺)

A12: The hydrogenation was carried out using 5-(4-nitrophenyl)-1-phenylpenta-2,4-dien-1-one (100.0 mg, 0.36 mmol). Yield = 96.0 mg (95%); ¹H NMR (500 MHz, TMS, CDCl₃, δ): 1.76 – 1.82 (m, 4H, CH₂), 2.78 – 2.81 (t, 2H, CH₂), 3.01 – 3.04 (t, 2H, CH₂), 7.34 – 7.36 (m, 2H, aromatic), 7.46 – 7.49 (m, 2H, aromatic), 7.56 – 7.59 (m, 1H, aromatic), 7.95 – 7.97 (m, 2H, aromatic), 8.14 – 8.16 (m, 2H, aromatic) ppm. ¹³C NMR (125 MHz, TMS, CDCl₃, δ): 23.71, 30.52, 35.75, 38.12, 123.65, 127.99, 128.62, 129.18, 133.08, 136.9, 146.13, 150.12, 199.84 ppm. GC-MS (m/z) = 283 (M⁺)

A13: The hydrogenation was carried out using 1,10-diphenylnona-1,3,7,9-tetraen-5-one (100.0 mg, 0.34 mmol). Yield = 96.0 mg (94%); ¹H NMR (500 MHz, TMS, CDCl₃, δ): 1.51 – 1.54 (m, 8H, CH₂), 2.29 – 2.32 (m, 4H,

CH₂), 2.51 – 2.54 (m, 4H, CH₂), 7.07 – 7.1 (m, 6H, aromatic), 7.17 – 7.19 (m, 4H, aromatic) ppm. ¹³C NMR (125 MHz, TMS, CDCl₃, δ): 23.5, 31.03, 35.77, 42.61, 125.77, 128.32, 128.4, 142.23, 211.01 ppm.

4.5.2.2 Suzuki coupling catalyzed by PdG₁

B1: The reaction was carried out using phenylboronic acid (50.0 mg, 0.4 mmol) and iodobenzene (82.0 mg, 0.4 mmol). Yield = 60.0 mg (97%); ¹H NMR (500 MHz, TMS, CDCl₃, δ): 7.314 – 7.346 (m, 2H, aromatic), 7.408 – 7.438 (m, 4H, aromatic), 7.574 – 7.592 (m, 4H, aromatic) ppm. ¹³C NMR (125 MHz, TMS, CDCl₃, δ): 127.23, 128.77, 128.87, 141.29 ppm.

B2: The reaction was carried out using phenylboronic acid (50.0 mg, 0.4 mmol) and 4-iodotoluene (93.0 mg, 0.4 mmol). Yield = 65.0 mg (95%); ¹H NMR (500 MHz, TMS, CDCl₃, δ): 2.39 (s, 3H, CH₃), 7.24 – 7.26 (d, 2H, aromatic), 7.32 – 7.33 (m, 1H, aromatic), 7.41 – 7.44 (t, 2H, aromatic), 7.48 – 7.5 (d, 2H, aromatic), 7.57 – 7.58 (d, 2H, aromatic) ppm.

B3: The reaction was carried out using phenylboronic acid (50.0 mg, 0.4 mmol) and 4-iodoanisole (100.0 mg, 0.4 mmol). Yield = 70.0 mg (95%); ¹H NMR (500 MHz, TMS, CDCl₃, δ): 3.84 (s, 3H, OCH₃), 6.96 – 6.98 (m, 2H, aromatic), 7.23 (m, 1H, aromatic), 7.28 – 7.31 (m, 2H, aromatic), 7.39 – 7.4 (m, 4H, aromatic) ppm. ¹³C NMR (125 MHz, TMS, CDCl₃, δ): 55.36, 114.21, 126.67, 126.75, 128.17, 128.74, 133.79, 140.84, 159.15 ppm.

B4: The reaction was carried out using phenylboronic acid (50.0 mg, 0.4 mmol) and 1-iodo-4-nitrobenzene (99.0 mg, 0.4 mmol). Yield = 76.0 mg (96%); ¹H NMR (500 MHz, TMS, CDCl₃, δ): 7.424 – 7.504 (m, 3H, aromatic),

7.508 – 7.51 (m, 2H, aromatic), 7.603 – 7.73 (m, 2H, aromatic), 8.25 – 8.35 (m, 2H, aromatic) ppm. ¹³C NMR (125 MHz, TMS, CDCl₃, δ): 124.11, 127.39, 127.80, 128.94, 129.17, 138.76, 147.08, 147.63 ppm.

B5: The reaction was carried out using phenylboronic acid (50.0 mg, 0.4 mmol) and 4-iodobenzoic acid (99.0 mg, 0.4 mmol). Yield = 67.0 mg (85%); ¹H NMR (500 MHz, TMS, CDCl₃, δ): 7.35 – 7.36 (m, 1H, aromatic), 7.4 – 7.43 (t, 2H, aromatic), 7.57 – 7.59 (d, 2H, aromatic), 7.63 – 7.65 (d, 2H, aromatic), 8.11 – 8.13 (d, 2H, aromatic) ppm. ¹³C NMR (125 MHz, TMS, CDCl₃, δ): 126.16, 126.31, 126.92, 127.27, 127.95, 129.72, 138.88, 145.47, 169.9 ppm.

B6: The reaction was carried out using phenylboronic acid (50.0 mg, 0.4 mmol) and 4-bromoanisole (75.0 mg, 0.4 mmol). Yield = 66.0 mg (89%). Product is same as in **B3**.

B7: The reaction was carried out using naphthalene-1-ylboronic acid (73.0 mg, 0.4 mmol) and 4-iodotoluene (91.0 mg, 0.4 mmol). Yield = 86.0 mg (94%); ¹H NMR (500 MHz, TMS, CDCl₃, δ): 2.46 (s, 3H, CH₃), 7.3 – 7.31 (m, 2H, aromatic), 7.39 – 7.43 (m, 4H, aromatic), 7.47 – 7.53 (m, 2H, aromatic), 7.84 – 7.85 (m, 1H, aromatic), 7.89 – 7.93 (m, 2H, aromatic) ppm.

B8: The reaction was carried out using naphthalene-1-ylboronic acid (73.0 mg, 0.4 mmol) and 4-iodoanisole (100.0 mg, 0.4 mmol). Yield = 92.0 mg (93%); ¹H NMR (500 MHz, TMS, CDCl₃, δ): 3.89 (s, 3 H, OCH₃), 7.02 – 7.04 (d, 2H, aromatic), 7.4 – 7.44 (m, 4 H, aromatic), 7.47 – 7.52 (m, 2H, aromatic), 7.83 – 7.84 (d, 1H, aromatic), 7.89 – 7.93 (q, 2H, aromatic) ppm.

¹³C NMR (125 MHz, TMS, CDCl₃, δ): 55.37, 113.73, 125.41, 125.71, 125.93, 126.08, 126.92, 127.34, 128.27, 131.12, 131.84, 133.14, 133.85, 139.92, 158.95 ppm.

B9: The reaction was carried out using 1-naphthylboronic acid (73.0 mg, 0.4 mmol) and 1-iodo-4-nitrobenzene (104.0 mg, 0.4 mmol). Yield = 99.0 mg (95%); ¹H NMR (500 MHz, TMS, CDCl₃, δ): 7.416 – 7.430 (m, 1H, aromatic), 7.457 – 7.490 (m, 1H, aromatic), 7.518 – 7.569 (m, 2H, aromatic), 7.648 – 7.675 (m, 2H, aromatic), 7.77 – 7.787 (d, 1H, aromatic), 7.921 – 7.946 (m, 2H, aromatic), 8.335 – 8.362 (d, 2H, aromatic) ppm. ¹³C NMR (125 MHz, TMS, CDCl₃, δ): 123.6, 124.85, 125.14, 125.33, 126.24, 126.75, 127.1, 128.58, 128.97, 130.93, 133.79, 137.79, 138.67, 147.69 ppm.

B10: The reaction was carried out using naphthalene-1-ylboronic acid (73.0 mg, 0.4 mmol) and 4-iodobenzoic acid (104.0 mg, 0.4 mmol). Yield = 92.0 mg (88%); ¹H NMR (500 MHz, TMS, CDCl₃, δ): 7.46 – 7.5 (m, 2H, aromatic), 7.53 – 7.59 (m, 2H, aromatic), 7.64 – 7.66 (m, 2H, aromatic), 7.87 – 7.89 (m, 1H, aromatic), 7.92 – 7.96 (m, 2H, aromatic), 8.26 – 8.29 (m, 2H, aromatic) ppm.

B11: The reaction was carried out using naphthalene-1-ylboronic acid (138.0 mg, 0.8 mmol) and 4-bromoanisole (0.1 mL, 0.8 mmol). Yield = 154.0 mg (82%). Product is same as in **B8**.

B12: The reaction was carried out using 4-cyanophenylboronic acid (132.0 mg, 0.9 mmol) and 4-iodobenzene (0.1 mL, 0.9 mmol). Yield = 116.0 mg (72%). ¹H NMR (500 MHz, TMS, CDCl₃, δ): 7.34 – 7.37 (m, 1H,

aromatic), 7.4 – 7.43 (m, 2H, aromatic), 7.51 – 7.53 (m, 2H, aromatic), 7.6 – 7.62 (m, 2H, aromatic), 7.65 – 7.67 (m, 2H, aromatic) ppm. ¹³C NMR (125 MHz, TMS, CDCl₃, δ): 110.74, 118.81, 127.08, 127.59, 128.51, 128.96, 132.45, 139.02, 145.53 ppm.

B13: The reaction was carried out using 4-cyanophenylboronic acid (120 mg, 0.8 mmol) and 4-iodoanisole (187.0 mg, 0.8 mmol). Yield = 120.0 mg (70%). ¹H NMR (500 MHz, TMS, CDCl₃, δ): 3.84 (s, 3H, OCH₃), 6.96 – 6.98 (m, 2H, aromatic), 7.28 – 7.31 (m, 2H, aromatic), 7.39 – 7.4 (m, 4H, aromatic) ppm. ¹³C NMR (125 MHz, TMS, CDCl₃, δ): 55.36, 114.21, 126.67, 126.75, 128.17, 128.74, 133.79, 140.84, 159.15 ppm.

B14: The reaction was carried out using 4-cyanophenylboronic acid (100.0 mg, 0.7 mmol) and 4-iodonitrobenzene (169.0 mg, 0.7 mmol). Yield = 145.0 mg (95%). ¹H NMR (500 MHz, TMS, CDCl₃, δ): 7.735 – 7.816 (m, 6H, aromatic), 8.343 – 8.36 (d, 2H, aromatic) ppm. ¹³C NMR (125 MHz, TMS, CDCl₃, δ): 112.67, 118.36, 124.37, 128.11, 128.17, 132.92, 143.13, 145.39, 147.91 ppm.

B15: The reaction was carried out using phenylboronic acid (52.0 mg, 0.43 mmol) and 3-iodopyridine (87.0 mg, 0.43 mmol). Yield = 50.0 mg (75%); ¹H NMR (500 MHz, TMS, CDCl₃, δ): 7.354 – 7.417 (m, 2H, aromatic), 7.46 – 7.49 (m, 2H, aromatic), 7.567 – 7.585 (m, 2H, aromatic), 7.866 – 7.89 (m, 1H, aromatic), 8.579 – 8.591 (m, 1H, aromatic), 8.846 – 8.85 (m, 1H, aromatic) ppm. ¹³C NMR (125 MHz, TMS, CDCl₃, δ): 123.66, 127.34, 128.17, 129.55, 134.55, 136.76, 137.72, 148.16, 148.28 ppm.

B16: The reaction was carried out using 1-naphthylboronic acid (100.0 mg, 0.58 mmol) and 3-iodopyridine (119.0 mg, 0.58 mmol). Yield = 73.0 mg (61%); ¹H NMR (500 MHz, TMS, CDCl₃, δ): 7.22 – 7.28 (m, 2H, aromatic), 7.296 – 7.312 (m, 1H, aromatic), 7.339 – 7.391 (m, 2H, aromatic), 7.627 – 7.666 (m, 2H, aromatic), 7.733 – 7.769 (t, 2H, aromatic), 8.526 – 8.538 (d, 1H, aromatic), 8.617 (s, 1H, aromatic) ppm. ¹³C NMR (125 MHz, TMS, CDCl₃, δ): 122.1, 124.29, 125, 125.46, 126.3, 127.45, 130.34, 132.69, 135.29, 136.3, 147.38, 149.37 ppm.

B17: The reaction was carried out using 3-nitrophenylboronic acid (97.0 mg, 58 mmol) and 3-iodopyridine (119.0 mg, 58 mmol). Yield = 70.0 mg (60%); ¹H NMR (500 MHz, TMS, CDCl₃, δ): 7.362 – 7.387 (m, 1H, aromatic), 7.594 – 7.625 (t, 1H, aromatic), 7.848 – 7.875 (t, 2H, aromatic), 8.192 – 8.209 (d, 1H, aromatic), 8.38 (s, 1H, aromatic), 8.617 (s, 1H, aromatic), 8.823 (s, 1H, aromatic) ppm. ¹³C NMR (125 MHz, TMS, CDCl₃, δ): 121.02, 121.87, 122.82, 129.15, 132, 133.32, 133.47, 138.55, 147.19, 147.83, 148.71 ppm.

B18: The reaction was carried out using phenylboronic acid (113.0 mg, 0.9 mmol) and 2,5-dichloriodobenzene (245.0 mg, 0.9 mmol). Yield = 150.0 mg (75%); ¹H NMR (500 MHz, TMS, CDCl₃, δ): 7.196 – 7.218 (m, 1H, aromatic), 7.31 – 7.315 (d, 1H, aromatic), 7.342 – 7.406 (m, 6H, aromatic) ppm. ¹³C NMR (125 MHz, TMS, CDCl₃, δ): 128.2, 128.3, 128.55, 129.37, 130.94, 131.12, 131.27, 132.66, 138.26, 142.05 ppm.

B19: The reaction was carried out using 3-nitrophenylboronic acid (150.0 mg, 0.9 mmol) and 2,5-dichloriodobenzene (245.0 mg, 0.9 mmol). Yield =

147 mg (61%); ¹H NMR (500 MHz, TMS, CDCl₃, δ): 7.332 – 7.37 (m, 2H, aromatic), 7.445 – 7.462 (d, 1H, aromatic), 7.622 – 7.654 (t, 1H, aromatic), 7.762 – 7.783 (d, 1H, aromatic), 8.266 – 8.308 (m, 2H, aromatic) ppm. ¹³C NMR (125 MHz, TMS, CDCl₃, δ): 123.17, 124.47, 129.29, 129.67, 130.9, 131.34, 133.07, 135.45, 139.58, 148.11 ppm.

B20: The reaction was carried out using 4-chlorophenylboronic acid (100.0 mg, 0.6 mmol) and 1-iodo-4-nitrobenzene (159.0 mg, 0.6 mmol). Yield = 90.0 mg (60%); ¹H NMR (500 MHz, TMS, CDCl₃, δ): 7.456 – 7.483 (d, 2H, aromatic), 7.545 – 7.572 (d, 2H, aromatic), 7.691 – 7.718 (d, 2H, aromatic), 8.284 – 8.312 (d, 2H, aromatic) ppm. ¹³C NMR (125 MHz, TMS, CDCl₃, δ): 124.32, 127.69, 128.67, 129.44, 135.27, 137.19, 146.32, 147.25 ppm.

B21: The reaction was carried out using 4-chlorophenylboronic acid (100.0 mg, 0.6 mmol) and 3-iodopyridine (131.0 mg, 0.6 mmol). Yield = 73.0 mg (60%); ¹H NMR (500 MHz, TMS, CDCl₃, δ): 7.299 – 7.309 (m, 1H, aromatic), 7.365 – 7.386 (d, 2H, aromatic), 7.42 – 7.446 (d, 2H, aromatic), 7.755 – 7.778 (m, 1H, aromatic), 8.521 – 8.529 (d, 1H, aromatic), 8.736 (s, 1H, aromatic) ppm. ¹³C NMR (125 MHz, TMS, CDCl₃, δ): 123.62, 128.34, 128.48, 129.31, 134.31, 135.54, 136.23, 147.97, 148.79 ppm.

4.5.2.3 Stille coupling catalyzed by PdG₁

C1: The reaction was carried out using trimethylphenyltin (165.0 mg, 0.68 mmol) and iodobenzene (139.0 mg, 0.68 mmol). Yield = 90.0 mg (85%). Product is same as in **B1**.

C2: The reaction was carried out using trimethylphenyltin (165.0 mg, 0.68 mmol) and 4-iodotoluene (149.0 mg, 0.68 mmol). Yield = 84.0 mg (73%). Product is same as in **B2**.

C3: The reaction was carried out using trimethylphenyltin (165.0 mg, 0.68 mmol) and 4-iodoanisole (160.0 mg, 0.68 mmol). Yield = 101.0 mg (80%). Product is same as in **B3**.

C4: The reaction was carried out using trimethylphenyltin (165.0 mg, 0.68 mmol) and 1-iodo-4-nitrobenzene (169.0 mg, 0.68 mmol). Yield = 130.0 mg (96%). Product is same as in **B4**.

C5: The reaction was carried out using trimethylphenyltin (165.0 mg, 0.68 mmol) and 4-iodobenzoic acid (168.0 mg, 0.68 mmol). Yield = 110.0 mg (81%). Product is same as in **B5**.

4.5.2.4 Hiyama coupling catalyzed by PdG₁

D1: The reaction was carried out using phenyltrimethoxysilane (397.0 mg, 2.0 mmol) and iodobenzene (205.0 mg, 1 mmol). Yield = 115 mg (75%). Product is same as in **B1**.

D2: The reaction was carried out using phenyltrimethoxysilane (397.0 mg, 2.0 mmol) and 4-iodotoluene (218 mg, 1 mmol). Yield = 100 mg (60%). Product is same as in **B2**.

D3: The reaction was carried out using phenyltrimethoxysilane (397.0 mg, 2.0 mmol) and 4-iodoanisole (234.0 mg, 1.0 mmol). Yield = 110 mg (61%). Product is same as in **B3**.

D4: The reaction was carried out using phenyltrimethoxysilane (198.5 mg, 1.0 mmol) and 1-iodo-4-nitrobenzene (124.5 mg, 0.5 mmol). Yield = 82 mg (82%). Product is same as in **B5**.

4.5.2.5 Heck reaction catalyzed by PdG₁

E1: The reaction was carried out using iodobenzene (1.0 g, 5 mmol) and styrene (0.5 g, 5 mmol). Yield = 311 mg (36%), ¹H NMR (300 MHz, TMS, CDCl₃, δ): 6.87 – 6.95 (m, 2H), 7.23 – 7.69 (m, 10H) ppm.

E2: The reaction was carried out using 4-iodotoluene (1.0 g, 5 mmol) and styrene (0.5 g, 5 mmol). Yield = 356 mg (40%), ¹H NMR (300 MHz, TMS, CDCl₃, δ): 2.3 (s, 3H, CH₃), 6.91 – 6.97 (m, 2H), 7.18 – 7.62 (m, 10H) ppm.

E3: The reaction was carried out using 4-iodoanisole (1.17 g, 5 mmol) and styrene (0.55 mL, 5 mmol). Yield = 390 mg (39%), ¹H NMR (500 MHz, TMS, CDCl₃, δ): 3.83 (s, 3H, OCH₃), 6.89 – 6.91 (m, 2H), 6.96 – 6.99 (m, 1H), 7.05 – 7.08 (m, 1H), 7.23 – 7.25 (m, 1H), 7.33 – 7.36 (t, 2H), 7.44 – 7.49 (m, 4H) ppm. ¹³C NMR (125 MHz, CDCl₃, δ): 55.33, 114.14, 126.25, 126.63, 127.21, 127.72, 128.22, 128.64, 130.16, 137.66, 159.31 ppm.

E4: The reaction was carried out using 1-iodo-4-nitrobenzene (1.25 g, 5 mmol) and styrene (0.55 mL, 5 mmol). Yield = 530 mg (49%), ¹H NMR (500 MHz, TMS, CDCl₃, δ): 7.1 – 7.16 (m, 1H), 7.29 – 7.42 (m, 4H), 7.53 – 7.56 (d, 2H), 7.6 – 7.63 (d, 2H), 8.19 – 8.22 (d, 2H, aromatic) ppm. ¹³C NMR (125 MHz, TMS, CDCl₃, δ): 123.13, 125.26, 125.84, 126, 127.83, 127.88, 132.29, 135.15, 142.83, 145.74 ppm.

List of Publications

- (i) Synthesis and Characterization of Gold-Nanoparticle Cored Dendrimers Stabilized by Metal–Carbon Bonds.
V. K. Ratheesh Kumar and K. R. Gopidas, *Chem. Asian J.* **2010**, *5*, 887-896.
- (ii) Palladium Nanoparticle-Cored G₁-Dendrimer Stabilized by Carbon-Pd Bonds: Synthesis, Characterization and Use as Chemoselective, Room Temperature Hydrogenation Catalyst.
V. K. Ratheesh Kumar and K. R. Gopidas, *Catal. Commun.* (*accepted for publication*)
- (iii) Cu(II)-Mediated Generation of Triarylamine Radical Cations and their Dimerization. An Easy Route to Tetraarylbenzidines.
K. Sreenath, C. V, Suneesh, **V. K. Ratheesh Kumar** and K. R. Gopidas, *J. Org. Chem.* **2008**, *73*, 3245-3251.

Posters Presented at National and International Conferences

- (i) Synthesis and Characterization of Gold-Nanoparticle Cored Dendrimers with Direct Metal-Carbon Linkage.
V. K. Ratheesh Kumar and K. R. Gopidas in 'International Conference on Advanced Nanomaterials and Nanotechnology' held at IIT Guwahati, Assam, December 9-11, 2009.
- (ii) Metal-Carbon Stabilized Palladium Nanoparticle-Cored Dendrimers as Chemoselective Hydrogenation Catalysts.

V. K. Ratheesh Kumar and K. R. Gopidas in '*5th Mid-CRSI Symposium on Chemistry*' held at NIIST (CSIR), Thiruvananthapuram, July 23-24, 2010.

(iii) Metal Nanoparticle-Cored Dendrimers: Synthesis, Characterization and their Use as Catalyst for Selected Organic Transformations.

V. K. Ratheesh Kumar and K. R. Gopidas in '*International Conference and Humboldt Kolleg on Interface between Chemistry and Biology: A Perspective*' held at ICT, Hyderabad, September 21-24, 2010.

References

- Adenier, A.; Combellas, C.; Kanoufi, F.; Pinson, J.; Podvorica, F. I. 'Formation of Polyphenylene Films on Metal Electrodes by Electrochemical Reduction of Benzenediazonium Salts', *Chem. Mater.* 18, **2006**, 2021-2029.
- Aiken, J. D.; Finke, R. G. 'A Review of Modern Transition-Metal Nanoclusters: Their Synthesis, Characterization, and Applications in Catalysis', *J. Mol. Catal. A: Chem.* 145, **1999**, 1-44.
- Allmond, C. E.; Sellinger, A. T.; Gogick, K.; Fitz-Gerald, J. M. 'Photo-Chemical Synthesis and Deposition of Noble Metal Nanoparticles', *Appl. Phys. A* 86, **2007**, 477-480.
- Allongue, P.; de Villeneuve, C. H.; Cherouvrier, G.; Cortés, R.; Bernard, M. C. 'Phenyl Layers on H-Si(111) by Electrochemical Reduction of Diazonium Salts: Monolayer versus Multilayer Formation', *J. Electroanal. Chem.* 550, **2003**, 161-174.
- Allongue, P.; Delamar, M.; Desbat, B.; Fagebaume, O.; Hitmi, R.; Pinson, J.; Savéant, J.-M. 'Covalent Modification of Carbon Surfaces by Aryl Radicals Generated from the Electrochemical Reduction of Diazonium Salts', *J. Am. Chem. Soc.* 119, **1997**, 201-207.
- Alvarez, M. M.; Khoury, J. T.; Schaaff, T. G.; Shafigullin, M. N.; Vezmar, I.; Whetten, R. L. 'Optical Absorption Spectra of Nanocrystal Gold Molecules', *J. Phys. Chem. B* 101, **1997**, 3706-3712.

- Anariba, F.; DuVall, S. H.; McCreery, R. L. 'Mono- and Multilayer Formation by Diazonium Reduction on Carbon Surfaces Monitored with Atomic Force Microscopy Scratching', *Anal. Chem.* 75, **2003**, 3837-3844.
- Angel, P. D.; Dominguez, J. M.; Angel, G. D.; Montoya, J. A.; Lamy-Pitara, E.; Labruquere, S.; Barbier, J. 'Aggregation State of Pt-Au/C Bimetallic Catalysts Prepared by Surface Redox Reactions', *Langmuir* 16, **2000**, 7210-7217.
- Astruc, D. 'Palladium Nanoparticles as Efficient Green Homogeneous and Heterogeneous Carbon-Carbon Coupling Precatalysts: A Unifying View', *Inorg. Chem.* 46, **2007**, 1884-1894.
- Astruc, D.; Lu, F.; Aranzaes, J. R. 'Nanoparticles as Recyclable Catalysts: The Frontier between Homogeneous and Heterogeneous Catalysis', *Angew. Chem. Int. Ed.* 44, **2005**, 7852 - 7872.
- Badia, A.; Singh, S.; Demers, L.; Cuccia, L.; Brown, G. R.; Lennox, R. B. 'Self-Assembled Monolayers on Gold Nanoparticles', *Chem. Eur. J.* 2, **1996**, 359-363.
- Balogh, L.; Tomalia, D. A. 'Poly(amidoamine) Dendrimer-Templated Nanocomposites. 1. Synthesis of Zerovalent Copper Nanoclusters', *J. Am. Chem. Soc.* 120, **1998**, 7355-7356.
- Bars, J. L.; Specht, U.; Bradley, J. S.; Blackmond, D. G. 'A Catalytic Probe of the Surface of Colloidal Palladium Particles Using Heck Coupling Reactions', *Langmuir* 15, **1999**, 7621-7625.
- Battistuzzi, G.; Cacchi, S.; Fabrizi, G. 'A Molten *n*-Bu₄NOAc/*n*-Bu₄NBr Mixture as an Efficient Medium for the Stereoselective Synthesis of (*E*)- and (*Z*)-3,3-Diarylacrylates', *Synlett* 3, **2002**, 0439-0442.

- Beletskaya, I. P.; Cheprakov, A. V. 'The Heck Reaction as a Sharpening Stone of Palladium Catalysis', *Chem. Rev.* 100, **2000**, 3009-3066.
- Beller, M.; Lohmer, G.; Kühlein, K.; Reisinger, C. P.; Herrmann, W. A. 'First Palladium-Catalyzed Heck Reactions with Efficient Colloidal Catalyst Systems', *J. Organomet. Chem.* 520, **1996**, 257-259.
- Bergbreiter, D. E.; Tian, J.; Hongfa, C. 'Using Soluble Polymer Supports to Facilitate Homogeneous Catalysis', *Chem. Rev.* 109, **2009**, 530-582.
- Bernard, M.-C.; Chaussé, A.; Cabet-Deliry, E.; Chehimi, M. M.; Pinson, J.; Podvorica, F.; Vautrin-UI, C. 'Organic Layers Bonded to Industrial, Coinage, and Noble Metals through Electrochemical Reduction of Aryldiazonium Salts', *Chem. Mater.* 15, **2003**, 3450-3462.
- Bernechea, M.; de Jesús, E.; López-Mardomingo, C.; Terreros, P. 'Dendrimer-Encapsulated Pd Nanoparticles versus Palladium Acetate as Catalytic Precursors in the Stille Reaction in Water', *Inorg. Chem.* 48, **2009**, 4491-4496.
- Bhattacharjee, S.; Dotzauer, D. M.; Bruening, M. L. 'Selectivity as a Function of Nanoparticle Size in the Catalytic Hydrogenation of Unsaturated Alcohols', *J. Am. Chem. Soc.* 131, **2009**, 3601-3610.
- Bradley J. S. *Clusters and Colloids: From Theory to Applications*; Schmid, G., (Ed.) VCH: Weinheim, 1994; pp 523-536.
- Brieger, G.; Nestruck, T. J. 'Catalytic Transfer Hydrogenation', *Chem. Rev.* 74, **1974**, 567-580.
- Brust, M.; Walker, M.; Bethel, D.; Schiffrin, D. J.; Whyman, R. 'Synthesis of Thiol-Derivatized Gold Nanoparticles in a Two-Phase Liquid-Liquid System', *J. Chem. Soc., Chem. Commun.* **1994**, 801-802.

- Burton, W. K.; Cabrera, N. 'Crystal Growth and Surface Structure. Part I', *Disc. Faraday Soc.* 5, **1949**, 33-39.
- Callis, N. M.; Thiery, E.; Bras, J. L.; Muzart, J. 'Palladium Nanoparticles-Catalyzed Chemoselective Hydrogenations, a Recyclable System in Water', *Tetrahedron Lett.* 48, **2007**, 8128-8131.
- Calò, V.; Nacci, A.; Monopoli, A.; Montingelli, F. 'Pd Nanoparticles as Efficient Catalysts for Suzuki and Stille Coupling Reactions of Aryl Halides in Ionic Liquids', *J. Org. Chem.* 70, **2005**, 6040-6044.
- Canning, P. S. J.; Maskill, H.; McCrudden, K.; Sexton, B. 'A Product Analytical Study of the Thermal and Photolytic Decomposition of Some Arenediazonium Salts in Solution', *Bull. Chem. Soc. Jpn.* 75, **2002**, 789-800.
- Cao, G. *Nanostructures and Nanomaterials: Synthesis, Properties and Applications*, 2008, Imperial College Press, London.
- Cassol, C. C.; Umpierre, A. P.; Machado, G.; Wolke, S. I.; Dupont, J. 'The Role of Pd Nanoparticles in Ionic Liquid in the Heck Reaction', *J. Am. Chem. Soc.* 127, **2005**, 3298-3299.
- Červený, L. 'Palladium Catalysts in Hydrogenation Reactions', *Chem. Eng. Comm.* 83, **1989**, 31-63.
- Cha, D. Y.; Parravano, G. 'Surface Reactivity of Supported Gold: I. Oxygen Transfer Between CO and CO₂', *J. Catal.* 18, **1970**, 200-211.
- Chechik, V.; Crooks, R. M. 'Dendrimer-Encapsulated Pd Nanoparticles as Fluorous Phase-Soluble Catalysts', *J. Am. Chem. Soc.* 122, **2000**, 1243-1244.

- Cheng, C.; Wang, X.; Xing, L.; Liu, B.; Zhu, R.; Hu, Y. 'An Efficient and Practical Method for Highly Chemoselective Hydrogenation of Nitrobenzylamines to Aminobenzylamine Hydrochlorides', *Adv. Synth. Catal.* **349**, **2007**, 1775-1780.
- Chum, P. W.; Wilson, S. E. 'Reduction of Alkynes and Monosubstituted Alkenes with Lithium Aluminum Hydride and Titanium Tetrachloride', *Tetrahedron Lett.* **1976**, 15-16.
- Chung, Y.-M.; Rhee, H.-K. 'Partial Hydrogenation of 1,3-Cyclooctadiene Using Dendrimer-Encapsulated Pd-Rh Bimetallic Nanoparticles', *J. Mol. Catal. A* **206**, **2003**, 291-298.
- Chung, Y.-M.; Rhee, H.-K. 'Pt-Pd Bimetallic Nanoparticles Encapsulated in Dendrimer Nanoreactor', *Catal. Lett.* **85**, **2003**, 159-164.
- Colquhoun, H. M.; Holton, J.; Thompson, D. J.; Twigg, M. V. *New Pathways for Organic Synthesis: Practical Applications of Transition Metals* Plenum Press, New York, 1984, Ch. 7, p. 265-338.
- Combella, C.; Jiang, D.; Kanoufi, F.; Pinson, J.; Podvorica, F. I. 'Steric Effects in the Reaction of Aryl Radicals on Surfaces', *Langmuir* **25**, **2009**, 286-293.
- Combella, C.; Kanoufi, F.; Pinson, J.; Podvorica, F. I. 'Sterically Hindered Diazonium Salts for the Grafting of a Monolayer on Metals', *J. Am. Chem. Soc.* **130**, **2008**, 8576-8577.
- Combella, C.; Kanoufi, F.; Pinson, J.; Podvorica, F. I. 'Time-of-Flight Secondary Ion Mass Spectroscopy Characterization of the Covalent Bonding between a Carbon Surface and Aryl Groups', *Langmuir* **21**, **2005**, 280-286.

- Crooks, R. M.; Zhao, M.; Sun, L.; Chechik, V.; Yeung, L. K. 'Dendrimer-Encapsulated Metal Nanoparticles: Synthesis, Characterization, and Applications to Catalysis', *Acc. Chem. Res.* 34, **2001**, 181-190.
- Cutler, E. C.; Lundin, E.; Garabato, B. D.; Choi, D.; Shon, Y.-S. 'Dendritic Functionalization of Monolayer Protected Gold Nanoparticles', *Mater. Res. Bull.* 42, **2007**, 1178-1185.
- Daniel, M.-C.; Ruiz, J.; Nlate, S.; Blais, J.-C.; Astruc, D. 'Nanoscopic Assemblies between Supramolecular Redox Active Metallodendrons and Gold Nanoparticles: Synthesis, Characterization, and Selective Recognition of H_2PO_4^- , HSO_4^- , and Adenosine-5'-Triphosphate (ATP^{2-}) Anions', *J. Am. Chem. Soc.* 125, **2003**, 2617-2628.
- de Villeneuve, C. H.; Pinson, J.; Bernard, M. C.; Allongue, P. 'Electrochemical Formation of Close-Packed Phenyl Layers on Si(111)', *J. Phys. Chem. B* 101, **1997**, 2415-2420.
- de Vries, J. G. 'A Unifying Mechanism for all High-Temperature Heck Reactions. The Role of Palladium Colloids and Anionic Species', *Dalton Trans.* **2006**, 421-429.
- Delamar, M.; Désarmot, G.; Fagebaume, O.; Hitmi, R.; Pinson, J.; Savéant, J.-M. 'Modification of Carbon Fiber Surfaces by Electrochemical Reduction of Aryl Diazonium Salts: Application to Carbon Epoxy Composites', *Carbon* 35, **1997**, 801-807.
- Delamarche, E.; Michel, B.; Kang, H.; Gerber, Ch. 'Thermal Stability of Self-Assembled Monolayers', *Langmuir* 10, **1994**, 4103-4108.

- Denmark, S. E.; Baird, J. D. 'Palladium-Catalyzed Cross-Coupling Reactions of Silanolates: A Paradigm Shift in Silicon-Based Cross-Coupling Reactions', *Chem. Eur. J.* **12**, **2006**, 4954–4963.
- Denmark, S. E.; Sweis, R. F. 'Design and Implementation of New, Silicon-Based, Cross-Coupling Reactions: Importance of Silicon-Oxygen Bonds', *Acc. Chem. Res.* **35**, **2002**, 835-846.
- Deshmukh, R. R.; Rajagopal, R.; Srinivasan, K. V. 'Ultrasound Promoted C–C Bond Formation Heck Reaction at Ambient Conditions in Room Temperature Ionic Liquids', *Chem. Commun.* **2001**, 1544–1545.
- Devenish, R. W.; Goulding, T.; Heaton, B. T.; Whyman, R. 'Preparation, Characterisation and Properties of Groups VIII and IB Metal Nanoparticles', *J. Chem. Soc., Dalton Trans.*, **1996**, 673-679.
- Diallo, A. K.; Ornelas, C.; Salmon, L.; Aranzaes, J. R.; Astruc, D. 'Homeopathic Catalytic Activity and Atom-Leaching Mechanism in Miyaura–Suzuki Reactions under Ambient Conditions with Precise Dendrimer-Stabilized Pd Nanoparticles', *Angew. Chem. Int. Ed.* **46**, **2007**, 8644 – 8648.
- Ding, J. H.; Gin, D. L. 'Catalytic Pd Nanoparticles Synthesized Using a Lyotropic Liquid Crystal Polymer Template', *Chem. Mater.* **12**, **2000**, 22-24.
- Dumartin, G.; Fouquet, E.; Pereyre, M.; Rabtier, M. 'Towards Non-polluting Organotin Reagents for Synthesis', *Appl. Org. Chem.* **9**, **1995**, 591-595.
- Dupont, J.; Fonseca, G. S.; Umpierre, A. P.; Fichtner, P. F. P.; Teixeira, S. R. 'Transition-Metal Nanoparticles in Imidazolium Ionic Liquids:

- Recyclable Catalysts for Biphasic Hydrogenation Reactions', *J. Am. Chem. Soc.* 124, **2002**, 4228-4229.
- Dyke, C. A.; Tour, J. M. 'Unbundled and Highly Functionalized Carbon Nanotubes from Aqueous Reactions', *Nano Lett.* 3, **2003**, 1215-1218.
- El-Sayed, M. A. 'Some Interesting Properties of Metals Confined in Time and Nanometer Space of Different Shapes', *Acc. Chem. Res.* 34, **2001**, 257-264.
- El-Sayed, M. A. 'Small is Different: Shape-, Size-, and Composition-Dependent Properties of Some Colloidal Semiconductor Nanocrystals', *Acc. Chem. Res.* 37, **2004**, 326-333.
- Entwistle, I. D.; Jackson, A. E.; Johnston, R. A. W.; Telford, R. P. 'Reduction of Nitro-Compounds', *J. Chem. Soc., Perkin Trans. 1*, **1977**, 443-444.
- Esumi, K.; Suzuki, A.; Aihara, N.; Usui, K.; Torigoe, K. 'Preparation of Gold Colloids with UV Irradiation Using Dendrimers as Stabilizer', *Langmuir* 14, **1998**, 3157-3159.
- Faraday, M. 'The Bakerian Lecture: Experimental Relations of Gold (and Other Metals) to Light', *Philos. Trans. R. Soc. London* 147, **1857**, 145-181.
- Feldheim, D. L.; Foss, C. A., Jr. (Eds.) *Metal Nanoparticles: Synthesis, Characterization and Applications*; Marcell Dekker: New York, 2002.
- Fink, J.; Kiely, C. J.; Bethell, D.; Schiffrin, D. J. 'Self-Organization of Nanosized Gold Particles', *Chem. Mater.* 10, **1998**, 922-926.
- Fréchet, J. M. J.; Tomalia, D. A. (Eds.), *Dendrimers and Other Dendritic Polymers*, John Wiley & Sons, Chichester, (UK), 2001.

- Garcia-Martinez, J. C.; Lezutekong, R.; Crooks, R. M. 'Dendrimer-Encapsulated Pd Nanoparticles as Aqueous, Room-Temperature Catalysts for the Stille Reaction', *J. Am. Chem. Soc.* 127, **2005**, 5097-5103.
- Ghosh, D.; Chen, S. 'Palladium Nanoparticles Passivated by Metal-Carbon Covalent Linkages', *J. Mater. Chem.* 18, **2008**, 755-762.
- Ghosh, D.; Chen, S. 'Solid-State Electronic Conductivity of Ruthenium Nanoparticles Passivated by Metal-Carbon Covalent Bonds', *Chem. Phys. Lett.* 465, **2008**, 115-119.
- Ghosh, D.; Pradhan, S.; Chen, W.; Chen, S. 'Titanium Nanoparticles Stabilized by Ti-C Covalent Bonds', *Chem. Mater.* 20, **2008**, 1248-1250.
- Ghosh, S. K.; Pal, T. 'Interparticle Coupling Effect on the Surface Plasmon Resonance of Gold Nanoparticles: From Theory to Applications', *Chem. Rev.* 107, **2007**, 4797-4862.
- Gittins, D. I.; Caruso, F. 'Spontaneous Phase Transfer of Nanoparticulate Metals from Organic to Aqueous Media', *Angew. Chem. Int. Ed.* 40, **2001**, 3001-3004.
- Glöckler, J.; Klütze, S.; Meyer-Zaika, W.; Reller, A.; García-García, F. J.; Strehblow, H.-H.; Keller, P.; Rentschler, E.; Kläui, W. 'With Phosphinophosphonic Acids to Nanostructured, Water-Soluble, and Catalytically Active Rhodium Clusters', *Angew. Chem. Int. Ed.* 46, **2007**, 1164-1167.
- Gopidas, K. R.; Whitesell, J. K.; Fox, M. A. 'Metal-Core-Organic Shell Dendrimers as Unimolecular Micelles', *J. Am. Chem. Soc.* 125, **2003**, 14168-14180.

- Gopidas, K. R.; Whitesell, J. K.; Fox, M. A. 'Nanoparticle-Cored Dendrimers: Synthesis and Characterization', *J. Am. Chem. Soc.* 125, **2003**, 6491-6502.
- Gopidas, K. R.; Whitesell, J. K.; Fox, M. A. 'Synthesis, Characterization, and Catalytic Applications of a Palladium-Nanoparticle-Cored Dendrimer', *Nano Lett.* 3, **2003**, 1757-1760.
- Gouda, K.; Hagiwara, E.; Hatanaka, Y.; Hiyama, T. 'Cross-Coupling Reactions of Aryl Chlorides with Organochlorosilanes: Highly Effective Methods for Arylation or Alkenylation of Aryl Chlorides', *J. Org. Chem.* 61, **1996**, 7232-7233.
- Grayson, S. M.; Fréchet, J. M. J. 'Convergent Dendrons and Dendrimers: from Synthesis to Applications', *Chem. Rev.* 101, **2001**, 3819-3867.
- Gröschel, L. R.; Haidar, A.; Beyer, K.-H.; Reichert, R.; Schomäcker, R. 'Characterization of Palladium Nanoparticles Adsorbed on Polyacrylic Acid Particles as Hydrogenation Catalyst', *Catal. Lett.* 95, **2004**, 67-75.
- Guo, W.; Li, J. J.; Wang, Y. A.; Peng, X. 'Luminescent CdSe/CdS Core/Shell Nanocrystals in Dendron Boxes: Superior Chemical, Photochemical and Thermal Stability', *J. Am. Chem. Soc.* 125, **2003**, 3901-3909.
- Hagiwara, Y.; Gouda, K.-I.; Hatanaka, Y.; Hiyama, T. 'NaOH-Promoted Cross-Coupling Reactions of Organosilicon Compounds with Organic Halides: Practical Routes to Biaryls, Alkenylarenes and Conjugated Dienes', *Tetrahedron Lett.* 38, **1997**, 439-442.
- Hamill, N. A.; Hardacre, C.; McMath, S. E. J. 'In situ XAFS Investigation of Palladium Species Present During the Heck Reaction in Room Temperature Ionic Liquids', *Green Chem.* 4, **2002**, 139-142.

- Haruta, M.; Kobayashi, T.; Sano, H.; Yamada, N. 'Novel Gold Catalysts of Carbon Monoxide at a Temperature Far Below 0 °C', *Chem. Lett.* **1987**, 405-408.
- Haruta, M.; Tsuboda, S.; Kobayashi, T.; Kagehama, H.; Genet, M. J.; Delmon, B. 'Low-Temperature Oxidation of CO over Gold Supported on TiO₂, α-Fe₂O₃, and Co₃O₄', *J. Catal.* **144**, **1993**, 175-192.
- Haruta, M.; Yamada, N.; Kobayashi, T.; Iijima, S. 'Gold Catalysts Prepared by Coprecipitation for Low-Temperature Oxidation of Hydrogen and of Carbon Monoxide', *J. Catal.* **115**, **1989**, 301-309.
- Hassan, J.; Sévignon, M.; Gozzi, C.; Schulz, E.; Lemaire, M. 'Aryl-Aryl Bond Formation One Century after the Discovery of the Ullmann Reaction', *Chem. Rev.* **102**, **2002**, 1359-1469.
- Hatanaka, Y.; Goda, K.; Okahara, Y.; Hiyama, T. 'Highly Selective Cross-Coupling Reactions of Aryl(halo)silanes with Aryl Halides: A General and Practical Route to Functionalized Biaryls', *Tetrahedron* **50**, **1994**, 8301-8316.
- Hatanaka, Y.; Hiyama, T. 'A Wide Range of Organosilicon Compounds Couples with Enol and Aryl Triflates in the Presence of Pd Catalyst and Fluoride Ion', *Tetrahedron Lett.* **31**, **1990**, 2719-2722.
- Hatanaka, Y.; Fukushima, S.; Hiyama, T. 'Selective Synthesis of Unsymmetrical Biaryls via Palladium-Catalyzed Cross-Coupling of Arylfluorosilanes with Aryl Iodides', *Chem. Lett.* **1989**, 1711-1714.

- Hattori, K.; Sajiki, H.; Hirota, K. 'Chemoselective Control of Hydrogenation among Aromatic Carbonyl and Benzyl Alcohol Derivatives Using Pd/C(en) Catalyst', *Tetrahedron* 57, **2001**, 4817-4824.
- Hattori, K.; Sajiki, H.; Hirota, K. 'Undesirable Deprotection of O-TBDMS Groups By Pd/C-Catalyzed Hydrogenation and Chemoselective Hydrogenation Using a Pd/C(en) Catalyst' *Tetrahedron* 57, **2001**, 2109-2114.
- Hawker, C. J.; Fréchet, J. M. J. 'Control of Surface Functionality in the Synthesis of Dendritic Macromolecules Using the Convergent-Growth Approach', *Macromolecules* 23, **1990**, 4726-4729.
- Hawker, C. J.; Fréchet, J. M. J. 'Preparation of Polymers with Controlled Molecular Architecture. A New Convergent Approach to Dendritic Macromolecules', *J. Am. Chem. Soc.* 112, **1990**, 7638-7647.
- Hawker, C.; Fréchet, J. M. J. 'A New Convergent Approach to Monodisperse Dendritic Macromolecules', *J. Chem. Soc., Chem. Commun.* **1990**, 1010-1013.
- Hayat, M. A. (Ed.) *Colloidal Gold: Principles, Methods and Applications*; Academic: San Diego, 1991.
- He, J.-A.; Valluzzi, R.; Yang, K.; Dolukhanyan, T.; Sung, C.; Kumar, J.; Tripathy, S. K. 'Electrostatic Multilayer Deposition of a Gold-Dendrimer Nanocomposite', *Chem. Mater.* 11, **1999**, 3268-3274.
- Heck, R. F. 'Acylation, Methylation, and Carboxyalkylation of Olefins by Group VIII Metal Derivatives', *J. Am. Chem. Soc.* 90, **1968**, 5518-5526.
- Heck, R. F. 'Allylation of Aromatic Compounds with Organopalladium Salts', *J. Am. Chem. Soc.* 90, **1968**, 5531-5534.

- Heck, R. F. 'Aromatic Haloethylation with Palladium and Copper Halides', *J. Am. Chem. Soc.* 90, **1968**, 5538-5542.
- Heck, R. F. 'The Arylation of Allylic Alcohols with Organopalladium Compounds. A New Synthesis of 3-Aryl Aldehydes and Ketones', *J. Am. Chem. Soc.* 90, **1968**, 5526-5531.
- Heck, R. F.; Nolley, J. P. 'Palladium-Catalyzed Vinylic Hydrogen Substitution Reactions with Aryl, Benzyl, and Styryl Halides', *J. Org. Chem.* 37, **1972**, 2320-2322.
- Henglein, A. 'Small-Particle Research: Physicochemical Properties of Extremely Small Colloidal Metal and Semiconductor Particles', *Chem. Rev.* 89, **1989**, 1861-1873.
- Hirai, H.; Nakao, Y.; Toshima, N. 'Preparation of Colloidal Rhodium in Poly(vinyl Alcohol) by Reduction with Methanol', *J. Macromol. Sci. Chem. A* 12, **1978**, 1117-1141.
- Hirai, H.; Nakao, Y.; Toshima, N. 'Preparation of Colloidal Transition Metals in Polymers by Reduction with Alcohols or Ethers', *J. Macromol. Sci. Chem. A* 13, **1979**, 727-750.
- Homsí, F.; Hosoi, K.; Nozaki, K.; Hiyama, T. 'Solid Phase Cross-Coupling Reaction of Aryl(halo)silanes with 4-Iodobenzoic Acid', *J. Organomet. Chem.* 624, **2001**, 208-216.
- Hostetler, M. J.; Wingate, J. E.; Zhong, C.-J.; Harris, J. E.; Vachet, R. W.; Clark, M. R.; Londono, J. D.; Green, S. J.; Stokes, J. J.; Wignall, G. D.; Glish, G. L.; Porter, M. D.; Evans, N. D.; Murray, R. W. 'Alkanethiolate Gold Cluster Molecules with Core Diameters from 1.5 to 5.2 nm: Core and

- Monolayer Properties as a Function of Core Size', *Langmuir* 14, **1998**, 17-30.
- Hou, W.; Dasog, M.; Scott, R. W. J. 'Probing the Relative Stability of Thiolate- and Dithiolate-Protected Au Monolayer-Protected Clusters', *Langmuir* 25, **2009**, 12954-12961.
- Howard, A.; Mitchell, C. E. J.; Egdell, R. G. 'Real Time STM Observation of Ostwald Ripening of Pd Nanoparticles on TiO₂(110) at Elevated Temperature', *Surf. Sci.* 515, **2002**, L504-L508.
- Hu, J.; Liu, Y. 'Pd Nanoparticle Aging and Its Implications in the Suzuki Cross-Coupling Reaction', *Langmuir* 21, **2005**, 2121-2123.
- Huang, J.; Hemminger, J. C. 'Photooxidation of Thiols in Self-Assembled Monolayers on Gold', *J. Am. Chem. Soc.* 115, **1993**, 3342-3343.
- Huang, W.; Kuhn, J. N.; Tsung, C.-K.; Zhang, Y.; Habas, S. E.; Yang, P.; Somorjai, G. A. 'Dendrimer Templated Synthesis of One Nanometer Rh and Pt Particles Supported on Mesoporous Silica: Catalytic Activity for Ethylene and Pyrrole Hydrogenation', *Nano Lett.* 8, **2008**, 2027-2034.
- Hurley, B. L.; McCreery, R. L. 'Covalent Bonding of Organic Molecules to Cu and Al Alloy 2024 T3 Surfaces via Diazonium Ion Reduction', *J. Electrochem. Soc.* 151, **2004**, B252-B259.
- Ikawa, T.; Sajiki, H.; Hirota, K. 'Highly Chemoselective Hydrogenation Method Using Novel Finely Dispersed Palladium Catalyst on Silk-Fibroin: Its Preparation and Activity', *Tetrahedron* 61, **2005**, 2217-2231.

- Imre, A.; Beke, D. L.; Gontier-Moya, E.; Szabo, I. A.; Gillet, E. 'Surface Ostwald Ripening of Pd Nanoparticles on the MgO (100) Surface', *Appl.Phys. A* 71, **2000**, 19-22.
- Jain, P. K.; Huang, X.; El-Sayed, I. H.; El-Sayed, M. A. 'Noble Metals on the Nanoscale: Optical and Photothermal Properties and Some Applications in Imaging, Sensing, Biology, and Medicine', *Acc. Chem. Res.* 41, **2008**, 1578-1586.
- Jeffery, T. 'On the Efficiency of Tetraalkylammonium Salts in Heck Type Reactions', *Tetrahedron* 52, **1996**, 10113-10130.
- Jeffery, T.; David, M. '[Pd/Base/QX] Catalyst Systems for Directing Heck-Type Reactions', *Tetrahedron Lett.* 39, **1998**, 5751-5754.
- Jiang, D.; Sumpter, B. G.; Dai, S. 'Structure and Bonding between an Aryl Group and Metal Surfaces', *J. Am. Chem. Soc.* 128, **2006**, 6030-6031.
- Jiang, G.; Wang, L.; Chen, T.; Yu, H.; Chen, C. 'Preparation of Gold Nanoparticles in the Presence of Poly(benzyl Ether) Alcohol Dendrons', *Mater. Chem. Phys.* 98, **2006**, 76-82.
- Jiang, G.; Wang, L.; Chen, T.; Yu, H.; Wang, J. 'Studies of Preparation of Palladium Nanoparticles Protected by Dendrons', *Nanotechnology* 15, **2004**, 1716-1719.
- Jordan, R.; West, N.; Ulman, A.; Chou, Y.-M.; Nuyken, O. 'Nanocomposites by Surface-Initiated Living Cationic Polymerization of 2-Oxazolines on Functionalized Gold Nanoparticles', *Macromolecules* 34, **2001**, 1606-1611.

- Jurčík, V.; Nolan, S. P.; Cazin, C. S. J. 'Hydrogenation of C-C Multiple Bonds Mediated by [Pd(NHC)(PCy₃)] (NHC=N-Heterocyclic Carbene) under Mild Reaction Conditions', *Chem. Eur. J.* 15, **2009**, 2509 – 2511.
- Kariuki, J. K.; McDermott, M. T. 'Formation of Multilayers on Glassy Carbon Electrodes via the Reduction of Diazonium Salts', *Langmuir* 17, **2001**, 5947-5951.
- Kariuki, J. K.; McDermott, M. T. 'Nucleation and Growth of Functionalized Aryl Films on Graphite Electrodes', *Langmuir* 15, **1999**, 6534-6540.
- Kavanagh, K. E.; Nord, F. F. 'Systematic Studies on Palladium-Synthetic High Polymer Catalysts', *J. Am. Chem. Soc.* 65, **1943**, 2121-2122.
- Kim, M.-K.; Jeon, Y.-M.; Jeon, W. S.; Kim, H.-J.; Hong, S. G.; Park, C. G.; Kim, K. 'Novel Dendron-Stabilized Gold Nanoparticles with High Stability and Narrow Size Distribution', *Chem. Commun.* **2001**, 667–668.
- Kim, S.-W.; Kim, M.; Lee, W. Y.; Hyeon, T. 'Fabrication of Hollow Palladium Spheres and their Successful Application to the Recyclable Heterogeneous Catalyst for Suzuki Coupling Reactions', *J. Am. Chem. Soc.* 124, **2002**, 7642-7643.
- Kitamura, Y.; Tanaka, A.; Sato, M.; Oono, K.; Ikawa, T.; Maegawa, T.; Monguchi, Y.; Sajiki, H. 'Development of a Practical and Scalable Preparation using Sonication of Pd/Fibroin Catalyst for Chemoselective Hydrogenation', *Synth. Commun.* 37, **2007**, 4381–4388.
- Klingelhöfer, S.; Heitz, W.; Greiner, A.; Oestreich, S.; Förster, S.; Antonietti, M. 'Preparation of Palladium Colloids in Block Copolymer Micelles and their Use for the Catalysis of the Heck Reaction', *J. Am. Chem. Soc.* 119, **1997**, 10116-10120.

- Kogan, V.; Aizenshtat, Z.; Neumann, R. 'Preferential Catalytic Hydrogenation of Aromatic Compounds versus Ketones with a Palladium Substituted Polyoxometalate as Pre-Catalyst', *New J. Chem.* **26**, **2002**, 272-274.
- Kogan, V.; Aizenshtat, Z.; Popovitz-Biro, R.; Neumann, R. 'Carbon-Carbon and Carbon-Nitrogen Coupling Reactions Catalyzed by Palladium Nanoparticles Derived from a Palladium Substituted Keggin-Type Polyoxometalate', *Org. Lett.* **4**, **2002**, 3529-3532.
- Köllhofer, A.; Pullmann, T.; Plenio, H. 'A Versatile Catalyst for the Sonogashira Coupling of Aryl Chlorides', *Angew. Chem. Int. Ed.* **42**, **2003**, 1056-1058.
- Komine, Y.; Ueda, I.; Goto, T.; Fujihara, H. 'Dendritic Effects on the Ordered Assembly and the Interfacial One-Electron Oxidation of Redox-Active Dendron-Functionalized Gold Nanoparticles', *Chem. Commun.* **2006**, 302-304.
- Kumar, K.; Zapf, A.; Michalik, D.; Tillack, A.; Heinrich, T.; Böttcher, H.; Arlt, M.; Beller, M. 'Palladium-Catalyzed Carbonylation of Haloindoles: No Need for Protecting Groups', *Org. Lett.* **6**, **2004**, 7-10.
- Kwock, E. W.; Neenan, T. X.; Miller, T. M. 'Convergent Synthesis of Monodisperse Aryl Ester Dendrimers', *Chem. Mater.* **3**, **1991**, 775-777.
- Leemans, L.; Fayt, R.; Teyssié, Ph.; de Jaeger, N. C. 'Poly(alkyl Methacrylate-*b*-sulfonated Glycidyl Methacrylate). A New Amphiphilic Polymeric Surfactant for the Preparation and Stabilization of Polymer Acrylic Latices in Aqueous Medium', *Macromolecules* **24**, **1991**, 5922-5925.

- Lewis, L. N. 'Chemical Catalysis by Colloids and Clusters', *Chem. Rev.* 93, **1993**, 2693-2730.
- Li, G.; Luo, Y. 'Preparation and Characterization of Dendrimer-Templated Ag-Cu Bimetallic Nanoclusters', *Inorg. Chem.* 47, **2008**, 360-364.
- Li, J.-H.; Tang, B.-X.; Tao, L.-M.; Xie, Y.-X.; Liang, Y.; Zhang, M.-B. 'Reusable Copper-Catalyzed Cross-Coupling Reactions of Aryl Halides with Organotin in Inexpensive Ionic Liquids', *J. Org. Chem.* 71, **2006**, 7488-7490.
- Li, Y.; El-Sayed, M. A. 'The Effect of Stabilizers on the Catalytic Activity and Stability of Pd Colloidal Nanoparticles in the Suzuki Reactions in Aqueous Solution', *J. Phys. Chem. B* 105, **2001**, 8938-8943.
- Li, Y.; Hong, X. M.; Collard, D. M.; El-Sayed, M. A. 'Suzuki Cross-Coupling Reactions Catalyzed by Palladium Nanoparticles in Aqueous Solution', *Org. Lett.* 2, **2000**, 2385-2388.
- Littke, A. F.; Fu, G. C. 'Palladium-Catalyzed Coupling Reactions of Aryl Chlorides', *Angew. Chem. Int. Ed.* 41, **2002**, 4176-4211.
- Liu, G.; Böcking, T.; Gooding, J. J. 'Diazonium Salts: Stable Monolayers on Gold Electrodes for Sensing Applications', *J. Electroanal. Chem.* 600, **2007**, 335-344.
- Liu, Y.-C.; McCreery, R. L. 'Reactions of Organic Monolayers on Carbon Surfaces Observed with Unenhanced Raman Spectroscopy', *J. Am. Chem. Soc.* 117, **1995**, 11254-11259.
- Love, C. S.; Chechik, V.; Smith, D. K.; Brennan, C. 'Dendron-Stabilised Gold Nanoparticles: Generation Dependence of Core Size and Thermal Stability', *J. Mater. Chem.* 14, **2004**, 919-923.

- Lynch, C. T. (Ed.) *CRC Handbook of Materials Chemistry*, Vol. 1, CRC Press, 1974, pp. 78, 87
- Maegawa, T.; Fujita, Y.; Sakurai, A.; Akashi, A.; Sato, M.; Oono, K.; Sajiki, H. 'Pd/C(en) Catalyzed Chemoselective Hydrogenation in the Presence of Aryl Nitriles', *Chem. Pharm. Bull.* 55, **2007**, 837-839.
- Maegawa, T.; Takahashi, T.; Yoshimura, M.; Suzuka, H.; Monguchi, Y.; Sajiki, H. 'Development of Molecular Sieves-Supported Palladium Catalyst and Chemoselective Hydrogenation of Unsaturated Bonds in the Presence of Nitro Groups', *Adv. Synth. Catal.* 351, **2009**, 2091-2095.
- Mayer, A. B. R.; Mark, J. E. 'Transition Metal Nanoparticles Protected by Amphiphilic Block Copolymers as Tailored Catalyst Systems', *Colloid Polym. Sci.* 275, **1997**, 333-340.
- Mekelburger, H.-B.; Vögtle, F.; Jaworek, W. 'Dendrimers, Arborols, and Cascade Molecules: Breakthrough into Generations of New Materials', *Angew. Chem. Int. Ed.* 31, **1992**, 1571-1576.
- Micheaud, C.; Marécot, P.; Guérin, M.; Barbier, J. 'Preparation of Alumina Supported Palladium-Platinum Catalysts by Surface Redox Reactions. Activity for Complete Hydrocarbon Oxidation', *Appl. Catal. A* 171, **1998**, 229-239.
- Mirkhalaf, F.; Paprotny, J.; Schiffrin, D. J. 'Synthesis of Metal Nanoparticles Stabilized by Metal-Carbon Bonds', *J. Am. Chem. Soc.* 128, **2006**, 7400-7401.
- Miyaura, N.; Suzuki, A. 'Palladium-Catalyzed Cross-Coupling Reactions of Organoboron Compounds', *Chem. Rev.* 95, **1995**, 2457-2483.

- Miyaura, N.; Yamada, K.; Suzuki, A. 'A New Stereospecific Cross-Coupling by the Palladium Catalyzed Reaction of 1-Alkenylboranes with 1-Alkenyl or 1-Alkynyl Halides', *Tetrahedron Lett.* 20, **1979**, 3437-3440.
- Mizoroki, T.; Mori, K.; Ozaki, A. 'Arylation of Olefin with Aryl Iodide Catalyzed by Palladium', *Bull. Chem. Soc. Jpn.* 44, **1971**, 581.
- Mizukoshi, Y.; Okitsu, K.; Maeda, Y.; Yamamoto, T. A.; Oshima, R.; Nagata, Y. 'Sonochemical Preparation of Bimetallic Nanoparticles of Gold/Palladium in Aqueous Solution', *J. Phys. Chem. B* 101, **1997**, 7033-7037.
- Mori, A.; Miyakawa, Y.; Ohashi, E.; Haga, T.; Maegawa, T.; Sajiki, H. 'Pd/C-Catalyzed Chemoselective Hydrogenation in the Presence of Diphenylsulfide', *Org. Lett.* 8, **2006**, 3279-3281.
- Mori, A.; Mizusaki, T.; Kawase, M.; Maegawa, T.; Monguchi, Y.; Takao, S.; Takagi, Y.; Sajiki, H. 'Novel Palladium-on-Carbon/Diphenyl Sulfide Complex for Chemoselective Hydrogenation: Preparation, Characterization, and Application', *Adv. Synth. Catal.* 350, **2008**, 406 – 410.
- Mulvaney, P. 'Surface Plasmon Spectroscopy of Nanosized Metal Particles', *Langmuir* 12, **1996**, 788-800.
- Myers, S. V.; Frenkel, A. I.; Crooks, R. M. 'X-ray Absorption Study of PdCu Bimetallic Alloy Nanoparticles Containing an Average of ~64 Atoms', *Chem. Mater.* 21, **2009**, 4824–4829.
- Nakamura, I.; Yamanoi, Y.; Yonezawa, T.; Imaoka, T.; Yamamoto, K.; Nishihara, H. 'Nanocage Catalysts—Rhodium Nanoclusters Encapsulated with Dendrimers as Accessible and Stable Catalysts for

- Olefin and Nitroarene Hydrogenations', *Chem. Commun.* **2008**, 5716–5718.
- Nakao, S.; Torigoe, K.; Kon-No, K.; Yonezawa, T. 'Self-Assembled One-Dimensional Arrays of Gold-Dendron Nanocomposites', *J. Phys. Chem. B* **106**, **2002**, 12097-12100.
- Narayanan, R.; El-Sayed, M. A. 'Catalysis with Transition Metal Nanoparticles in Colloidal Solution: Nanoparticle Shape Dependence and Stability', *J. Phys. Chem. B* **109**, **2005**, 12663-12676.
- Narayanan, R.; El-sayed, M. A. 'Effect of Catalysis on the Stability of Metallic Nanoparticles: Suzuki Reaction Catalyzed by PVP-Palladium Nanoparticles', *J. Am. Chem. Soc.* **125**, **2003**, 8340-8347.
- Narayanan, R.; El-Sayed, M. A. 'Effect of Colloidal Catalysis on the Nanoparticle Size Distribution: Dendrimer-Pd vs PVP-Pd Nanoparticles Catalyzing the Suzuki Coupling Reaction', *J. Phys. Chem. B* **108**, **2004**, 8572-8580.
- Narayanan, R.; El-Sayed, M. A. 'Effect of Colloidal Nanocatalysis on the Metallic Nanoparticle Shape: The Suzuki Reaction', *Langmuir* **21**, **2005**, 2027-2033.
- Narayanan, R.; El-Sayed, M. A. 'FTIR Study of the Mode of Binding of the Reactants on the Pd Nanoparticle Surface during the Catalysis of the Suzuki Reaction', *J. Phys. Chem. B* **109**, **2005**, 4357-4360.
- Narayanan, R.; Tabor, C.; El-Sayed, M. A. 'Can the Observed Changes in the Size or Shape of a Colloidal Nanocatalyst Reveal the Nanocatalysis Mechanism Type: Homogeneous or Heterogeneous?' *Top. Catal.* **48**, **2008**, 60–74.

- Navaladian, S.; Viswanathan, B.; Viswanath, R. P.; Varadarajan, T. K. 'Thermal Decomposition as Route for Silver Nanoparticles', *Nanoscale Res. Lett.* **2**, **2007**, 44-48.
- Negishi, E.-I.; Baba, S. 'Novel Stereoselective Alkenyl-Aryl Coupling via Nickel-Catalyzed Reaction of Alkenylalanes with Aryl Halides', *J. Chem. Soc., Chem. Comm.* **1976**, 596-597.
- Negishi, E.-I.; King, A. O.; Okukado, N. 'Selective Carbon-Carbon Bond Formation via Transition Metal Catalysis. 3. A Highly Selective Synthesis of Unsymmetrical Biaryls and Diarylmethanes by the Nickel- or Palladium-Catalyzed Reaction of Aryl- and Benzylzinc Derivatives with Aryl Halides', *J. Org. Chem.* **42**, **1977**, 1821-1823.
- Nemamcha, A.; Rehspringer, J.-L.; Khatmi, D. 'Synthesis of Palladium Nanoparticles by Sonochemical Reduction of Palladium(II) Nitrate in Aqueous Solution', *J. Phys. Chem. B* **110**, **2006**, 383-387.
- Newkome, G. R.; Yao, Z.; Baker, G. R.; Gupta, V. K. 'Cascade Molecules: A New Approach to Micelles. A [27]-Arborol', *J. Org. Chem.* **50**, **1985**, 2003-2004.
- Niemantsverdriet, J. W. *Spectroscopy in Catalysis: An Introduction* 2nd Edition, 2000, Wiley-VCH, Chapter 7, p 167-175.
- Niu, Y.; Crooks, R. M. 'Preparation of Dendrimer-Encapsulated Metal Nanoparticles Using Organic Solvents', *Chem. Mater.* **15**, **2003**, 3463-3467.
- Niu, Y.; Yeung, L. K.; Crooks, R. M. 'Size-Selective Hydrogenation of Olefins by Dendrimer-Encapsulated Palladium Nanoparticles', *J. Am. Chem. Soc.* **123**, **2001**, 6840-6846.

- Nunomura, N.; Hori, H.; Teranishi, T.; Miyake, M.; Yamada, S. 'Magnetic Properties of Nanoparticles in Pd/Ni Alloys', *Phys. Lett. A* 249, **1998**, 524-530.
- Nuzzo, R. G.; Dubois, L. H.; Allara, D. L. 'Fundamental Studies of Microscopic Wetting on Organic Surfaces. 1. Formation and Structural Characterization of a Self-Consistent Series of Polyfunctional Organic Monolayers', *J. Am. Chem. Soc.* 112, **1990**, 558-569.
- Ooe, M.; Murata, M.; Mizugaki, T.; Ebitani, K.; Kaneda, K. 'Dendritic Nanoreactors Encapsulating Pd Particles for Substrate-Specific Hydrogenation of Olefins', *Nano Lett.* 2, **2002**, 999-1002.
- Oosterom, G. E.; Reek, J. N. H.; Kamer, P. C. J.; van Leeuwen, P. W. N. M. 'Transition Metal Catalysis Using Functionalized Dendrimers', *Angew. Chem. Int. Ed.* 40, **2001**, 1828-1849.
- Ornelas, C.; Aranzaes, J. R.; Salmon, L.; Astruc, D. 'Click Dendrimers: Synthesis, Redox Sensing of Pd(OAc)₂, and Remarkable Catalytic Hydrogenation Activity of Precise Pd Nanoparticles Stabilized by 1,2,3-Triazole-Containing Dendrimers', *Chem. Eur. J.* 14, **2008**, 50-64.
- Ornelas, C.; Ruiz, J.; Salmon, L.; Astruc, D. 'Sulphonated Click Dendrimer-Stabilized Palladium Nanoparticles as Highly Efficient Catalysts for Olefin Hydrogenation and Suzuki Coupling Reactions under Ambient Conditions in Aqueous Media', *Adv. Synth. Catal.* 350, **2008**, 837-845.
- Pachón, L. D.; Rothenberg, G. 'Transition-Metal Nanoparticles: Synthesis, Stability and the Leaching Issue', *Appl. Organometal. Chem.* 22, **2008**, 288-299.

- Pachón, L. D.; Thathagar, M. B.; Hartl, F.; Rothenberg, G. 'Palladium-Coated Nickel Nanoclusters: New Hiyama Cross-Coupling Catalysts', *Phys. Chem. Chem. Phys.* **8**, **2006**, 151–157.
- Pathak, S.; Greci, M. T.; Kwong, R. C.; Mercado, K.; Prakash, G. K. S.; Olah, G. A.; Thompson, M. E. 'Synthesis and Applications of Palladium-Coated Poly(vinylpyridine) Nanospheres', *Chem. Mater.* **12**, **2000**, 1985-1989.
- Paulik, M. G.; Brooksby, P. A.; Abell, A. D.; Downard, A. J. 'Grafting Aryl Diazonium Cations to Polycrystalline Gold: Insights into Film Structure Using Gold Oxide Reduction, Redox Probe Electrochemistry, and Contact Angle Behavior', *J. Phys. Chem. C* **111**, **2007**, 7808-7815.
- Percec, V.; Aqad, E.; Peterca, M.; Rudick, J. G.; Lemon, L.; Ronda, J. C.; De, B. B.; Heiney, P. A.; Meijer, E. W. 'Steric Communication of Chiral Information Observed in Dendronized Polyacetylenes', *J. Am. Chem. Soc.* **128**, **2006**, 16365-16372.
- Phan, N. T. S.; Sluys, M. V. D.; Jones, C. W. 'On the Nature of the Active Species in Palladium Catalyzed Mizoroki–Heck and Suzuki–Miyaura Couplings – Homogeneous or Heterogeneous Catalysis, A Critical Review', *Adv. Synth. Catal.* **348**, **2006**, 609 – 679.
- Pilcher, A. S.; DeShong, P. 'Utilization of Tetrabutylammonium Triphenyldifluorosilicate as a Fluoride Source for Silicon-Carbon Bond Cleavage', *J. Org. Chem.* **61**, **1996**, 6901-6905.
- Pinson, J.; Podvorica, F. 'Attachment of Organic Layers to Conductive or Semiconductive Surfaces by Reduction of Diazonium Salts', *Chem. Soc. Rev.* **34**, **2005**, 429–439.

- Rahim, E. H.; Kamounah, F. S.; Frederiksen, J.; Christensen, J. B. 'Heck Reactions Catalyzed by PAMAM-Dendrimer Encapsulated Pd(0) Nanoparticles', *Nano Lett.* **1**, **2001**, 499-501.
- Rampino, L. D.; Nord, F. F. 'Applicability of Palladium Synthetic High Polymer Catalysts', *J. Am. Chem. Soc.* **63**, **1941**, 3268.
- Rampino, L. D.; Nord, F. F. 'Preparation of Palladium and Platinum Synthetic High Polymer Catalysts and the Relationship between Particle Size and Rate of Hydrogenation', *J. Am. Chem. Soc.* **63**, **1941**, 2745-2746.
- Reetz, M. T.; Breinbauer, R.; Wanninger, K. 'Suzuki and Heck Reactions Catalyzed by Preformed Palladium Clusters and Palladium/Nickel Bimetallic Clusters', *Tetrahedron Lett.* **37**, **1996**, 4499-4502.
- Reetz, M. T.; de Vries, J. G. 'Ligand-Free Heck Reactions Using Low Pd-loading', *Chem. Commun.* **2004**, 1559-1563.
- Reetz, M. T.; Helbig W. 'Size-Selective Synthesis of Nanostructured Transition Metal Clusters', *J. Am. Chem. Soc.* **116**, **1994**, 7401-7402.
- Reetz, M. T.; Lohmer, G. 'Propylene Carbonate Stabilized Nanostructured Palladium Clusters as Catalysts in Heck Reactions', *Chem. Commun.* **1996**, 1921-1922.
- Reetz, M. T.; Quaiser, S. A. 'A New Method for the Preparation of Nanostructured Metal Clusters', *Angew. Chem. Int. Ed.* **34**, **1995**, 2240-2241.
- Reetz, M.; Westermann, E. 'Phosphane-Free Palladium-Catalyzed Coupling Reactions: The Decisive Role of Pd Nanoparticles', *Angew. Chem. Int. Ed.* **39**, **2000**, 165-168.

- Rieley, H.; Price, N. J.; Smith, T. L.; Yang, S. 'Photo-Oxidation and Photo-Reduction in Alkylthiol Monolayers Self-Assembled on Gold', *J. Chem. Soc., Faraday Trans.* 92, **1996**, 3629-3634.
- Rocaboy, C.; Gladysz, J. A. 'Highly Active Thermomorphic Fluorous Palladacycle Catalyst Precursors for the Heck Reaction; Evidence for a Palladium Nanoparticle Pathway', *Org. Lett.* 4, **2002**, 1993-1996.
- Roucoux, A.; Schulz, J.; Patin, H. 'Reduced Transition Metal Colloids: A Novel Family of Reusable Catalysts?' *Chem. Rev.* 102, **2002**, 3757-3778.
- Russel, T. W.; Duncan, D. M.; Hansen, S. C. 'Catalytic Reduction. 4. Hydrogenation of Aldehydes over Borohydride Reduced Nickel and Palladium', *J. Org. Chem.* 42, **1977**, 551-554.
- Sajiki, H.; Mori, S.; Ohkubo, T.; Ikawa, T.; Kume, A.; Maegawa, T.; Monguchi, Y. 'Partial Hydrogenation of Alkynesto cis-Olefins by Using a Novel Pd⁰- Polyethyleneimine Catalyst' *Chem. Eur. J.* 14, **2008**, 5109 -5111.
- Schmidt, G., (Ed.) *Clusters and Colloids*; VCH: Weinheim, 1994.
- Schoenfisch, M. H.; Pemberton, J. E. 'Air Stability of Alkanethiol Self-Assembled Monolayers on Silver and Gold Surfaces', *J. Am. Chem. Soc.* 120, **1998**, 4502-4513.
- Schütz, J.; Herdtweck, E.; Herrmann, W. A. 'Synthesis and Catalytic Application of Palladium Pyrazolin-3-ylidene Complexes', *Organometallics* 23, **2004**, 6084-6086.
- Scott, R. W. J.; Datye, A. K.; Crooks, R. M. 'Bimetallic Palladium-Platinum Dendrimer-Encapsulated Catalysts', *J. Am. Chem. Soc.* 125, **2003**, 3708-3709.

- Scott, R. W. J.; Wilson, O. M.; Crooks, R. M. 'Synthesis, Characterization, and Applications of Dendrimer-Encapsulated Nanoparticles', *J. Phys. Chem. B* 109, **2005**, 692-704.
- Scott, R. W. J.; Wilson, O. M.; Oh, S.-K.; Kenik, E. A.; Crooks, R. M. 'Bimetallic Palladium-Gold Dendrimer-Encapsulated Catalysts', *J. Am. Chem. Soc.* 126, **2004**, 15583-15591.
- Sharma, A.; Kumar, V.; Sinha, A. K. 'A Chemoselective Hydrogenation of the Olefinic Bond of α,β -Unsaturated Carbonyl Compounds in Aqueous Medium under Microwave Irradiation', *Adv. Synth. Catal.* 348, **2006**, 354-360.
- Shen, Q.; Shekhar, S.; Stambuli, J. P.; Hartwig, J. F. 'Highly Reactive, General, and Long-Lived Catalysts for Coupling Heteroaryl and Aryl Chlorides with Primary Nitrogen Nucleophiles', *Angew. Chem. Int. Ed.* 44, **2005**, 1371 -1375.
- Shenhar, R.; Rotello, V. M. 'Nanoparticles: Scaffolds and Building Blocks', *Acc. Chem. Res.* 36, **2003**, 549-561.
- Shewchuk, D. M.; McDermott, M. T. 'Comparison of Diazonium Salt Derived and Thiol Derived Nitrobenzene Layers on Gold', *Langmuir* 25, **2009**, 4556-4563.
- Shimura, T.; Aramaki, K. 'Preparation of a Self-Assembled Monolayer on Iron by the Formation of a Covalent Bond between Carbon and Iron Atoms', *Corros. Sci.* 48, **2006**, 3784-3801.
- Shirakawa, E.; Murota, Y.; Nakao, Y.; Hiyama, T. 'Homocoupling of Organostannanes Catalyzed by Iminophosphine-Palladium', *Synlett* **1997**, 1143-1144.

- Shon, Y.-S.; Choi, D. 'A Route to Redox-Active Nanoparticle-Cored Dendrimers: Post-Encapsulation of Ferrocene', *Chem. Lett.* 35, **2006**, 644-645.
- Shon, Y.-S.; Choi, D. 'Dendritic Functionalization of Metal Nanoparticles for Nanoparticle-Cored Dendrimers', *Curr. Nanosci.* 3, **2007**, 245-254.
- Song, R. G.; Yamaguchi, M.; Nishimura, O.; Suzuki, M. 'Investigation of Metal Nanoparticles Produced by Laser Ablation and their Catalytic Activity', *Appl. Surf. Sci.* 253, **2007**, 3093-3097.
- Stewart, M. P.; Maya, F.; Kosynkin, D. V.; Dirk, S. M.; Stapleton, J. J.; McGuinness, C. L.; Allara, D. L.; Tour, J. M. 'Direct Covalent Grafting of Conjugated Molecules onto Si, GaAs, and Pd Surfaces from Aryldiazonium Salts', *J. Am. Chem. Soc.* 126, **2004**, 370-378.
- Stille, J. K. 'The Palladium-Catalyzed Cross-Coupling Reactions of Organotin Reagents with Organic Electrophiles [New Synthetic Methods (58)]', *Angew. Chem., Int. Ed.* 25, **1986**, 508-524.
- Suzuki, A. 'Recent Advances in the Cross-Coupling Reactions of Organoboron Derivatives with Organic Electrophiles, 1995-1998', *J. Organomet. Chem.* 576, **1999**, 147-168.
- Swanson, D. R.; Huang, B.; Abdelhady, H. G.; Tomalia, D. A. 'Unique Steric and Geometry Induced Stoichiometries Observed in the Divergent Synthesis of Poly(ester-acrylate/amine) (PEA) Dendrimers', *New J. Chem.* 31, **2007**, 1368-1378.
- Takasaki, M.; Motoyama, Y.; Higashi, K.; Yoon, S.-H.; Mochida, I.; Nagashima, H. 'Chemoselective Hydrogenation of Nitroarenes with

- Carbon Nanofiber-Supported Platinum and Palladium Nanoparticles', *Org. Lett.* 10, **2008**, 1601-1604.
- Tang, H.; Menzel, K.; Fu, G. C. 'Ligands for Palladium-Catalyzed Cross-Couplings of Alkyl Halides: Use of an Alkyldiaminophosphane Expands the Scope of the Stille Reaction', *Angew. Chem. Int. Ed.* 42, **2003**, 5079 – 5082.
- Taratula, O.; Chen, A. M.; Zhang, J.; Chaudry, J.; Nagahara, L.; Banerjee, I.; He, H. 'Highly Aligned Ribbon-Shaped Pd Nanoparticle Assemblies by Spontaneous Organization', *J. Phys. Chem. C* 111, **2007**, 7666-7670.
- Tarlov, M. J.; Burgess Jr., D. R. F.; Gillen, G. 'UV Photopatterning of Alkanethiolate Monolayers Self-Assembled on Gold and Silver', *J. Am. Chem. Soc.* 115, **1993**, 5305-5306.
- Tarlov, M. J.; Newman, J. G. 'Static Secondary Ion Mass Spectrometry of Self-Assembled Alkanethiol Monolayers on Gold', *Langmuir* 8, **1992**, 1398-1405.
- Temperley, H. N. V. 'Statistical Mechanics and the Partition of Numbers. II. The Form of Crystal Surfaces', *Proc. Cambridge Phil. Soc.* 48, **1952**, 683-697.
- Terrill, R. H.; Postlethwaite, T. A.; Chen, C.-H.; Poon, C.-D.; Terzis, A.; Chen, A.; Hutchison, J. E.; Clark, M. R.; Wignall, G.; Londono, J. D.; Superfine, R.; Flavo, M.; Johnson Jr., C. S.; Samulski, E. T.; Murray, R. W. 'Monolayers in Three Dimensions: NMR, SAXS, Thermal and Electron Hopping Studies of Alkanethiol Stabilized Gold Clusters', *J. Am. Chem. Soc.* 117, **1995**, 12537-12548.
- Tomalia, D. A. 'The Dendritic State', *Mater. Today* 8, **2005**, 34-46.

- Tomalia, D. A.; Baker, H.; Dewald, J.; Hall, M.; Kallos, G.; Martin, S.; Roeck, J.; Ryder, J.; Smith, P. 'A New Class of Polymers: Starburst-Dendritic Macromolecules', *Polymer J.* 17, **1985**, 117-132.
- Tomalia, D. A.; Naylor, A. M.; Goddard III, W. A. 'Starburst Dendrimers: Molecular-Level Control of Size, Shape, Surface Chemistry, Topology, and Flexibility from Atoms to Macroscopic Matter', *Angew. Chem. Int. Ed. Engl.* 29, **1990**, 138-175.
- Tsuji, J. *Palladium Reagents and Catalysts: Innovations in Organic Synthesis*; Wiley: New York, 1995.
- Turkevich, J.; Kim, G. 'Palladium: Preparation and Catalytic Properties of Particles of Uniform Size', *Science* 169, **1970**, 873-879.
- Turkevich, J.; Stevenson, P. C.; Hillier, J. 'A Study of the Nucleation and Growth Processes in the Synthesis of Colloidal Gold', *Faraday Discuss. Chem. Soc.* 11, **1951**, 55-75.
- Vasylyev, M. V.; Maayan, G.; Hovav, Y.; Haimov, A.; Neumann, R. 'Palladium Nanoparticles Stabilized by Alkylated Polyethyleneimine as Aqueous Biphasic Catalysts for the Chemoselective Stereocontrolled Hydrogenation of Alkenes', *Org. Lett.* 8, **2006**, 5445-5448.
- Walker, S. D.; Barder, T. E.; Martinelli, J. R.; Buchwald, S. L. 'A Rationally Designed Universal Catalyst for Suzuki–Miyaura Coupling Processes', *Angew. Chem. Int. Ed.* 43, **2004**, 1871–1876.
- Wang, J.; Firestone, M. A.; Uciello, O.; Carlisle, J. A. 'Surface Functionalization of Ultrananocrystalline Diamond Films by Electrochemical Reduction of Aryldiazonium Salts', *Langmuir* 20, **2004**, 11450-11456.

- Wang, R.; Yang, J.; Zheng, Z.; Carducci, M. D.; Jiao, J.; Seraphin, S. 'Dendron-Controlled Nucleation and Growth of Gold Nanoparticles', *Angew. Chem. Int. Ed.* **40**, **2001**, 549-542.
- Wang, Y. A.; Li, J. J.; Chen, H.; Peng, X. 'Stabilization of Inorganic Nanocrystals by Organic Dendrons', *J. Am. Chem. Soc.* **124**, **2002**, 2293-2298.
- Wooley, K. L.; Hawker, C. J.; Fréchet, J. M. J. 'Polymers with Controlled Molecular Architecture: Control of Surface Functionality in the Synthesis of Dendritic Hyperbranched Macromolecules Using the Convergent Approach', *J. Chem. Soc., Perkin Trans. I*, **5**, **1991**, 1059-1076.
- Wu, L.; Li, B.-L.; Huang, Y.-Y.; Zhou, H.-F.; He, Y.-M.; Fan, Q.-H. 'Phosphine Dendrimer-Stabilized Palladium Nanoparticles, as Highly Active and Recyclable Catalyst for the Suzuki-Miyaura Reaction and Hydrogenation', *Org. Lett.* **8**, **2006**, 3605-3608.
- Wu, L.; Li, Z.-W.; Zhang, F.; He, Y.-M.; Fan, Q.-H. 'Air-Stable and Highly Active Dendritic Phosphine Oxide-Stabilized Palladium Nanoparticles: Preparation, Characterization and Applications in the Carbon-Carbon Bond Formation and Hydrogenation Reactions', *Adv. Synth. Catal.* **350**, **2008**, 846-862.
- Wu, M.; O'Neill, S. A.; Brousseau, L. C.; McConnell, W. P.; Shultz, D. A.; Linderman, R. J.; Feldheim, D. L. 'Synthesis of Nanometer-Sized Hollow Polymer Capsules from Alkanethiol-Coated Gold Particles', *Chem. Commun.* **2000**, 775-776.

- Xiong, Y.; Cai, H.; Wiley, B. J.; Wang, J.; Kim, M. J.; Xia, Y. 'Synthesis and Mechanistic Study of Palladium Nanobars and Nanorods', *J. Am. Chem. Soc.* 129, **2007**, 3665-3675.
- Yang, P.; Zhang, W.; Du, Y.; Wang, X. 'Hydrogenation of Nitrobenzenes Catalyzed by Platinum Nanoparticle Core-Polyaryl Ether Trisacetic Acid Ammonium Chloride Dendrimer Shell Nanocomposite', *J. Mol. Catal. A: Chem.* 260, **2006**, 4-10.
- Yang, W.; Chen, M.; Knoll, W.; Deng, H. 'Synthesis of Hexanedithiolate/Decanethiolate Mixed Monolayer Protected Gold Clusters and Scanning Tunneling Microscope Tip Induced Patterning on the Clusters/Au(111) Surface', *Langmuir* 18, **2002**, 4124-4130.
- Ye, H.; Scott, R. W. J.; Crooks, R. M. 'Synthesis, Characterization, and Surface Immobilization of Platinum and Palladium Nanoparticles Encapsulated within Amine-Terminated Poly(amidoamine) Dendrimers', *Langmuir* 20, **2004**, 2915-2920.
- Yeung, L. K.; Crooks, R. M. 'Heck Heterocoupling within a Dendritic Nanoreactor', *Nano Lett.* 1, **2001**, 14-17.
- Yin, L.; Liebscher, J. 'Carbon-Carbon Coupling Reactions Catalyzed by Heterogeneous Palladium Catalysts', *Chem. Rev.* 107, **2007**, 133-173.
- Yu, J.-Q.; Wu, H.-C.; Ramarao, C.; Spencer, J. B.; Ley, S. V. 'Transfer Hydrogenation Using Recyclable Polyurea-Encapsulated Palladium: Efficient and Chemoselective Reduction of Aryl Ketones', *Chem. Commun.* **2003**, 678-679.

-
- Zhao, M.; Crooks, R. M. 'Dendrimer-Encapsulated Pt Nanoparticles: Synthesis, Characterization, and Applications to Catalysis', *Adv. Mater.* **11**, **1999**, 217-220.
- Zhao, M.; Crooks, R. M. 'Intradendrimer Exchange of Metal Nanoparticles', *Chem. Mater.* **11**, **1999**, 3379-3385.
- Zhao, M.; Sun, L.; Crooks, R. M. 'Preparation of Cu Nanoclusters within Dendrimer Templates', *J. Am. Chem. Soc.* **120**, **1998**, 4877-4878.